uOttawa

L'Université canadienne
Canada's university

FACULTÉ DES ÉTUDES SUPÉRIEURES ET POSTOCTORALES

uOttawa

L'Université canadienne
Canada's university

FACULTY OF GRADUATE AND POSDOCTORAL STUDIES

Lan Lin

AUTEUR DE LA THÈSE / AUTHOR OF THESIS

Ph.D. (Civil Engineering)

GRADE / DEGREE

Department of Civil Engineering

FACULTÉ, ÉCOLE, DÉPARTEMENT / FACULTY, SCHOOL, DEPARTMENT

Development of Improved Intensity Measures for Probabilistic Seismic Demand Analysis

TITRE DE LA THÈSE / TITLE OF THESIS

Nove Naumoski

DIRECTEUR (DIRECTRICE) DE LA THÈSE / THESIS SUPERVISOR

Murat Saatcioglu

CO-DIRECTEUR (CO-DIRECTRICE) DE LA THÈSE / THESIS CO-SUPERVISOR

EXAMINATEURS (EXAMINATRICES) DE LA THÈSE / THESIS EXAMINERS

Hanping Hong

Dan Palermo

Jag Humar

Hiroshi Tanaka

Gary W. Slater

Le Doyen de la Faculté des études supérieures et postdoctorales / Dean of the Faculty of Graduate and Postdoctoral Studies

Development of Improved Intensity Measures for Probabilistic Seismic Demand Analysis

By

Lan Lin

Thesis Submitted to the Faculty of the Graduate and Postdoctoral Studies
in Partial Fulfillment of the Requirements for the Degree of
Doctor of Philosophy in Civil Engineering

Department of Civil Engineering
Faculty of Engineering
University of Ottawa

September 2008

Your file Votre référence
ISBN: 978-0-494-46515-8
Our file Notre référence
ISBN: 978-0-494-46515-8

Dedicated to my family,

Especially, my parents for their love and continuous support.

Acknowledgments

I wish to express my sincere gratitude to my supervisors Dr. Nove Naumoski and Dr. Murat Saatcioglu for their guidance and support during the course of this study.

I would like to thank Drs. Hiroshi Tanaka, Jag Humar, David Lau, Heng Khoo, and David Redekop for sharing their knowledge by offering the courses that helped me in my graduate studies.

Thanks and appreciation are due to Dr. John Adams and Mr. Stephen Halchuk of the Geological Survey of Canada for providing seismic hazard analysis results for use in this thesis.

I also wish to thank the Faculty of Graduate and Postdoctoral Studies at the University of Ottawa for awarding me an admission scholarship.

Abstract

Performance-Based Earthquake Engineering (PBEE) is a multidisciplinary procedure for seismic assessment of existing structures and design of new structures. One of the phases of PBEE is the determination of the mean annual frequencies of exceeding specified values of a structural response parameter (e.g., maximum interstorey drift) due to future earthquake motions. This is done using probabilistic seismic demand analysis (PSDA), which combines the seismic hazard at the location of the structure and the structural response obtained from nonlinear dynamic analysis for a selected set of earthquake records.

Past research work has shown that the PSDA results depend greatly on the intensity measure used for scaling the records for the computation of the structural response. This thesis is focused on the development of new intensity measures for use in PSDA. Three reinforced concrete frame buildings (4-storey, 10-storey, and 16-storey) designed for Vancouver were used in the study. Eighty ground motion records representative of seismic motions in the Vancouver region were selected for use in the analyses. Based on comprehensive analyses of the frames of the buildings, two intensity measures designated S_{N1} and S_{N2} are proposed. The intensity measure S_{N1} takes into account the first mode response and the period elongation of that mode during nonlinear response. This intensity measure is intended for short-period (i.e., first mode dominated) building structures. The intensity measure S_{N2} takes into account the contributions of the first and second modes to the response, and is suitable for long-period buildings. It is demonstrated in the thesis that both S_{N1} and S_{N2} are superior in the prediction of structural responses relative to the

intensity measure represented by the spectral acceleration at the first mode period, $Sa(T_1)$, which is currently the most used intensity measure. They are easy for use, provide reliable results, and are suitable for probabilistic seismic demand analysis of structures.

Table of Contents

List of Tables

List of Figures

Chapter 1

Introduction

1.1 Motivation

Performance-based earthquake engineering (PBEE) represents a new approach for seismic assessment of existing structures and design of new structures. The development of PBEE was initiated following the 1989 Loma Prietta and the 1994 Northridge, California earthquakes, that caused a relatively small number of casualties but very large economic losses due to property damage and business interruptions (Hamburger 2007). These earthquakes demonstrated that the performance objective of the codes – to prevent collapse (i.e., just life safety) during a 'rare' earthquake – is insufficient, and a new approach is needed for seismic design of structures to minimise both the fatalities and economical losses due to earthquakes.

A formal framework for performance-based earthquake engineering has been developed by the Pacific Earthquake Engineering Research (PEER) Center (Cornell and Krawinkler 2000). Given the uncertainties of the seismic motions at a given location, and the variability of the structural response for different seismic motions, a probabilistic approach has been used in the development of the PBEE methodology. Figure 1.1

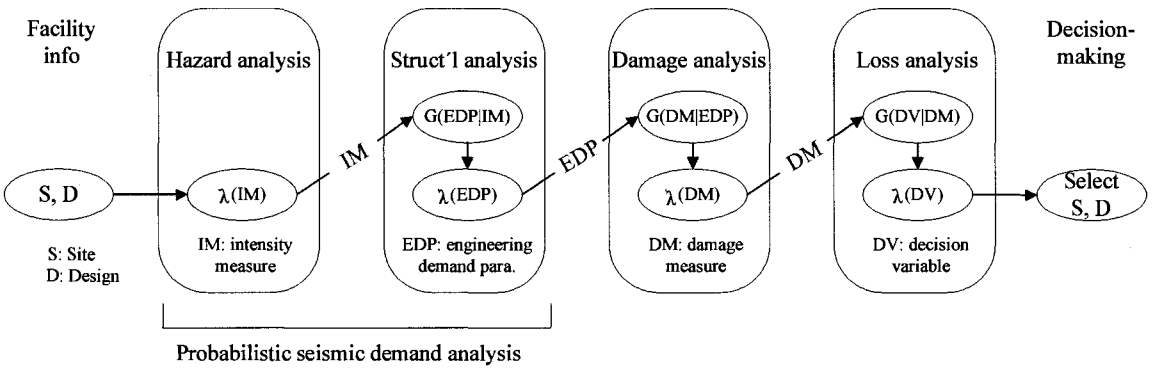

Figure 1.1 PEER framework methodology for performance-based earthquake engineering (Adapted from Moehle and Deierlein 2004).

illustrates schematically the PBEE methodology. It can be seen that the methodology consists of four analysis phases, i.e., seismic hazard analysis, structural response analysis, damage analysis, and loss analysis. The parameters used in Fig. 1.1 are as follows:

- *IM*[(1)] is an Intensity Measure (e.g., peak ground motion, spectral acceleration at the fundamental building period, or an advanced intensity measure consisting of more than one parameter, as discussed below in Section 1.3).
- *EDP* is an Engineering Demand Parameter (e.g., interstorey drift, ductility, floor acceleration, etc.).
- *DM* is a Damage Measure (quantitative representation of damage to structural elements, nonstructural elements, and contents); in the context of the PBEE framework, the *DM*s

(1) Note that *IM*, *EDP*, *DM*, and *DV* represent random variables. Each of these variables can have a series of values. The commonly accepted convention for denoting random variable names in uppercase letters and specific values of the variables in lowercase letters is adopted throughout this thesis (e.g., specific values of *IM*, *EDP*, *DM*, and *DV* are denoted as *im*, *edp*, *dm*, and *dv* respectively). In this section, only random variables are used, for short and also for consistency with the designations in the PBEE framework documents (i.e., Cornell and Krawinkler 2000, Moehle and Deierlein 2004).

must be defined in terms of fragility relations, which represent the probability of damage states as a function of *EDP* (Moehle and Deierlein 2004).

- *DV* is a Decision Variable (direct dollar losses, downtime (or restoration time), and casualties).

The other quantities in Fig. 1.1 are described in detail in Moehle and Deierlein (2004) and only a brief discussion is given in this section. The terms $G(EDP|IM)$[(2)], $G(DM|EDP)$, and $G(DV|DM)$ represent conditional probabilities of exceedance. As an example, assuming the *EDP* to be interstorey drift (*IDR*) and the *IM* to be the spectral acceleration at the first mode period ($Sa(T_1)$), then the term $G(EDP|IM)$ represents the probability of exceeding a specified *IDR* level, given a value of $Sa(T_1)$. Similarly, $G(DM|EDP)$ is the probability of exceeding *DM* given *EDP*, and $G(DV|DM)$ is the probability of exceeding *DV* given *DM*.

The terms $\lambda(IM)$[(3)], $\lambda(EDP)$, $\lambda(DM)$, and $\lambda(DV)$ are the *mean annual frequencies* of exceeding specified *IM*, *EDP*, *DM*, and *DV* values respectively. Of special importance for decision-makers (developers, building owners, and building officials) is the final result of the PBEE analysis, $\lambda(DV)$, which represents the annual frequency of the loss exceeding $DV=dv$ dollars, when the decision variable *DV* is a financial loss. As seen in Fig. 1.1, each

---

(2) Note that the terms $G(EDP|IM)$, $G(DM|EDP)$, and $G(DV|DM)$ are normally computed for series of values of *EDP*, *IM*, *DM*, and *DV*. For example, considering that *EDP* and *IM* have series of values designated *edp* and *im* respectively (see footnote (1)), then the term $G(EDP|IM)$ for a specified *EDP* level *edp* is computed for each *im* value of the *im*-series, and represents the probabilities of exceeding the specific *EDP* level *edp*, given different *im* values, i.e., $P(EDP>edp|IM=im)$. The computation of $G(EDP|IM)$ for another *EDP* level is the same. Figure 5.6 in Chapter 5 shows computed $G(EDP|IM)$ for selected *EDP* levels, where *EDP* is represented by interstorey drift (*IDR*), and *IM* is represented by the spectral acceleration at the first mode period ($Sa(T_1)$). This explanation for $G(EDP|IM)$ applies also to $G(DM|EDP)$ and $G(DV|DM)$.

(3) $\lambda(IM)$, $\lambda(EDP)$, $\lambda(DM)$, and $\lambda(DV)$ are typically computed for series of values of *IM*, *EDP*, *DM*, and *DV* respectively. In this thesis, $\lambda(IM)$ and $\lambda(EDP)$ are extensively used and are referred to as the seismic hazard curve and the demand hazard curve respectively. Figure 5.7 in Chapter 5 shows seismic hazard curves for *IM* represented by $Sa(T_1)$, and Figure 5.8 shows demand hazard curves for *EDP* represented by interstorey drift (*IDR*).

of the terms $\lambda(EDP)$, $\lambda(DM)$, and $\lambda(DV)$ is obtained by integrating the results from two consecutive analysis phases. For example, $\lambda(EDP)$ is obtained from $\lambda(IM)$ and $G(EDP|IM)$, $\lambda(DM)$ is obtained from $\lambda(EDP)$ and $G(DM|EDP)$, etc.

Based on the total probability theorem, the PBEE methodology is expressed mathematically as (Cornell and Krawinkler 2000, Moehle and Deierlein 2004):

$$\lambda(DV) = \iiint_{DM,EDP,IM} G(DV \mid DM) \cdot \left| dG(DM \mid EDP) \right| \cdot \left| dG(EDP \mid IM) \right| \cdot \left| d\lambda(IM) \right| \qquad (1.1)$$

The parameters included in Equation (1.1) are described above. Both Equation (1.1) and Fig. 1.1 show that PBEE is formulated in such a way that each of the four analysis phases is effectively independent. This allows the phases to be studied and executed independently, and then linked back together using the *intermediate variables*, *IM*, *EDP*, and *DM* (Fig. 1.1). An important assumption in the methodology is that the outcome from each phase depends only on the corresponding (i.e., preceding) intermediate variable. For example, the structural response is assumed to depend *only* upon the intensity measure (*IM*) of the ground motion. Further, it is assumed (for simplicity) that the intermediate variables are chosen such that conditional probability is not carried over from one analysis phase to the next (e.g., given knowledge of *EDP*, the damage analysis does not depend on *IM*).

It is seen from the foregoing discussion that the intermediate variables *IM*, *EDP*, and *DM* are essential in performance-based earthquake engineering. This thesis focuses on the intensity measure (*IM*). Since the intensity measure connects the ground motion hazard with the structural response (Fig. 1.1), the investigation of *IM* requires considerations of both the seismic hazard analysis and the response analysis. The final results obtained by linking these two analyses represent the annual frequencies of exceeding specified *EDP*

levels, designated $\lambda(EDP)$ in Fig. 1.1. The analysis method for the computation of $\lambda(EDP)$ is well established and is referred to as the *probabilistic seismic demand analysis*. To illustrate the need for the improvement of the intensity measure, the main features of the probabilistic seismic demand analysis, and a summary of the intensity measures that are currently available are presented hereafter.

1.2 Overview of probabilistic seismic demand analysis

As mentioned above, the goal of probabilistic seismic demand analysis (PSDA) is to compute the mean annual frequencies of exceeding given levels of structural response. This is done by integrating probabilistic structural response over all potential levels of ground motion intensity. Using the designations for the intensity measure (*IM*) and the engineering demand parameter (*EDP*), described above, the computation of the mean annual frequency of exceeding a given *EDP* level *edp* can be expressed mathematically as (Baker and Cornell 2005):

$$\lambda_{EDP}(edp) = \int_{im} P(EDP > edp \mid IM = im) \cdot \left| \frac{d\lambda_{IM}(im)}{d(im)} \right| \cdot d(im) \tag{1.2}$$

Note that this equation represents the last two terms of Equation (1.1), but written in extended forms (i.e., including the specific values of *EDP* and *IM* designated as *edp* and *im* respectively). In Equation (1.2), the term $P(EDP>edp|IM=im)$ is the conditional probability of exceeding a specified *EDP* level *edp*, given a level of $IM=im$, and the term $\lambda_{IM}(im)$ is the mean annual frequency of exceeding a given *IM* value *im*. Note that $\lambda_{IM}(im)$ is commonly called the *ground motion* or *seismic hazard curve*, and is computed using probabilistic

seismic hazard analysis (PSHA), as described in Adams and Halchuk (2003), and in Atkinson (2004).

As seen in Equation (1.2), the PSDA for a given building structure involves computations of: (i) the engineering demand parameter (*EDP*) (e.g., maximum interstorey drift, maximum ductility, maximum floor acceleration, etc.) for different *IM* levels *im*, (ii) the conditional probabilities $P(EDP>edp|IM=im)$ for each *IM* level, and (iii) the seismic hazard curve $\lambda_{IM}(im)$. The computation of the *EDP* is done by nonlinear time history analysis of the structural model subjected to a set of selected seismic motions scaled to a series of *IM* levels *im*. It can be recognised that for a selected *EDP*, the accuracy of $\lambda_{EDP}(edp)$ depends greatly on the intensity measure *IM*. Given this, substantial research has been conducted in recent years on the improvement of the intensity measures, as described below. The importance of the intensity measure in PSDA was also the reason for the development of improved intensity measures, presented in this thesis.

1.3 Review of existing intensity measures

Based on literature review, two types of intensity measures (*IM*s) are commonly used in PSDA. The first type is a scalar (i.e., single-parameter) intensity measure, and the second type is a vector-valued intensity measure that contains more than one parameter. In this section, the scalar *IM*s are discussed first, followed by the vector-valued *IM*s.

The peak ground acceleration (*PGA*) of a ground motion was a commonly used scalar *IM* in the past. More recently, 5% damped spectral acceleration at the first mode period of vibration ($Sa(T_1)$) has been the most used scalar *IM*. Spectral acceleration at T_1 has been found to be an effective *IM* (Shome et al. 1998), but among records with the same

value of $Sa(T_1)$, there is still significant variability in the level of structural response (Baker and Cornell 2005). This is because $Sa(T_1)$ does not include the effects of the period elongation during nonlinear response and the contribution of the higher modes to the structural response.

Another scalar *IM* is the *inelastic* spectral displacement, *Sdi* (Tothong and Luco 2007, Ruiz-Garcia and Miranda 2005). For a given frame of a building, *Sdi* is computed for an equivalent bilinear single-degree-of-freedom (SDOF) system that has the same elastic period as the *fundamental* period of the frame, and provides displacement responses to ground motions that are similar to the roof displacements of the frame. The same as $Sa(T_1)$, *Sdi* does not include the contributions of the higher modes to the response of the structure. However, *Sdi* is intended to take into account the effects of the elongation of the fundamental period during nonlinear response. This is because the period of the equivalent SDOF system elongates during the response, and therefore *Sdi* depends, to some extent, on the ground motion spectral characteristics for periods longer than the elastic period of the SDOF system.

The inelastic spectral displacement, *Sdi*, has a disadvantage compared to $Sa(T_1)$ since no 'standard' attenuation relation that can be widely used is available for *Sdi*. Note that attenuation relation is needed for *Sdi* (as an *IM*) in order to compute the seismic hazard curve, $\lambda_{IM}(im)$, that is used in PSDA. Tothong and Cornell (2007) developed an attenuation relation for *Sdi* using earthquake records from California and from the 1999 Chi-Chi, Taiwan earthquake. Since the number of the records from the Chi-Chi earthquake is about one third of the total number of records used in the analysis, the applicability of the attenuation relation for western Canada needs to be verified.

Luco and Cornell (2007) proposed a scalar *IM* called $IM_{1E\&2E}$, where $1E$ designates 1st mode-Elastic, and $2E$ designates 2nd mode-Elastic. As indicated by the subscript ($1E\&2E$), this *IM* takes into account the effects of the 1st and 2nd modes of vibration in the estimation of the *elastic* structural response. This is an improvement compared to $Sa(T_1)$. However, this *IM* is deficient in representing the inelastic response. To overcome this deficiency of $IM_{1E\&2E}$, Luco and Cornell (2007) developed an improved *IM* called $IM_{1I\&2E}$, where $1I$ stands for 1st mode-Inelastic. The rationale for this *IM* is to take into account the contributions of the 1st and 2nd modes to the structural response, and the effects of the nonlinear response (i.e., the period elongation) of the first mode. From a practical point of view, $IM_{1I\&2E}$ is an appropriate *IM* since it captures the characteristics of structural behaviour with the increase of the excitation level. It is assumed in the formulation of this *IM* that at higher intensity levels, the first mode might respond in the inelastic range, while the second mode is still in the elastic range. It has been found that $IM_{1I\&2E}$ is effective for predicting the maximum drift response (Tothong and Luco 2007). However, the use of both the $IM_{1E\&2E}$ and $IM_{1I\&2E}$ is presently limited to research because (as for *Sdi*) no attenuation relations for a wide use are available for these *IM*s. Tothong and Cornell (2007) developed an approximate attenuation relation for $IM_{1I\&2E}$ based on the attenuation relation that they developed for *Sdi*. Considering the records used and the approximations involved in the development of the attenuation relation for $IM_{1I\&2E}$, further research is needed in order to verify the applicability of this relation.

It should also be mentioned that the determination of $IM_{1E\&2E}$ and $IM_{1I\&2E}$ for a given structure is not straightforward (compared to $Sa(T_1)$, for example). These *IM*s include modal participation factors and modal damping ratios for the first two modes of the

structure. In addition to these parameters, $IM_{1I\&2E}$ requires the yield displacement of an equivalent bilinear SDOF system of the structure, as described above in the discussion of the *IM* represented by inelastic spectral displacement *Sdi*.

Cordova et al. (2000) investigated an *IM* that takes into account the elongation of the first mode period during nonlinear response. This *IM* includes the ground motion spectral accelerations corresponding to the elastic and the elongated periods of the first mode of the structure considered. Investigations for this *IM* have been conducted using three composite moment-resisting frames consisting of reinforced concrete columns and steel beams (two 6-storey frames, and one 12-storey frame) and a 6-storey steel frame. The elongated period has been estimated from dynamic analyses of the frames using two sets of eight records each. It has been found that this *IM* leads to smaller dispersion of the responses compared to that corresponding to $Sa(T_1)$. The use of this *IM* is not difficult and attenuation relation can be derived based on available attenuation relations for spectral accelerations. However, given the limited investigations (for composite and steel frames, and small number of records), further research is needed for this *IM*, specifically for reinforced concrete buildings and using larger sets of records.

In addition to the scalar *IM*s, research has been conducted in recent years on the development of vector-valued *IM*s. Baker and Cornell (2005) proposed a vector-valued *IM* that consists of two parameters, i.e., the spectral acceleration at the first mode period ($Sa(T_1)$), and 'epsilon' (ε). The parameter ε is defined by engineering seismologists studying ground motions as a measure of the difference between the spectral acceleration of a record and the spectral acceleration from an attenuation relation at the given period. It has been found that the parameter ε is an indicator of the shape of the spectrum, which is known to

affect the structural response. Given this, the vector-valued $IM=\{Sa(T_1), \varepsilon\}$ includes the spectral acceleration at the fundamental period and the spectral shape of the ground motion. It takes into account the first mode effects (through $Sa(T_1)$), as well as the effects of the higher modes and the period elongation (through ε). The effectiveness of this *IM* in predicting inelastic structural responses has been shown to be significantly greater than that of $Sa(T_1)$ alone. However, this *IM* has not been used in practical applications primarily because structural engineers are not familiar with ε, and this parameter is not readily available for recorded motions.

It is seen from this review that advanced *IM*s are available for PSDA, but they are currently not used in practical applications because of different limitations, as discussed above. The advantages and the disadvantages of $Sa(T_1)$ relative to the other *IM*s can also be seen from the review. The advantage of $Sa(T_1)$ as *IM* is that it is simple to use, it can be easily computed from recorded motions, and attenuation relations are available for spectral accelerations. The disadvantage of $Sa(T_1)$ is that it does not include the effects of the period elongation during nonlinear response and the contribution of the higher modes to the structural response. Given this, additional studies are needed in order to develop improved intensity measures that are effective for predicting inelastic structural responses and are easy to use.

1.4 Objective and scope

The objective of this study is to develop improved intensity measures for use in probabilistic seismic demand analysis for reinforced concrete frame buildings. Considering the limitations of the existing intensity measures, the study is focused on the development

of intensity measures that take into account the contributions of the first and the second vibration modes to the structural response, and the effects of the period elongation during nonlinear response. To achieve this objective, the following tasks were carried out in this study:

(a) Design of three reinforced concrete frames of building structures located in Vancouver.

(b) Development of nonlinear models of the frames for use in response analyses.

(c) Selection of earthquake records representative of expected earthquake ground motions in the Vancouver region. These were used as excitation motions in the response analysis of the frames.

(d) Investigation of the effects of elastic and inelastic spectral displacements as intensity measures.

(e) Investigation of the period elongation during nonlinear response of the frames.

(f) Probabilistic seismic demand analysis for the frames using spectral accelerations at the fundamental periods of the frames ($Sa(T_1)$) as intensity measures.

(g) Development of improved intensity measures that take into account the contributions of the first and the second vibration modes to the structural response, and the effects of the elongation of the first mode period during nonlinear response.

(h) Validation of the improved intensity measures.

(i) Development of attenuation relations for the improved intensity measures based on existing attenuation relations for spectral accelerations.

(j) Probabilistic seismic demand analysis of the frames using the improved intensity measures, and comparisons of the results with those obtained for $Sa(T_1)$ as intensity measure.

1.5 Organization

The material in this thesis is presented in 9 chapters. Chapters 2 and 3 provide background material (design of frames, and selection of earthquake records) that is used in the research work presented in Chapters 4 through 8. The main conclusions from the research are given in Chapter 9.

Chapter 2 describes the design of the frames used in this study. Three reinforced concrete frames (4-storey, 10-storey, and 16-storey high) of building structures assumed to be located in Vancouver were designed according to the 2005 edition of the National Building Code of Canada. The dimensions of the frame members and the reinforcement determined from the design are presented in Appendix A. The development of nonlinear models of the frames for use in response analyses is also described in this chapter.

Chapter 3 discusses the selection of earthquake ground motion records, representative for the Vancouver region. For the purpose of the selection of the records, the seismic hazard for Vancouver is reviewed and the selection criteria are presented. The characteristics of the selected records are presented in Appendix B.

Chapter 4 investigates the effects of using inelastic and elastic spectral displacements as intensity measures. This was motivated by findings reported in literature, which show that the use of inelastic spectral displacement (*Sdi*) as an intensity measure leads to a smaller dispersion of structural responses than that from the use of elastic spectral

displacement (*Sde*). An investigation of the response dispersions for *Sdi* and *Sde* as intensity measures is presented in this chapter. It was found that for the frames used in this study, the intensity measures *Sdi* and *Sde* result in similar response dispersions, and therefore, *Sdi* was not further considered in this thesis.

Chapter 5 describes the use of probabilistic seismic demand analysis (PSDA) for reinforced concrete frame buildings. The computation steps in the PSDA procedure are described in detail. PSDA is applied to the three frames considered in this thesis. Maximum interstorey drift is used as an engineering demand parameter, and the spectral acceleration at the first mode period ($Sa(T_1)$) is used as an intensity measure. The estimation of the ultimate (i.e., the collapse) drift level and the inclusion of collapses of the frames in PSDA are discussed in depth. The discussion of various issues regarding the use of PSDA and the results from the analyses presented in this chapter are essential for the research described in the following chapters.

The development of improved intensity measures, which is the main objective of this thesis, is described in **Chapter 6**. Two new intensity measures, designated S_{N1} and S_{N2}, are introduced in this chapter, and their effectiveness is investigated for the frames considered in this thesis. The intensity measure S_{N1} takes into account the elongation of the first mode period during nonlinear response and is proposed for use in PSDA for first mode dominated frames (i.e., short-period frames). The intensity measure S_{N2} includes the contributions of the first and the second modes to the structural response, and is proposed for long-period frames.

Chapter 7 investigates the suitability of the proposed intensity measures for use in probabilistic seismic demand analysis. This is done by comparing the major characteristics

of the proposed intensity measures with those of the 'traditional' intensity measure represented by $Sa(T_1)$. It is found that the proposed intensity measures are superior compared to $Sa(T_1)$.

The use of the proposed intensity measures in PSDA for the frames considered in this thesis is illustrated in **Chapter 8**. The PSDA procedure is, in general, the same as that described in Chapter 5 for intensity measure represented by $Sa(T_1)$, except that new attenuation relations are required for the proposed intensity measures. The development of the attenuation relations is described in detail in Chapter 8. This is done using the existing attenuation relations for spectral accelerations for western Canada.

Finally, **Chapter 9** summarises the main findings and conclusions of this thesis, and provides recommendations for future research.

Chapter 2

Design and Modelling of Frames

2.1 Description of buildings

Three reinforced concrete frame buildings were used in this study. Figure 2.1 shows the plan and the elevations of the buildings. The buildings are for office use and are located in Vancouver, which is in a high seismic hazard zone (NRCC 2005). The buildings are identical in plan but have different heights. As shown in the figure, the buildings include a 4-storey, a 10-storey, and a 16-storey building, which are considered representative of low-rise, medium-rise and high-rise buildings respectively.

The configurations of the buildings were selected in consultation with an experienced structural designer from Vancouver (DeVall 2007) to represent typical office buildings. The plan of each building is 27.0 m x 63.0 m (Fig. 2.1). The storey heights are 3.65 m. The lateral load resisting system consists of moment-resisting reinforced concrete frames in both the longitudinal and the transverse directions. There are four frames in the longitudinal direction (designated *Le* and *Li* in Fig. 2.1; *Le* – exterior frames, and *Li* – interior frames) and eight frames in the transverse direction (*Te* and *Ti*). The distance between both the longitudinal and the transverse frames is 9.0 m. Secondary beams between the longitudinal frames are used at the floor levels in order to reduce the depth of

the floor slabs. The secondary beams are supported by the beams of the transverse frames. The floor system consists of a one-way slab spanning in the transverse direction, supported by the beams of the longitudinal frames and the secondary beams. The slab is cast integrally with the beams.

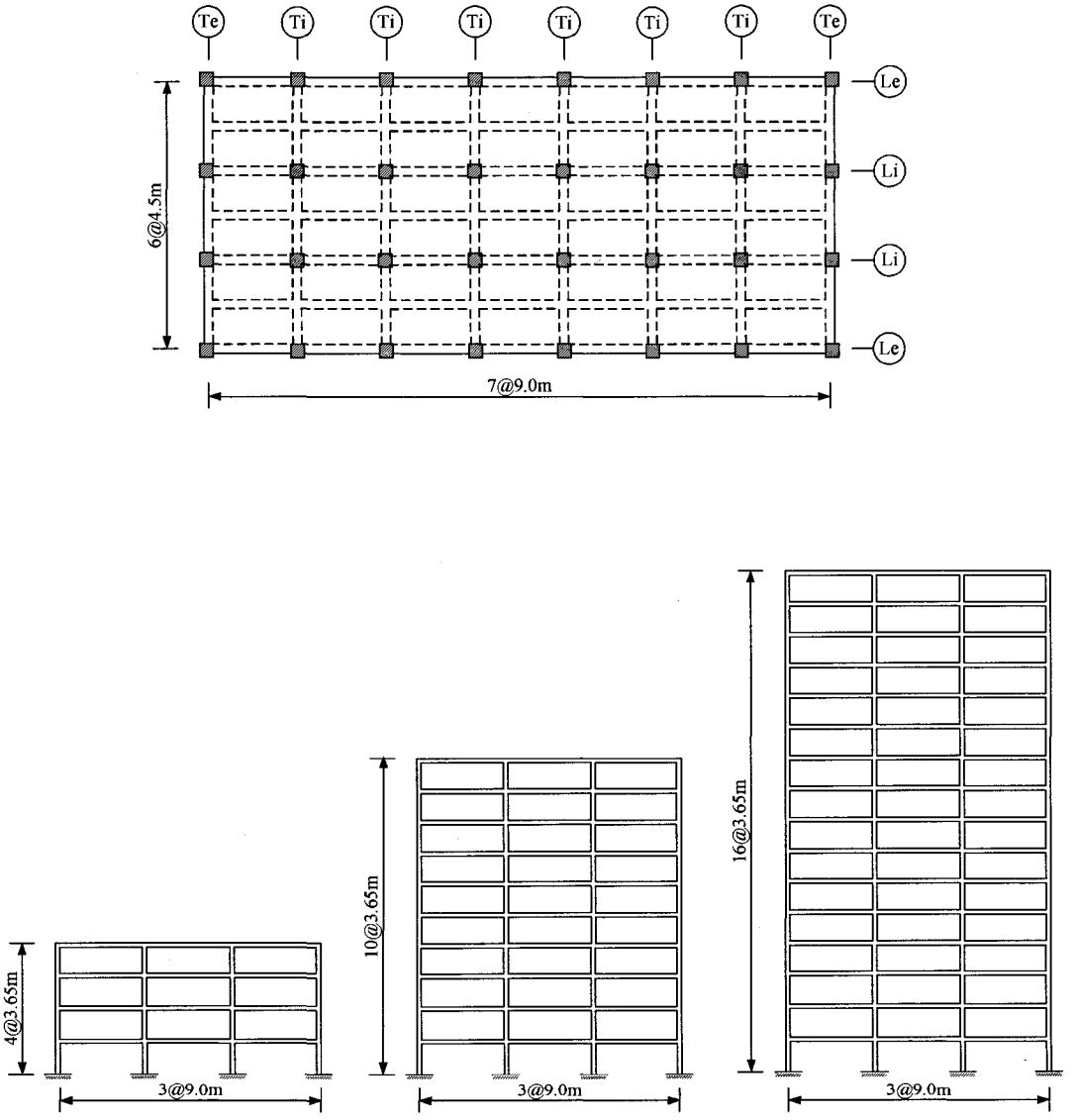

Figure 2.1 Plan of floors and elevations of transverse frames of the buildings.

2.2 Design of frames

In this study, only the interior transverse frames (*Ti*) of the buildings were considered. For ease of discussion, the 4-storey, the 10-storey, and the 16-storey frames are referred to as the 4S, the 10S, and the 16S frames respectively. The frames were designed as *ductile* reinforced concrete frames. The gravity and the seismic loads were determined according to the 2005 edition of the National Building Code of Canada (NBCC) (NRCC 2005). Each frame was treated as an individual structural unit with its own gravity and seismic loads. The gravity loads for the frames are shown in Appendix A, Table A.1.

The lateral loads due to earthquake motions were determined in accordance with NBCC using the equivalent static force procedure. 'Reference' ground conditions, represented by site class C in NBCC, were assumed at the building locations. The seismic base shear force for each frame, V, was computed according to the code formula:

$$V=S(T_a)\cdot M_V\cdot I_E\cdot W/(R_dR_o) \tag{2.1}$$

where, $S(T_a)$ is the design spectral acceleration at the fundamental lateral period of the frame, M_V is the higher mode effect factor, I_E is the importance factor, W is the total weight associated with the frame, R_d is the ductility-related force modification factor, and R_o is the overstrength-related force modification factor. The fundamental periods of the frames were computed according to the code formula for reinforced concrete moment-resisting frames, $T_a = 0.075h_n^{3/4}$, where h_n is the height of the frame above the base in meters. The design spectral accelerations, $S(T_a)$, were determined from the seismic design spectrum for Vancouver (Fig. 2.2). The values of the other parameters used in Equation (2.1), as specified in NBCC, are: $M_V = 1$, $I_E = 1$, $R_d = 4$, and $R_o = 1.7$. The weight W includes the self weight of the frame and the dead loads corresponding to the tributary areas of the frame of

9.0 m x 27.0 m (Fig. 2.1) at all floors. The design values for the fundamental periods of the frames, T_a, the spectral accelerations, $S(T_a)$, and the base shear coefficients, V/W, are listed in Table 2.1. The seismic forces for the frames are given in Appendix A.2.

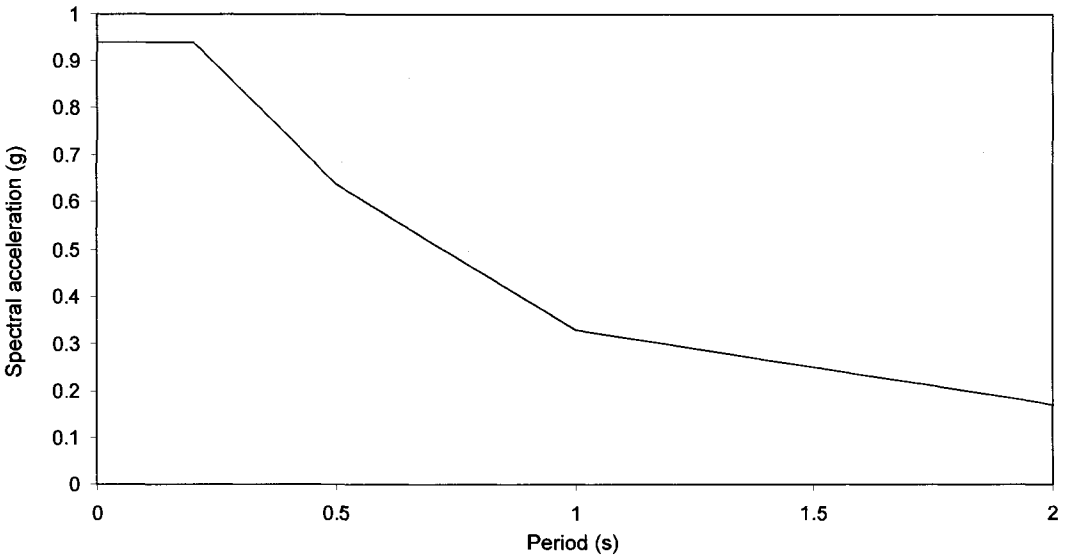

Figure 2.2 Seismic design spectrum for Vancouver, for site class C.

Table 2.1 Design parameters for the frames.

Design parameter	Frame		
	4S	10S	16S
Period, T_a (s)	0.56	1.11	1.58
$S(T_a)$ (g)	0.603	0.312	0.237
V/W	0.089	0.046	0.035
Max. drift (%)*	1.65	1.61	1.63

*Drifts are expressed as a percentage of the storey height.

The member forces for use in the design were determined by elastic analyses of the frames subjected to the combinations of gravity and seismic loads as specified in NBCC. The computer program SAP2000 (Computers and Structures, Inc. 2000) was used in the analysis. Rigid zones were used at the beam-column joints of the structural model. The

lengths of the rigid zones were selected to be the same as the depths of the beams and columns. The effects of cracking were included by using reduced member stiffnesses, i.e., 40% and 70% of the gross *EI* for beams and column respectively, where *E* is the modulus of elasticity of reinforced concrete (E = 27 000 MPa in this study), and *I* is the moment of inertia of the member section. The gross *EI* for the beams includes the slab with flange width as specified in the Canadian standard CSA A23.3-04 (CSA 2004). Load-deflection (P-Δ) effects were taken into account in the analysis. As specified in NBCC, maximum inelastic interstorey drifts were calculated as $R_d R_o$ times the drift obtained from the elastic analyses. The maximum calculated drifts for the frames are given in Table 2.1. It can be seen that the calculated drifts are smaller than the design drift of 2.5% allowed by NBCC.

The member forces obtained from the elastic analyses were used in the design of the frames. The design was conducted in accordance with the requirements for ductile moment-resisting frames specified in CSA standard A23.3-04 (CSA 2004). These requirements are based on the capacity design method (Paulay and Priestley 1992). The capacity method intends to provide a strong column - weak beam frame structure in which the inelastic deformations due to strong seismic motions occur in beams rather than in columns. Compressive strength of concrete f_c' = 30 MPa, and yield strength of reinforcement f_y = 400 MPa were used in the design. The dimensions and the reinforcement of the columns and the beams of the 4S, the 10S, and the 16S frames are shown in Appendix A, Tables A.3.1, A.3.2, and A.3.3 respectively. The thickness of the floor slab is 15 cm at all floors.

2.3 Modelling of frames for dynamic analysis

In this study, the computer program RUAUMOKO (Carr 2004) was used for the inelastic dynamic analysis of the frames subjected to seismic motions. It is a two-dimensional (2-D) analysis program, which provides a wide range of modelling options. The program includes different types of elements for modelling structural members and a number of hysteretic behaviour models.

For each frame, a 2-D inelastic model was developed for use in RUAUMOKO. Sensitivity analyses were performed to investigate the effects of various modelling parameters on the response of the 10S frame model. The modelling parameters presented hereafter are based on the results from the sensitivity analyses, and were used throughout this study.

The beams and columns were modelled by a 'beam-column' element, which is represented by a single component flexural spring. Inelastic deformations are assumed to occur at the ends of the element where plastic hinges can be formed. The effects of axial deformations in beams are neglected. Axial deformations are considered for columns, but no interaction between bending moment and axial load is taken into account.

For the purpose of the frame models, moment-curvature relationships for the end sections of each beam and column were determined using fibre analyses of the cross sections. The concrete stress-strain relationship included the effect of confinement based on the model proposed by Mander et al. (1988). Nominal values for material strengths (i.e., concrete and reinforcement resisting factors $\Phi_c = \Phi_s = 1$) were used in the fibre analysis. The axial forces used in the fibre analysis of the columns included the forces resulting from dead load and a half live load. For illustration, Figure 2.3 shows the moment-curvature

relationships for the first storey exterior column and the first floor beam of the 10S frame. The shapes of the relationships shown in the figure are representative of those of the columns and beams of the frames considered in this study. As can be seen in the figure, the

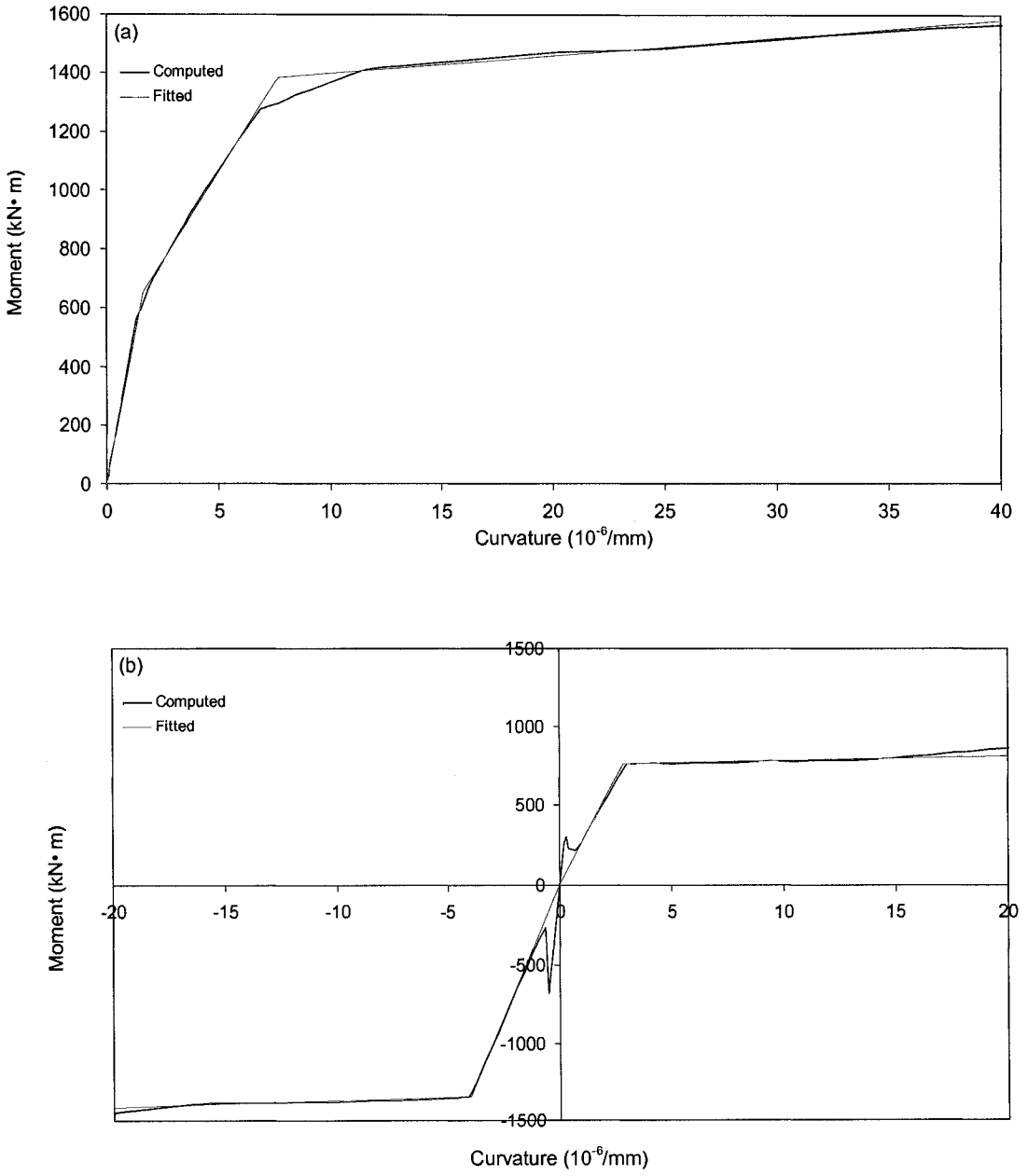

Figure 2.3 Moment-curvature relationships for a column and beam of the 10S frame: (a) exterior column at first storey, and (b) beam at first floor.

shapes of the computed moment-curvature relationships for columns and beams are quite different. This is because of the effects of the axial forces used in the fibre analysis of the columns, and the differences in the geometry and the reinforcement of the columns and the beams. While the cross sections and the reinforcement of the columns are symmetrical, the beams were treated as T-sections with different top and bottom reinforcement as obtained from the design.

The computed moment-curvature relationships for the columns were idealised by three linear segments, with the first segment corresponding to the uncracked stiffness, the second segment to the region between cracking and yielding, and the third segment to the post-yielding range (Fig. 2.3(a)). The beam moment-curvature relationships were approximated by two segments representing the pre- and post-yielding ranges (Fig. 2.3(b)). Based on the shapes of the moment-curvature relationships, a trilinear hysteretic model was selected for the columns, and a bilinear (modified Takeda) model was selected for the beams from the models available in RUAUMOKO, as shown in Fig. 2.4. Both models take into account the degradation of the stiffness during nonlinear response. The parameters of the trilinear model for each column were determined from the idealised moment-curvature relationships. Values for the coefficients α and β of 0.5 and 0.6 respectively were used for the bilinear model (Carr 2004).

Rigid zones were used at the beam-column joints of the structural models. The lengths of the rigid zones were selected to be the same as the depths of the beams and columns.

Gravity loads acting on the beams were applied as fixed-end moments and shear forces, as required by RUAUMOKO. These included dead loads and half of live loads.

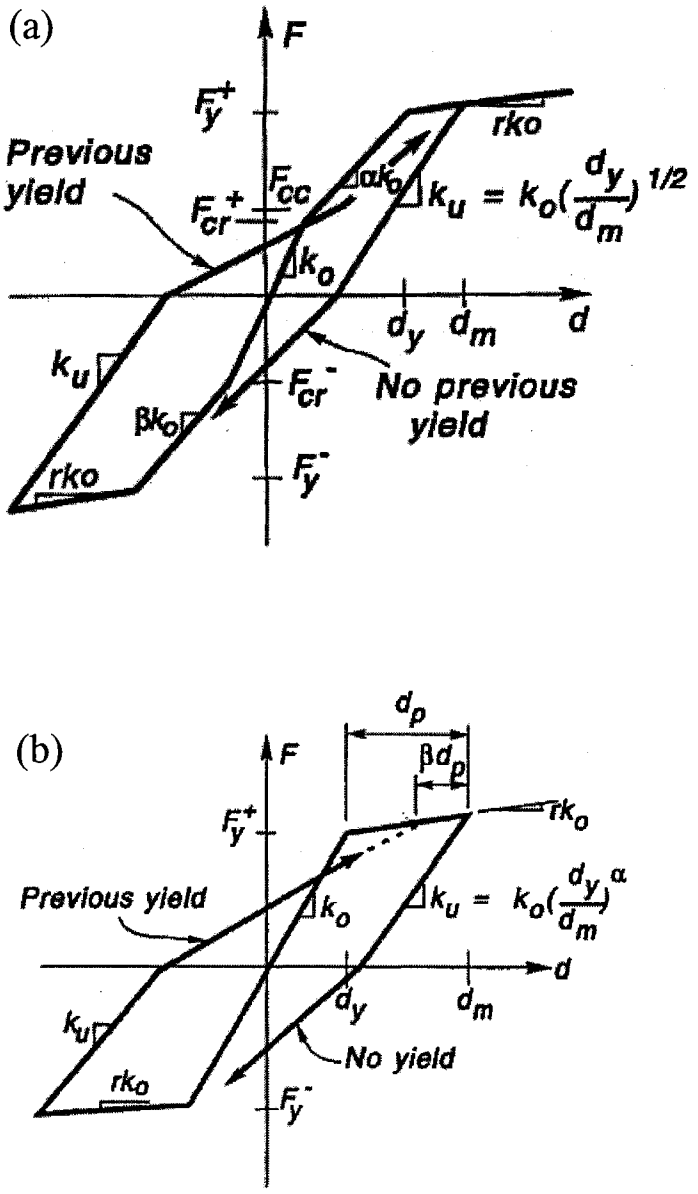

Figure 2.4 Hysteretic models used in this study: (a) for columns, and (b) for beams. (Adopted from Carr 2004).

Axial forces due to own weight of columns were applied at the ends of the column members. Lumped masses corresponding to dead loads were specified at the nodes of the structural models.

RUAUMOKO provides several damping models for nonlinear analysis. In this study, Rayleigh damping of 5% of critical was assigned to the first and the second vibration modes of the models. The damping was specified to be proportional to the initial stiffness of the models.

The natural periods of the first three vibration modes of the models, obtained by RUAUMOKO, are given in Table 2.2. The first mode periods are significantly larger than those used in the design (Table 2.1). This was expected since it is known that the code formula provides relatively small period values that lead to conservative seismic design forces.

Table 2.2 Natural periods of the frame models (in seconds).

Frame model	Mode No.		
	1	2	3
4S	0.94	0.29	0.14
10S	1.96	0.70	0.40
16S	2.75	1.02	0.60

Chapter 3

Selection of Earthquake Records

3.1 Overview of the seismic hazard for Vancouver

It is known that western British Columbia, where Vancouver is located, is characterized by highest seismic hazard in Canada (Adams and Halchuk 2003, Adams and Atkinson 2003). Specifically, many strong earthquakes have occurred in the past in the region within a radius of about 200 km around Vancouver, the strongest of which was the 1946 earthquake with a magnitude of 7.3 (Anglin et al. 1990). The seismic hazard for Vancouver comes from crustal earthquakes, deep subcrustal earthquakes, and from large subduction earthquakes likely to occur along the Cascadia subduction zone located west of Vancouver Island. Potential locations of the hypocenters of subduction earthquakes are estimated to be at a distance of about 140 km from Vancouver (Adams and Halchuk 2003). Present knowledge indicates that a great earthquake on the Cascadia subduction zone could have a magnitude larger than 8. The return period of such large Cascadia earthquakes is estimated to be about 600 years.

The Geological Survey of Canada has conducted seismic hazard analyses for the needs of the National Building Code of Canada (Adams and Halchuk 2003). The seismic hazard is represented by elastic acceleration spectra with the same probability of

exceedance of 2% in 50 years for periods between 0.1 s and 2.0 s. These spectra are called the uniform hazard spectra. The uniform hazard spectra show that the seismic hazard for Vancouver resulting from crustal and subcrustal earthquakes is higher than that from subduction earthquakes. Tremblay (1998) investigated the spectral characteristics of Cascadia earthquake motions and stated that "structures designed for crustal earthquakes in Vancouver should be able to safely sustain Cascadia subduction earthquakes". Tremblay and Atkinson (2001) also concluded that "structures located in Vancouver and designed for crustal earthquakes at the 2% in 50 year probability level would survive M 8.5 Cascadia earthquakes with limited damage".

In this thesis, ground motions from crustal earthquakes only were used in the analysis. Similar studies can be conducted for other types of earthquakes (e.g., deep subcrustal earthquakes, subduction earthquakes, etc.) following the approach presented in this thesis.

3.2 Predominant magnitude-distance scenarios for Vancouver

For the purpose of the selection of records for use in the analyses, it is important to know the magnitudes (M) and the distances (R) of the earthquakes that have the largest contributions to the seismic hazard. These earthquakes are referred to as the scenario earthquakes. There are two references that provide M-R scenarios for Vancouver. Halchuk et al. (2007) disaggregate the seismic hazard by computing the contributions to the hazard of selected magnitude-distance intervals (i.e., bins) of ΔM=0.25 and ΔR=20 km. The results from the disaggregation analysis for a given site provide a discrete joint distribution of the contributions to the hazard of earthquakes with different magnitudes and distances (hazard distribution vs. magnitude and distance). This distribution enables one to estimate the

predominant *M-R* pair for the site considered. Using this approach, Halchuk et al. (2007) have determined the predominant *M-R* values for Vancouver for spectral acceleration hazard at different periods. The *M-R* values corresponding to 2% in 50 years probability of exceedance are M=6.4 and R=54 km for period of 0.2 s, and M=6.8 and R=49 km for period of 2.0 s. Note that these M and R values are the *mean* (or weighted average) values for each period. The periods of 0.2 s and 2.0 s are used as representative of short- and long-period ground motions respectively.

Tremblay and Atkinson (2001) also provide predominant M and R values for Vancouver for a probability of exceedance of 2% in 50 years. They suggest using an event of M=6.5 at R=30 km to represent the short-period hazard, and an event of M=7.2 at R=70 km to represent the long-period hazard. As stated in the study, their values are based on hazard disaggregation analyses conducted by the U.S. Geological Survey for Northwestern Washington State and on experience from site-specific studies in the Vancouver region.

The differences in the M and R values of these two studies are obviously due to the differences in the methods used for determining predominant magnitudes and distances. While the method used in Halchuk et al. (2007) is based on rigorous disaggregation of the seismic hazard for Vancouver, the method in Tremblay and Atkinson (2001) involves certain approximations in the estimation of the M and R values as discussed above.

3.3 Selection of records

Ground motion records from earthquakes in the Vancouver region would be the most suitable for the analysis of the frames considered in this study. Since such records are not available, recorded ground motions from earthquakes in California were selected. It is

believed that the characteristics of crustal earthquakes that might occur in the Vancouver region are similar to those of California earthquakes (Atkinson 2006). In general, no distinction is made in literature between the characteristics of crustal earthquakes in different regions in western North America. For example, the attenuation relations for crustal earthquakes used for western Canada (Adams and Halchuk 2003) have been developed for western North America (Boore et al. 1997).

Earthquake records were selected from the strong motion database of the Pacific Earthquake Engineering Research (PEER) Center. The following searching criteria were specified in the selection of the records:

- Moment magnitude range: M=5.5 to M=8.0.
- Distance range: R=10 km to R=110 km.
- Records from earthquakes in California.
- Recording stations at sites with shear wave velocity between 360 m/s and 750 m/s. Note that this shear velocity range corresponds to the NBCC site class C, which was assumed in the design of the frames used in this study.
- Records from instruments on free field, in shelters, and in basements of buildings.
- Peak ground acceleration (PGA) range: PGA=0.03 g to 2.08 g (note that 2.08 g is the maximum PGA value in the PEER database).

The specified magnitude and distance ranges cover the predominant magnitude-distance scenarios for Vancouver, as discussed in Section 3.2.

In total 84 earthquake records were obtained from the search. Three sets were selected from these records, as described below. Note that each record consists of three components, i.e., two perpendicular horizontal components, and a vertical component. In this study, only the horizontal components of the records were used. For convenience, the term 'record' used further in this study refers to a single horizontal component.

The three sets selected for this study are referred to as the 80R set, the 40R set, and the 20R set, where 80, 40, and 20 indicate the number of recorded components contained in the sets. Attention was paid such that records from as large as possible number of earthquakes were included in the sets. Each of these sets was used for a specific research objective, as seen in the next chapters of this thesis. The main characteristics of the sets are as follows:

80R set: This set contains 80 horizontal components of records at 40 locations (i.e., both horizontal components of 40 records). The characteristics of the earthquakes and the records are given in Appendix B, Table B.1. The two horizontal components of each record are designated in the table as Comp. 1 and Comp. 2. The magnitude-distance distribution and the *PGA*-distance distribution of the records are shown in Fig. 3.1(a) and Fig. 3.2(a) respectively. The records of this set were obtained from 22 earthquakes with magnitudes ranging from 5.8 to 7.3. The records were taken at distances ranging from 10 km to 109 km. The *PGA* values of the records are between 0.04 g and 0.36 g.

40R set: It consists of the larger components of the records in the 80R set. The records are listed in Appendix B, Table B.2. The magnitude-distance distribution of the records is the same as that for the 80R set (Fig. 3.1(a)). The *PGA*-distance distribution is

shown in Fig. 3.2(b). The *PGA* values of the records in this set range between 0.05 g and 0.36 g.

20R set: The records of this set were randomly selected from the 80R set. The characteristics of the records are given in Appendix B, Table B.3. Figure 3.1(b) shows the magnitude-distance distribution, and Fig. 3.2(c) shows the PGA-distance distribution of the records. The magnitudes of the earthquakes are between 6.0 and 7.4, and the distances of the records are between 11.3 km and 90.6 km. The *PGA* values range from 0.10 g to 0.28 g.

Figure 3.3 shows the 5% damped acceleration response spectra of the selected records. The mean and the mean plus one standard deviation (i.e., 84% level) spectra are also included. For comparison, the design spectrum for Vancouver is superimposed in the figure. It can be seen that the design spectrum covers most of the spectra. The exceeding of the design spectrum by a few spectra of the records is not a surprise considering the probability level of 2% in 50 years used in defining the design spectrum.

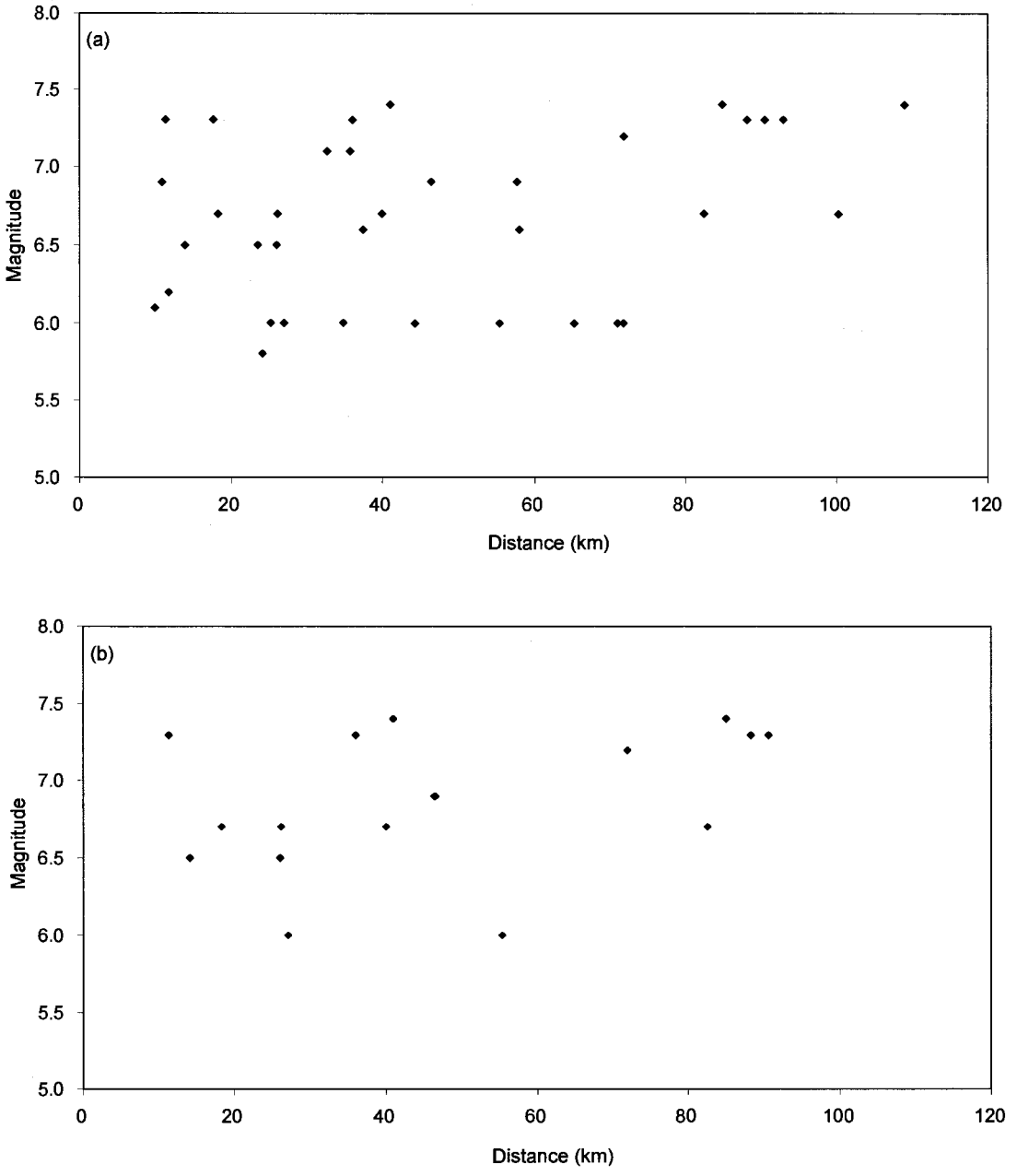

Figure 3.1 Magnitude-distance distributions for the selected records: (a) 80R and 40R sets, and (b) 20R set.

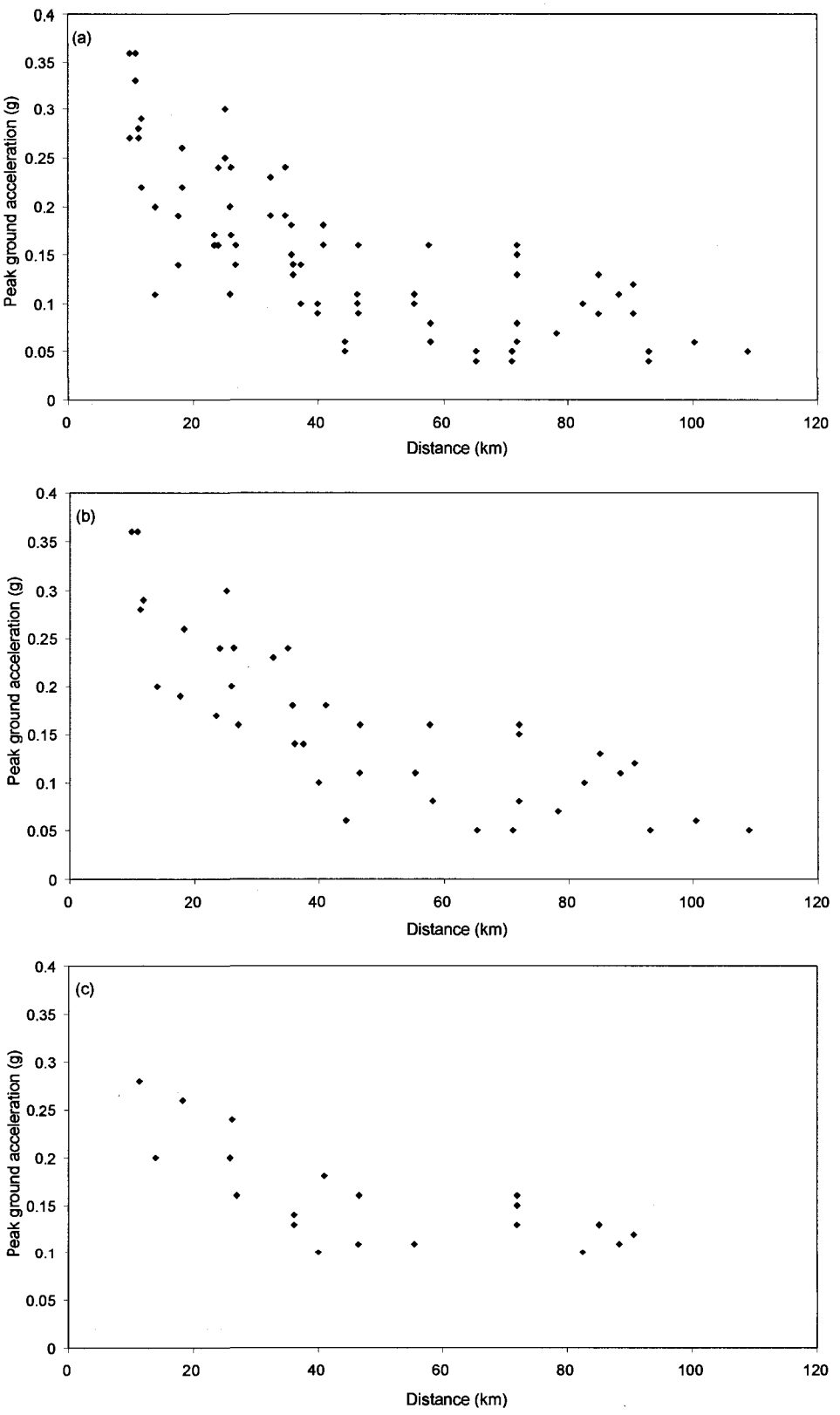

Figure 3.2 Peak ground acceleration-distance distributions for the selected records: (a) 80R set, (b) 40R set, and (c) 20R set.

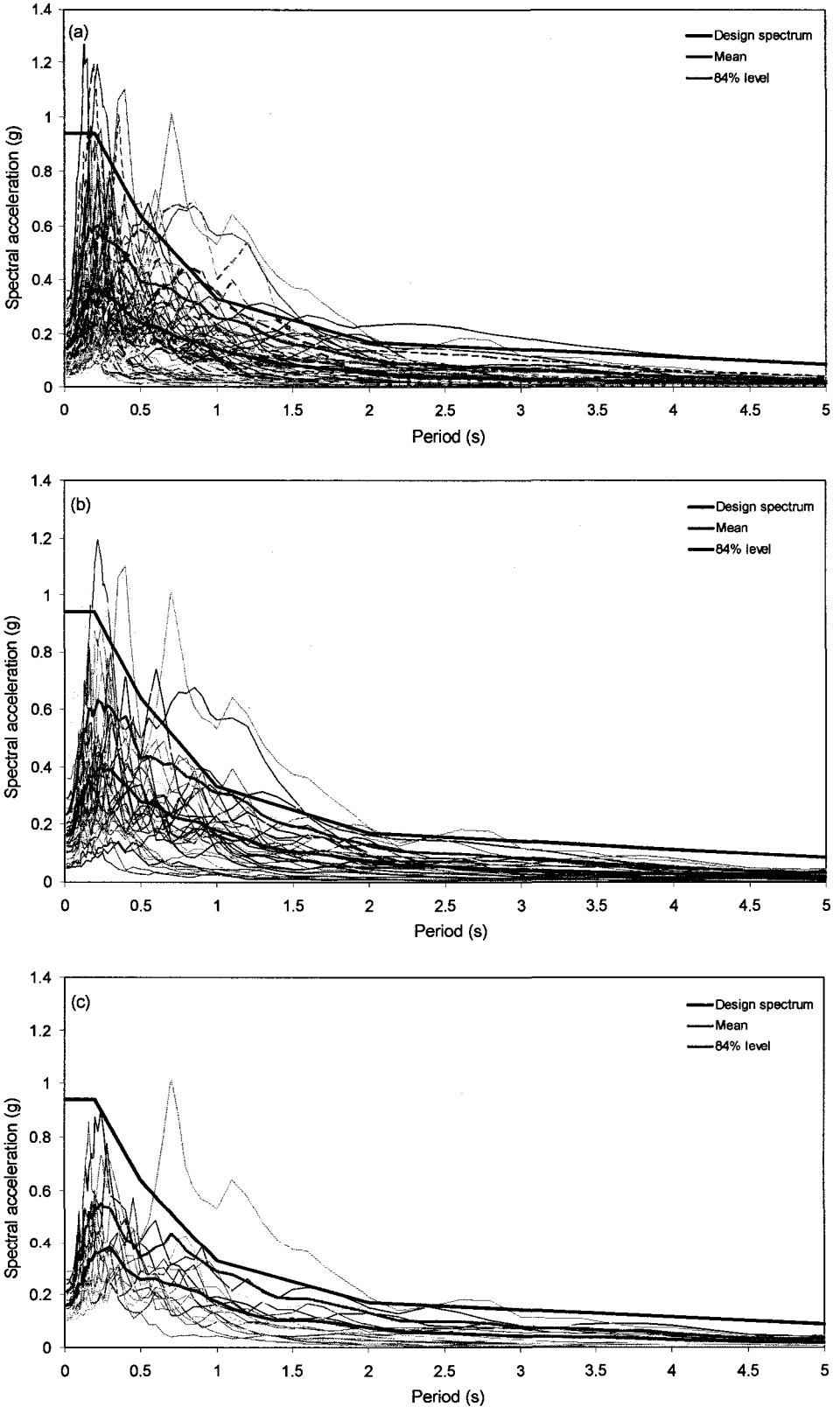

Figure 3.3 Acceleration response spectra for the selected records: (a) 80R set, (b) 40R set, and (c) 20R set; 5% damping.

Chapter 4

Inelastic Versus Elastic Displacement-Based Intensity Measures

4.1 Introduction

There are several studies in which the inelastic spectral displacement at the fundamental structural period, T_1 (i.e., $Sdi(T_1)$), rather than the elastic spectral displacement ($Sde(T_1)$), has been used as an intensity measure (*IM*) (e.g., Ruiz-Garcia and Miranda 2005, Tothong and Luco 2007). For simplicity, $Sdi(T_1)$ and $Sde(T_1)$ are referred to in this chapter as *Sdi* and *Sde* respectively. Note that the elastic spectral displacement (*Sde*) for a given period, T_1, is linearly proportional to the elastic spectral acceleration (*Sa*) for that period (i.e., $Sde=(T_1/2\pi)^2 \cdot Sa$), and therefore, *Sde* and *Sa* represent the same *IM*. For convenience, however, *Sde* rather than *Sa* is used in this chapter.

Ruiz-Garcia and Miranda (2005), and Tothong and Luco (2007) investigated the nonlinear responses of frame buildings subjected to sets of earthquake motions scaled to *Sde* and *Sdi*. They reported that the use of *Sdi* as *IM* leads to smaller dispersions of the interstorey drifts than those resulting from the use of *Sde*, and concluded that *Sdi* has advantages relative to *Sde* for the estimation of the seismic demands for frame buildings.

As a part of this thesis, the effects of the use of *Sde* and *Sdi* as *IM*s were investigated on the 4S, the 10S, and the 16S frames. The objective of the investigation was to compare the dispersions of the interstorey drifts resulting from these *IM*s, and to assess the potential for the use of *Sdi* as *IM*. For the purpose of this investigation, equivalent inelastic SDOF systems were developed for the frames. These were needed to determine the scaling factors for the records for scaling to *Sdi*. The characteristics of the equivalent SDOF systems are briefly described hereafter.

4.2 Equivalent inelastic SDOF systems for the frames

The method proposed by Fajfar (2000) for the development of an equivalent *inelastic* SDOF system for a multi-degree-of-freedom (MDOF) system was used in this study. The SDOF system was assumed to follow elastic-perfectly plastic force-displacement relationship. The method is developed to simplify the computation of the nonlinear response of MDOF structures. Namely, the top (i.e., roof) displacement response of a building structure subjected to a given ground motion can be determined approximately from the displacement response of the idealised SDOF system under the same motion. Detailed derivations of the parameters of the equivalent SDOF system are presented in Fajfar (2000), and only the final expressions are given in this section.

For each frame, the parameters of the inelastic SDOF system (designated with *) were determined as follows:

- Equivalent mass $m^* = \Sigma m_i \Phi_i$, where m_i is the mass of the frame at floor level i, and Φ_i is the value of the first mode shape Φ at level i; note that Φ is normalized to have a value of 1 at the roof.

- Yield displacement $D_y^*=D_y^t/\Gamma$, and yield strength $F_y^*=V_y/\Gamma$, where D_y^t and V_y are the top displacement and the base shear respectively, corresponding to the yield point of the idealised pushover curve for the frame (Fig. 4.1), and $\Gamma=m^*/\Sigma m_i\Phi_i^2$. The pushover curve for each frame was determined using the program RUAUMOKO; the distribution of the lateral forces along the height of the frame was the same as that of the design seismic forces (Chapter 2 and Appendix A.2).
- The elastic period of the equivalent SDOF system is $T^*=2\pi\sqrt{m^* D_y^*/F_y^*}$. Note that this is very close to the fundamental period (T_1) of the frame considered, and can be assumed that $T^*=T_1$; the proximity comes from the idealisation of the pushover curves (Fig. 4.1).

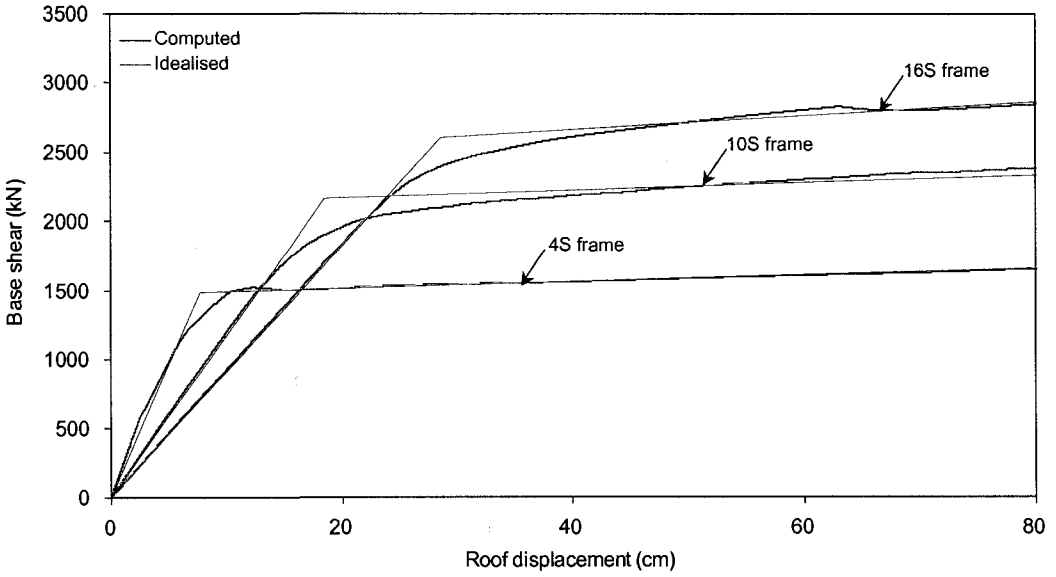

Figure 4.1 Pushover curves for the frames.

Having determined the parameters of the SDOF system for a given frame, the maximum value of the top (roof) displacement (D^t_{max}) of the frame subjected to a specified ground motion can be expressed as (Fajfar 2000):

$$D^{t}_{max} = \Gamma \cdot Sd \tag{4.1}$$

where Γ is as defined above, and *Sd* represents spectral displacement which can be elastic (if the maximum displacement response of the SDOF system is smaller than D_y^*), or inelastic (if the SDOF system response is larger than D_y^*).

4.3 Analysis and results

The frames were analysed using the records of the 40R set as excitation motions. For the purpose of comparisons, analyses were conducted by scaling the records to elastic spectral displacements *Sde*, and to inelastic spectral displacements *Sdi*.

Scaling to *Sde* is straightforward, and therefore the discussion that follows is primarily related to the scaling to *Sdi*. Scaling to *Sdi* requires considerations of the equivalent inelastic SDOF system of the frame that is analysed, and therefore it is useful to discuss briefly the expected response of the frame relative to the characteristics of the equivalent SDOF system. Theoretically, based on Equation (4.1) and the expressions used in the derivation of the equivalent SDOF system for a given frame, one might expect elastic responses of the frame for records scaled to $Sd \leq D_y^*$ and inelastic responses for records scaled to $Sd > D_y^*$ (as mentioned above, *Sd* denotes spectral displacement, in general, which can be elastic or inelastic). However, considering the assumptions and the approximations involved in the derivation of the equivalent SDOF system, the frame could experience *inelastic* responses for scaling to *Sd* levels even well below D_y^*. For simplicity, however, and following the practice in other studies (e.g., Ruiz-Garcia and Miranda 2005), the scaling in this chapter was based on *Sdi* for scaling levels $Sd > D_y^*$.

In this chapter, $Sd = D_y^*$ is called the *reference* spectral displacement, and is designated as Sd_{ref}. It represents (approximately) the highest scaling level associated with elastic responses of the frames. In other words, records scaled to Sd_{ref} are expected to produce responses corresponding to an average 'global' displacement ductility of approximately 1.0, where the 'global' ductility is represented by the ratio of the maximum roof displacement (D^t_{max}) obtained from nonlinear dynamic analysis of the frame, to the 'global' yield displacement (D_y^t) from the pushover curve (Fig. 4.1) (i.e., D^t_{max}/ D_y^t). The values for Sd_{ref} for the 4S, the 10S, and the 16S frames are listed in Table 4.1. The table also includes the corresponding reference spectral accelerations (Sa_{ref}) for the frames, which are used in the following chapters of this thesis. Note that Sa_{ref} is computed as $Sa_{ref}=(2\pi/ T_1)^2 \cdot Sd_{ref}$.

Table 4.1 Reference values for spectral displacement (Sd_{ref}) and spectral acceleration (Sa_{ref}) for the 4S, the 10S, and the 16S frames.

Frame	Reference spect. displac. Sd_{ref} (cm)	Reference spect. accel. Sa_{ref} (g)
4S (T_1=0.94s)	4.0	0.18
10S (T_1=1.96s)	13.4	0.14
16S (T_1=2.75s)	20.5	0.11

Five intensity levels were used in the analysis, i.e., $Sd=Sd_{ref}$ to $Sd=5Sd_{ref}$, which were intended to produce 'global' ductilities of approximately 1.0 to 5.0 respectively. For each intensity level, the records were scaled to both the *Sde* and *Sdi*. While the scaling to *Sde* is routine, the scaling to *Sdi* required a number of nonlinear time history analyses of the equivalent SDOF systems of the frames in order to determine the scaling factors for each of the intensity levels considered. Namely, for a given frame and intensity level, the scaling factor for each record was determined by incrementally increasing the intensity of the

record (i.e., by increasing the scaling factor) and conducting time history analyses on the equivalent SDOF system of the frame until the computed inelastic displacement of the SDOF system matched the prescribed intensity level.

Finally, time history analyses were conducted on the frames using the scaled records as excitation motions. Maximum interstorey drifts (*IDR*) over the height of the frames were determined for each excitation. Figures 4.2, 4.3, and 4.4 show the maximum interstorey drifts for the 4S, the 10S, and the 16S frame respectively. The figures contain the results from the scaling to *Sde* (graphs (a) in the figures), and those from the scaling to *Sdi* (graphs (b)). The 50% (i.e., the median), the 84%, and the 16% levels of the results are also shown in the figures.

The main objective of this investigation is to compare the dispersions of the responses for scaling to *Sde* and *Sdi*. The dispersion is an important indicator for the effectiveness of a given *IM*, i.e., smaller dispersion is always preferred (Tothong and Cornell 2007). The dispersions of the interstorey drifts of the frames can be assessed by considering the bands between the 84% and the 16% levels of the results in Figs. 4.2, 4.3, and 4.4. It is seen in the figures that the dispersions resulting from scaling to *Sde* and *Sdi* are quite close. This indicates that considering the dispersions, the use of *Sdi* as *IM* does not have advantage compared to the use of *Sde*, for the frames used in this study. However, this should not be generalised and additional research is needed regarding the use of *Sdi* as *IM*.

4.4 Summary

An investigation was conducted to determine the effects of the use of elastic and inelastic spectral displacements (*Sde* and *Sdi* respectively) as intensity measures. Time

history analyses were performed on the three frames using the records of the 40R set scaled to *Sde* and *Sdi*. The dispersions of the interstorey drifts for scaling to *Sde* and *Sdi* were compared to see which of these two parameters is more appropriate for scaling. The dispersion is an important indicator for the effectiveness of a given intensity measure, i.e., smaller dispersion is always preferred. It was found that the dispersions resulting from scaling to *Sde* and *Sdi* were quite close. Based on this it can be concluded that considering the dispersions, the use of *Sdi* as an intensity measure does not have an advantage when compared to the use of *Sde*, for the frames used in this thesis.

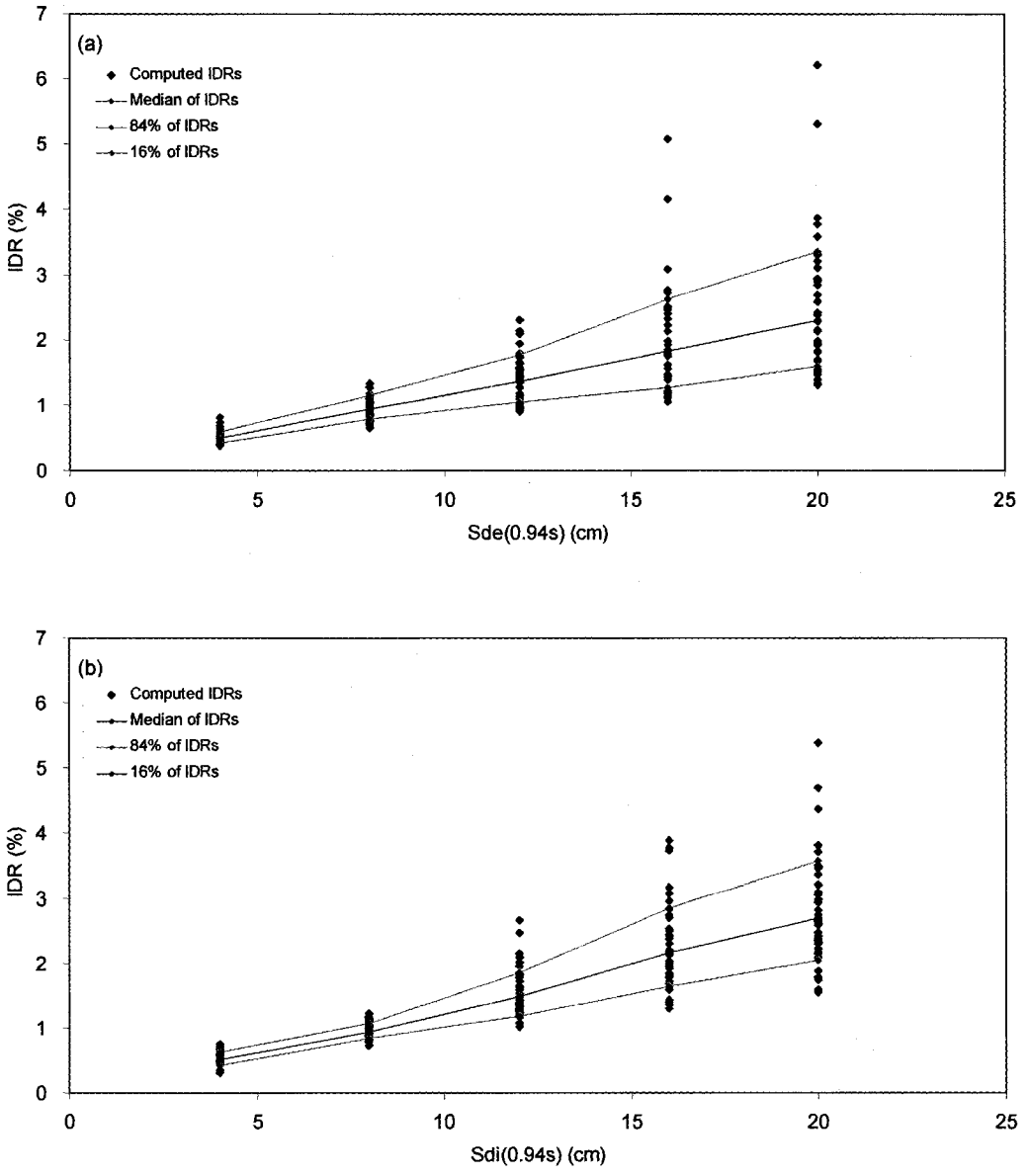

Figure 4.2 Variation of interstorey drifts for the 4S frame for intensity measures represented by elastic and inelastic spectral displacements, i.e., *Sde* and *Sdi* respectively: (a) *Sde*, and (b) *Sdi*.

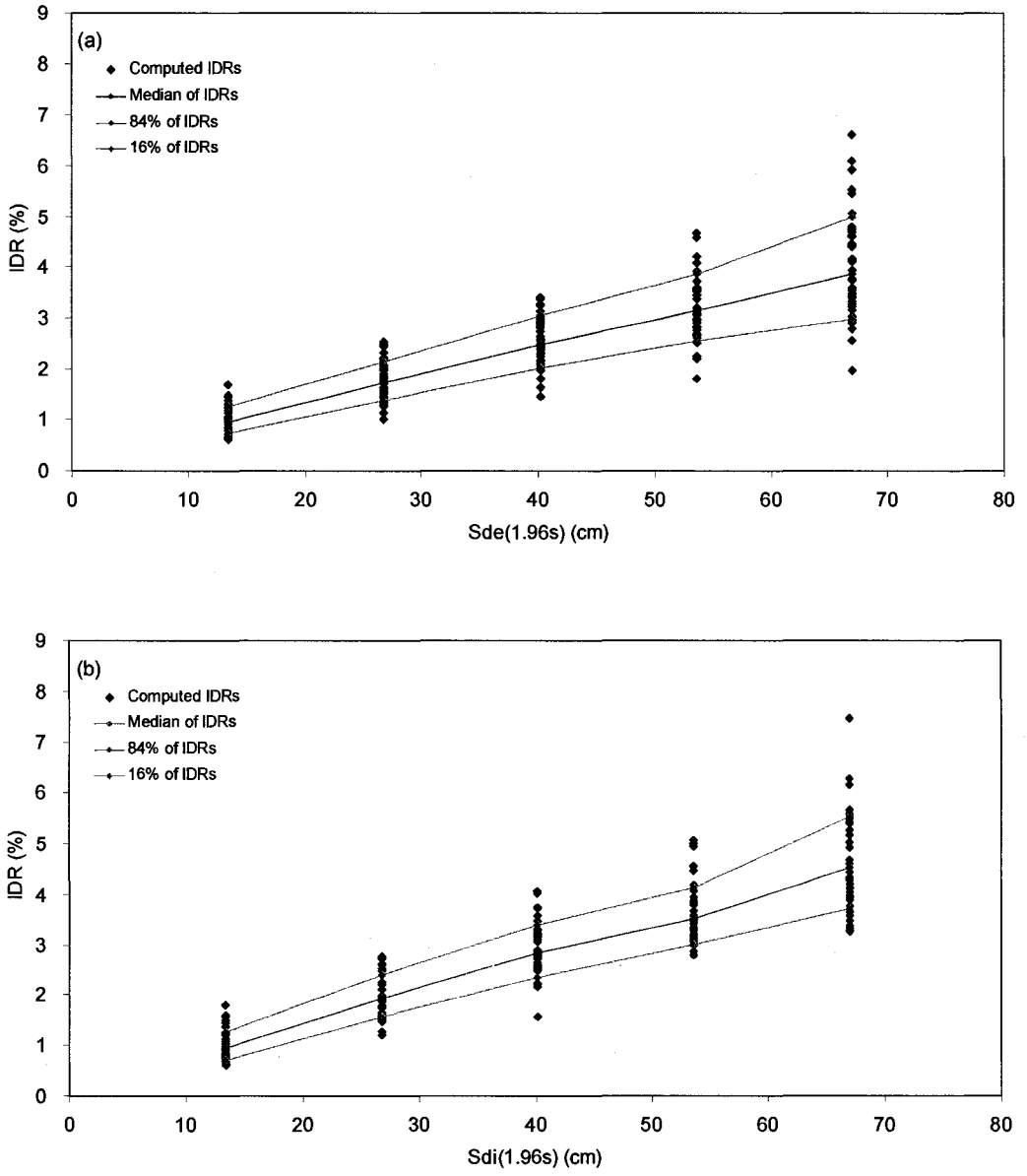

Figure 4.3 Variation of interstorey drifts for the 10S frame for intensity measures represented by elastic and inelastic spectral displacements , i.e., *Sde* and *Sdi* respectively: (a) *Sde*, and (b) *Sdi*.

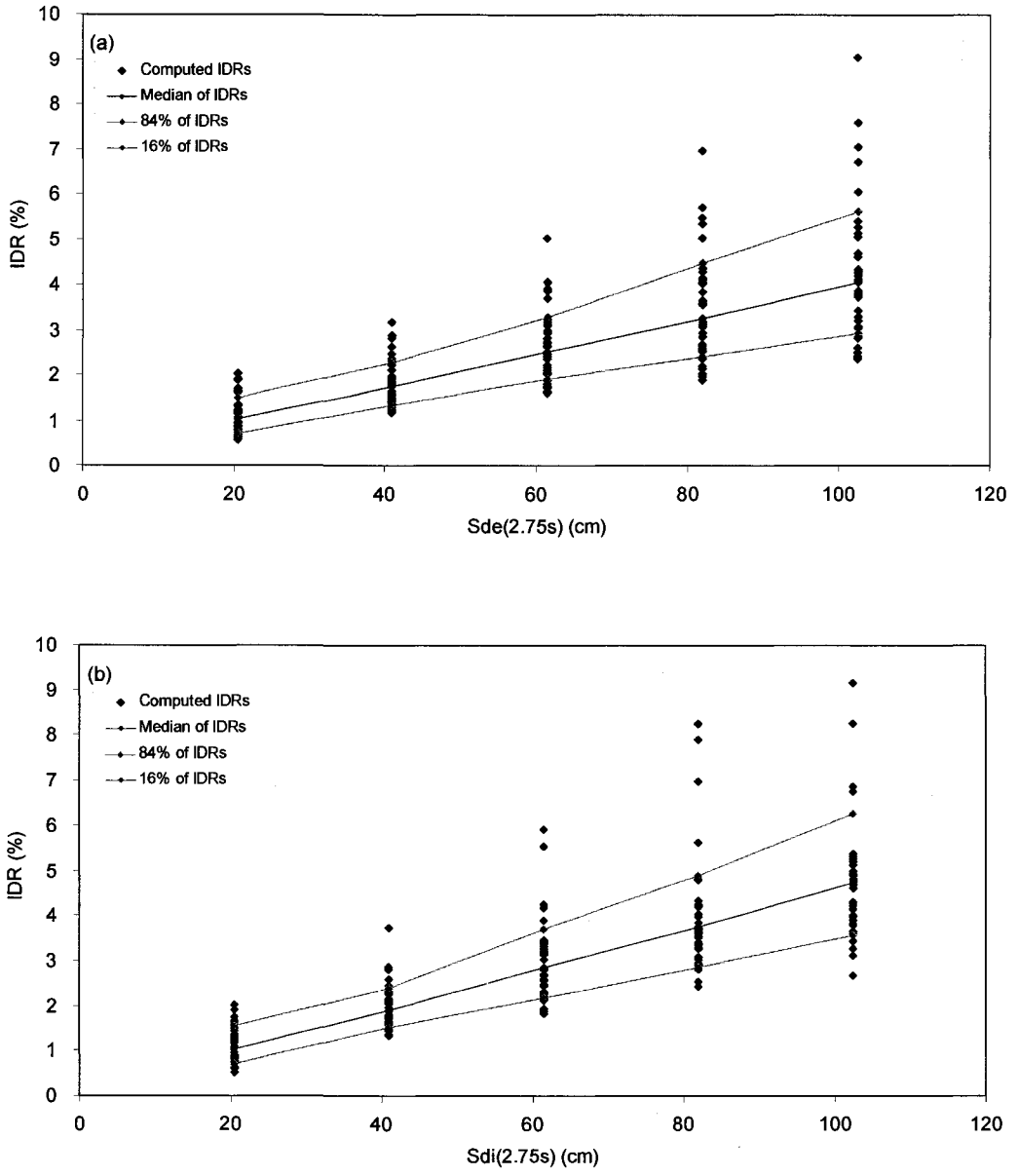

Figure 4.4 Variation of interstorey drifts for the 16S frame for intensity measures represented by elastic and inelastic spectral displacements, i.e., *Sde* and *Sdi* respectively: (a) *Sde*, and (b) *Sdi*.

Chapter 5

Probabilistic Seismic Demand Analysis Using $Sa(T_1)$ as Intensity Measure

5.1 Introduction

As discussed in the introduction of this thesis (Chapter 1), one of the main tasks in the performance-based seismic assessment or design of a given structure is the estimation of the response demand due to future earthquakes. This can be done by probabilistic seismic demand analysis (PSDA) as outlined in the PEER framework document (Cornell and Krawinkler 2000). PSDA combines the structural response of interest (obtained from nonlinear dynamic analysis) with the ground motion hazard at the location of the structure. The final results from PSDA for a given structure are the mean annual frequencies of exceeding specified levels of the response parameter considered.

This chapter presents an overview of the computations and the parameters involved in PSDA. The application of PSDA to the three frames considered in this thesis is discussed in detail. The analyses were conducted using maximum interstorey drift (*IDR*) as a structural response parameter, and spectral acceleration at the fundamental structural period ($Sa(T_1)$) as intensity parameter of the seismic motions. The description of the analysis and

the results for the frames presented in this chapter are essential for understanding the PSDA in general, as well as for understanding the improvements to the PSDA proposed in the following chapters.

5.2 Formulation of demand hazard curve

The goal of probabilistic seismic demand analysis is to compute the mean annual frequencies of exceeding given levels of structural response due to future earthquakes. Following PEER practice, the response demand in PSDA is quantified using an engineering demand parameter (*EDP*) (e.g., maximum interstorey drift, maximum ductility, etc.), and the intensity of the seismic motions is represented by an intensity measure (*IM*) (e.g., elastic spectral acceleration of the seismic motion at the fundamental period of the structure, inelastic spectral displacement, etc.). Using this terminology, the mean annual frequency of exceeding a given *EDP* value *edp*, designated $\lambda_{EDP}(edp)$, is calculated as (Baker and Cornell 2005):

$$\lambda_{EDP}(edp) = \int_{im} P(EDP > edp \mid IM = im) \cdot \left| \frac{d\lambda_{IM}(im)}{d(im)} \right| \cdot d(im) \tag{5.1}$$

$\lambda_{EDP}(edp)$ is also referred to as the demand hazard curve. In this equation, the term $P(EDP>edp|IM=im)$ is the conditional probability of exceeding a specified *EDP* level *edp*, given a level of $IM=im$. The term $\lambda_{IM}(im)$ is the mean annual frequency of exceeding a given *IM* value *im* (this is commonly referred to as the ground motion or seismic hazard curve). Note that the seismic hazard curve, $\lambda_{IM}(im)$, is normally determined by seismologists using probabilistic seismic hazard analysis (PSHA), a procedure that is well documented elsewhere (e.g., Adams and Halchuk 2003, Atkinson 2004).

It is seen from Equation (5.1) that *EDP* and *IM* are required in order to conduct PSDA. In this study, the maximum interstorey drift (*IDR*) over the height of the frames is used as *EDP*. It is a 'global' response parameter and has been used as *EDP* in a number of PEER studies (e.g., Baker and Cornell 2005, Baker 2007, Tothong and Cornell 2007, Tothong and Luco 2007, Luco and Cornell 2007, among others). The maximum *IDR* is also used in the NBCC seismic design provisions to limit the lateral deflections in the design for seismic loads (e.g., maximum drift of 2.5% of the storey height is allowed by NBCC for buildings of normal importance) (NRCC 2005). Most importantly, SEAOC (Vision 2000 Committee 1995) and ASCE (2000) have specified structural performance and damage levels in terms of maximum *IDR*. Such a link between damage and *IDR* is essential for the use of the drift hazard curve (Equation (5.1)) in the estimation of losses due to earthquakes, as discussed in Chapter 1.

In the selection of *IM*, it is important that the structural response is related to the *IM*, and an attenuation relation for the *IM* is available for use in PSHA. Elastic spectral acceleration at the fundamental structural period T_1 ($Sa(T_1)$) is currently the most used *IM*. The analyses in this chapter were conducted using $Sa(T_1)$ as *IM*. Improved *IM*s that take into account the elongation of the structural period, and the contributions of the first and the second modes to the response, are introduced in Chapter 6. The analysis conducted hereafter is of special importance for assessing the 'accuracy' of the PSDA results based on $Sa(T_1)$ relative to those corresponding to the improved *IM*s.

Using *IDR* as *EDP*, and $Sa(T_1)$ as *IM*, Equation (5.1) can be written as follows:

$$\lambda_{IDR}(idr) = \int_{sa} P(IDR > idr \mid Sa(T_1) = sa) \cdot \left| \frac{d\lambda_{Sa(T_1)}(sa)}{d(sa)} \right| \cdot d(sa) \tag{5.2}$$

Equation (5.2) is used in the further discussion in this chapter.

5.3 Analysis method

As seen in Equation (5.2), the PSDA for a given structure involves computations of: (i) the maximum *IDR*s of the structure for different $Sa(T_1)$ levels *sa*, (ii) the conditional probabilities $P(IDR>idr|Sa(T_1)=sa)$, and (iii) the spectral acceleration hazard curve $\lambda_{Sa(T_1)}(sa)$ for the location of the structure. The results for $P(IDR>idr|Sa(T_1)=sa)$ and $\lambda_{Sa(T_1)}(sa)$ are further combined to determine the drift hazard curve $\lambda_{IDR}(idr)$ for the structure. Figure 5.1 illustrates the flowchart for PSDA. The computations listed above were conducted to determine the drift hazard curves for the three frames used in this thesis. The numerical procedures used in the analysis and the results obtained for the frames are described in Sections 5.3.1 to 5.3.4 that follow.

5.3.1 Maximum *IDR*s

The responses of the frame models were computed using nonlinear time history analyses. The program RUAUMOKO (Carr 2004) was used for the analyses. The excitation motions were represented by the records of the 80R set (Table B.1 in Appendix B). As discussed in Chapter 3, this set consists of 80 records that were selected to be representative of the expected seismic motions in the Vancouver region, for which the frames were designed.

For each frame model, the records were scaled to have the same spectral acceleration at the first mode period of the model (i.e., T_1=0.94 s for the 4S frame, 1.96 s for the 10S frame, and 2.75 s for the 16S frame; Table 2.2 in Chapter 2). For illustration, Fig. 5.2 shows the 5% damped spectra of the scaled records to spectral acceleration of 0.15

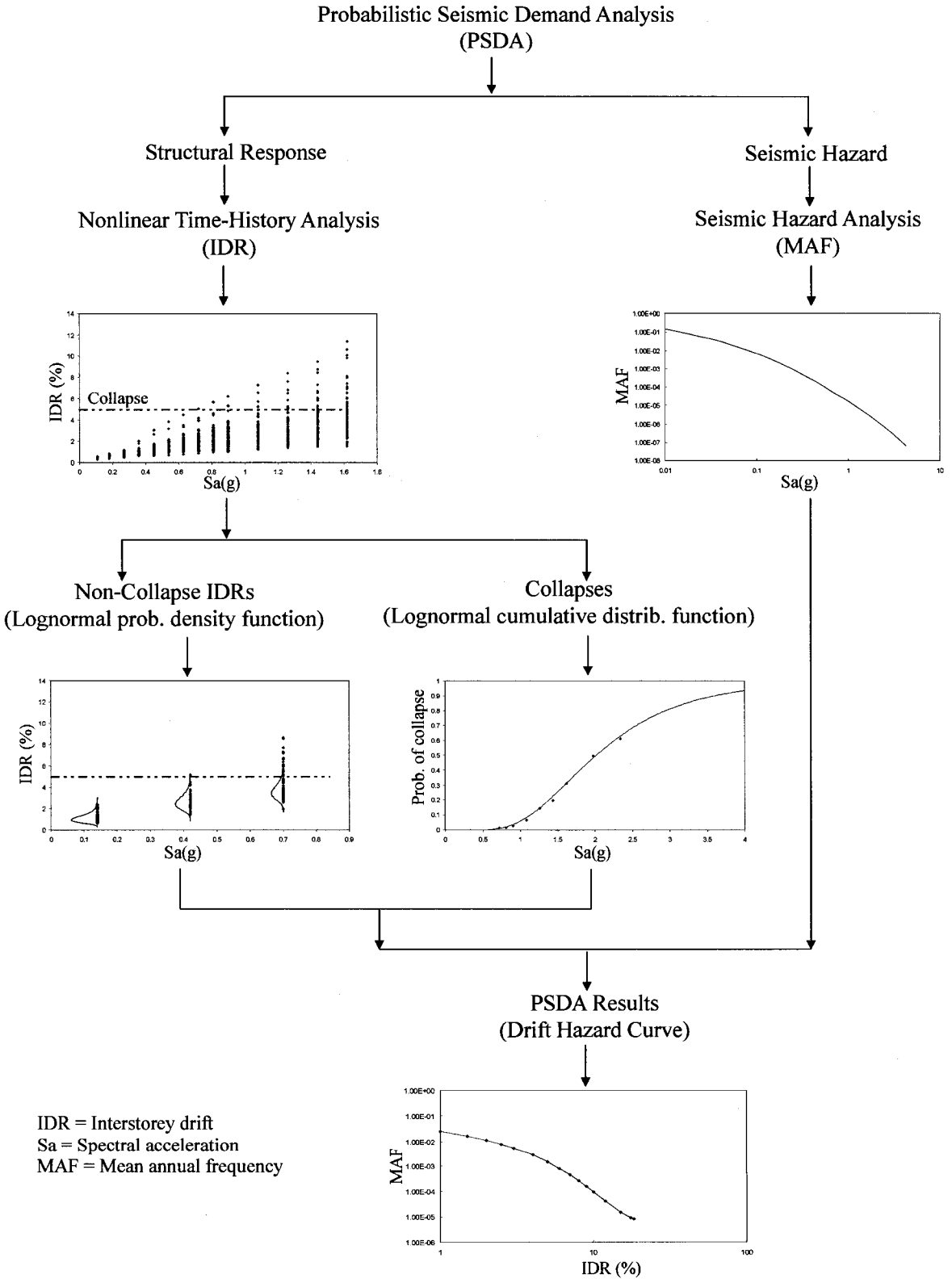

Figure 5.1 Flowchart for probabilistic seismic demand analysis.

g at the first mode period of the 10S frame, T_1=1.96 s. It can be seen that this scaling provides a relatively small dispersion of the spectra in the vicinity of T_1 and for long periods, but the dispersion is significant in the short period range.

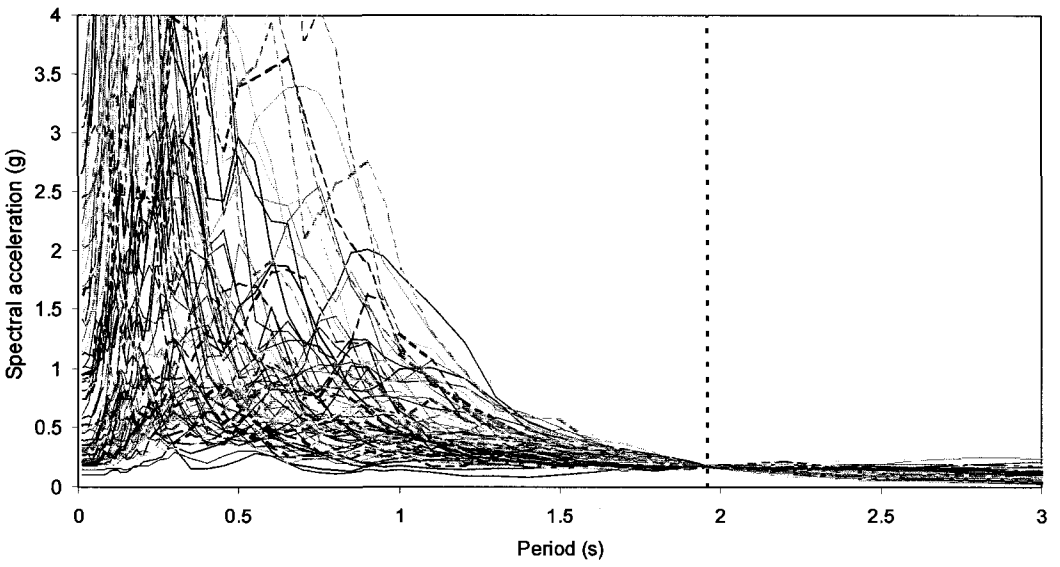

Figure 5.2 Acceleration response spectra for the records of the 80R set scaled to spectral acceleration of 0.15 g at the first mode period of the 10S frame, T_1=1.96 s; 5% damping.

To determine the maximum *IDR*s due to ground motions with different intensities, the records were scaled to a range of $Sa(T_1)$ intensity levels. In total 16 levels were used for the 4S frame, and 14 levels for each of the 10S and the 16S frames.The ranges of the $Sa(T_1)$ levels were from 0.11 g to 2.34 g for the 4S frame, from 0.04 g to 1.26 g for the 10S frame, and from 0.03 g to 0.99 g for the 16S frame. Expressed in terms of the *reference* spectral acceleration $Sa(T_1)_{ref}$ (Table 4.1), the $Sa(T_1)$ levels ranged from $0.6Sa(T_1)_{ref}$ to $13Sa(T_1)_{ref}$ for the 4S frame, and from $0.3Sa(T_1)_{ref}$ to $9Sa(T_1)_{ref}$ for the 10S and the 16S frames. Maximum *IDR*s were obtained from nonlinear time history analyses of the frame models subjected to the records scaled to each of the $Sa(T_1)$ levels. Figure 5.3 shows the computed *IDR*s versus the intensity levels $Sa(T_1)$. Each point in the figure represents the *IDR* for a

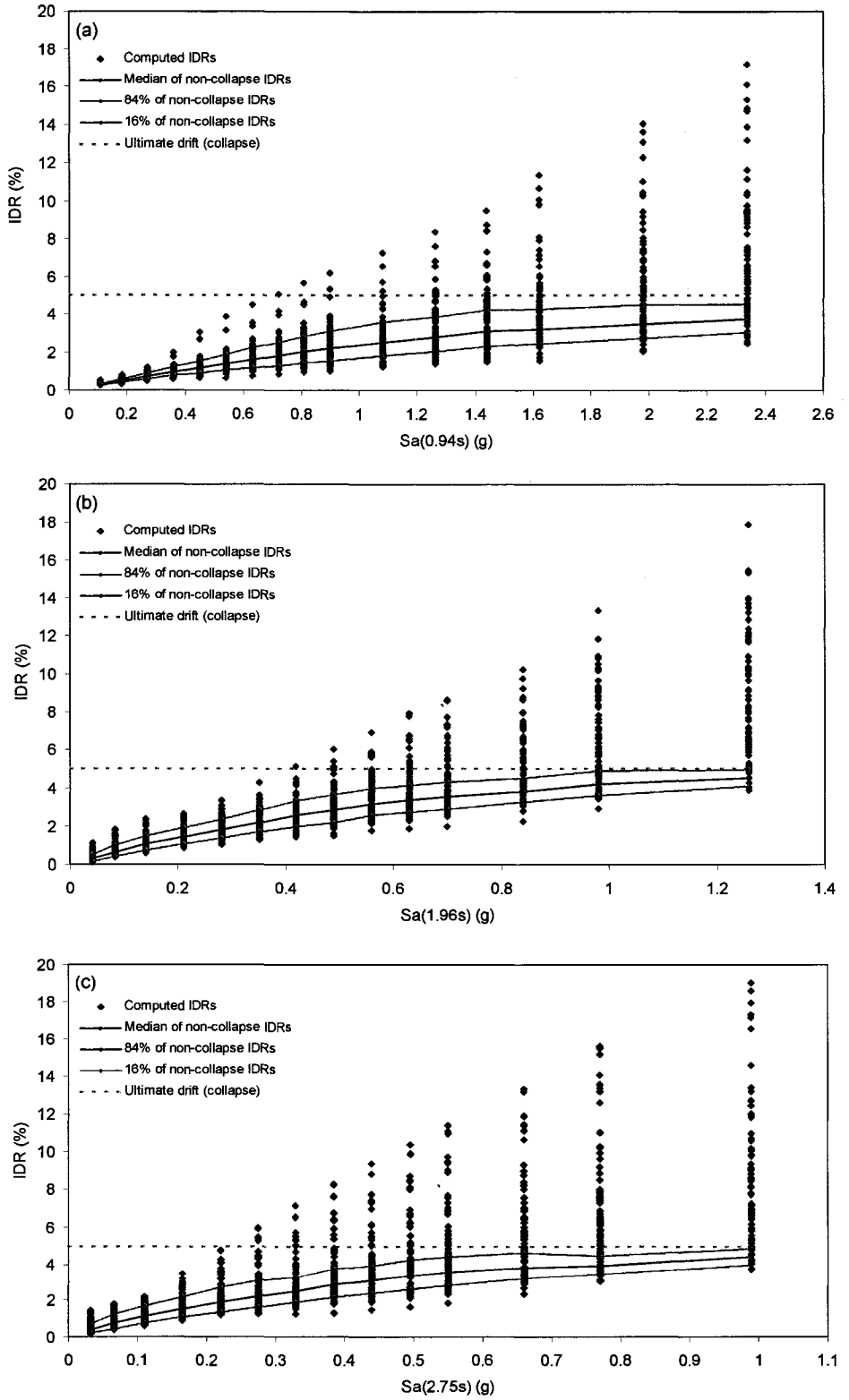

Figure 5.3 Computed maximum *IDR*s for records scaled to spectral acceleration at the first mode period, $Sa(T_1)$: (a) for the 4S frame, (b) for the 10S frame, and (c) for the 16S frame.

given record and intensity level. The ultimate drift level at 5% drift, shown in Fig. 5.3, is discussed below in this section.

It can be seen in the figure that the records scaled to the selected intensities produce *IDR*s ranging from very small to excessive values. As intended in the selection of the intensity levels, the largest *IDR*s corresponding to the highest levels are comparable for the three frames. This was necessary in order to develop drift hazard curves for the frames for approximately the same ranges of maximum *IDR*s. It is seen that highest intensity level was used for the 4S frame and lowest intensity was used for the 16S frame. This is because the 4S frame has largest lateral stiffness, and therefore, a higher intensity of the motions is required for this frame in order to obtain maximum *IDR* demands close to those of the 10S and the 16S frames.

Figure 5.3 shows quite large *IDR*s for the higher intensity levels. *IDR* values of the order of 15% and above can be seen for the highest $Sa(T_1)$ levels used in the analysis. Certainly, such large *IDR*s cannot be resisted by the frames, i.e., the frames would collapse when their *ultimate* drift capacities (i.e., collapse drift limits) are exceeded. It is important for this study to know how many records produce collapse at a given $Sa(T_1)$ intensity. Since the program RUAUMOKO does not identify the collapse, an estimate of the ultimate drift capacities of the frames is needed in order to determine which records cause collapse. In this study, the collapse was defined to occur if the *IDR* obtained from the dynamic analysis exceeds 5%. The considerations for the selection of the value of 5% as ultimate drift for the frames analysed in this study are discussed hereafter.

Estimation of ultimate drift

Since the frames are designed according to NBCC, it is useful first to consider the code requirements for the expected performance of buildings when subjected to strong seismic motions. As stated in Commentary J of NBCC, "a building designed according to the code would likely have extensive structural and nonstructural damage during the design ground motion but the building should not collapse". Referring to experience during past earthquakes, it is also stated in Commentary J (also in Heidebrecht 1997) that ductile structures with regular configurations in which the energy dissipation is distributed throughout the structure can sustain their integrity at ground motions considerably above the design ground motion level. These considerations indicate that the *ultimate* drifts for the frames used in this study (which were designed as ductile frames with careful considerations of the confinement and P-Δ requirements specified in the code) would be significantly larger than the maximum *design* drift of 2.5% allowed by the code.

An important document regarding the selection of the ultimate drift is the Prestandard for the Seismic Rehabilitation of Buildings prepared by the American Society of Civil Engineers (ASCE) for the U.S. Federal Emergency Management Agency (FEMA), known as FEMA 356 report (ASCE 2000). Depending on the seismic rehabilitation objectives, FEMA 356 specifies different structural performance levels. For each performance level, the expected structural damage due to earthquakes is described in this document. Of interest for this thesis is the *collapse prevention structural performance level* for a seismic hazard corresponding to that used in NBCC, i.e., 2% in 50 years seismic motion. The collapse prevention performance level is defined as "the post-earthquake damage state that includes damage to structural components such that the structure

continues to support gravity loads but retains no margin against collapse". The interstorey drift specified in FEMA 356 for this performance level is 4% for reinforced concrete frame buildings.

In addition to the foregoing code-related documents, a review of the research work related to this topic was conducted in order to quantify the ultimate drift for use in this thesis. The findings from few of these studies are summarised here.

One of the most comprehensive studies in this field was done by Perus et al. (2007, 2006). They compiled and statistically analysed the ultimate drifts obtained from experimental investigations of reinforced concrete columns. Results from testing of about 850 specimens are used in their study. Parameters that affect the ultimate drift are considered in the study. These include the effects of confinement, axial loads, shear span-to-depth ratio, concrete compressive strength, and longitudinal reinforcement. The mean ultimate drift was found to range between 4% and 6%, and the mean plus one standard deviation ultimate drift was found to be approximately between 6% and 8%.

Pujol et al. (2000) compared results from experimental studies on ultimate drifts of reinforced concrete columns. In total 29 specimens with different confinement ratios and axial loads were considered. It is shown that depending on the confinement and the axial loads, the ultimate drifts of columns can be well above 4%.

Based on experimental results, Saatcioglu and Razvi (2002) proposed an equation that relates the ultimate drift of columns with the confinement reinforcement, the properties of the concrete and the reinforcement, the applied axial load, and the nominal compressive capacity of the columns. The equation was used to determine the ultimate drifts for the first

storey columns of the frames used in this thesis. The computed ultimate drifts were between 6% and 9%.

In summary, the ultimate drift depends on a number of parameters which lead to a large scatter of results even from experiments with cyclic loading of columns. In a real situation, when a building is subjected to a strong earthquake, the problem is much more complex. The forces in the structural members and the deformations vary rapidly during earthquake response, and the collapse mechanism depends not only on the characteristics of the structural members but also on the characteristics of the earthquake motion.

In dynamic analyses, different approaches for defining the collapse have been used in different studies. Baker and Cornell (2005) define the collapse if the dynamic analysis algorithm fails to converge due to numerical instability or if the drift ratio at any storey exceeds 10%. Vamvatsikos and Cornell (2004) examine the curve representing the relationship between the intensity levels $Sa(T_1)$ (plotted on the vertical axis) and the computed maximum interstorey drifts (on the horizontal axis); the collapse (referred to as the global instability in Vamvatsikos and Cornell (2004)) is defined to occur when the curve becomes flat and any increase in the intensity results in practically infinite interstorey drift. Such simplified approaches are in use since the collapse mechanism is difficult to model and is not included in the available computer programs for nonlinear dynamic analysis.

Based on the foregoing considerations, 5% drift (i.e., twice the allowed design drift) was chosen as ultimate drift for the frames analysed in this thesis. Considering the results obtained from experiments discussed above, 5% ultimate drift level seems reasonable for well designed and detailed ductile reinforced concrete frames. One might even prefer using

somewhat higher value than 5% for *new* buildings since FEMA 356 requires 4% ultimate drift for *existing* buildings. Sensitivity analyses were conducted to investigate the effects of the ultimate drift on the PSDA final results (i.e., the drift hazard curves). It was found that the reduction of the ultimate drift to 4% results in very small differences between the drift hazard curves corresponding to 4% and 5% ultimate drifts. The differences increased when ultimate drifts lower than 4% were used. The increase of the ultimate drift up to 7% resulted in almost identical drift hazard curves to those obtained for 5% ultimate drift.

5.3.2 Calculation of the probability $P(IDR>idr|Sa(T_1)=sa)$

The PSDA described above requires the calculation of the probability of *IDR* exceeding a specified level *idr*, given a level $Sa(T_1)=sa$, i.e., $P(IDR>idr|Sa(T_1)=sa)$ (Equation 5.2). To calculate this probability, we should consider both the *IDR*s that are below the 5% ultimate drift (referred to as the non-collapse *IDR*s) and those that exceed the ultimate drift (referred to as the collapses) (Fig. 5.3); note that the term 'collapse *IDR*s' is intentionally avoided here because if there is a collapse, then *IDR* has no meaning. Having defined the non-collapse *IDR*s and the collapses for each $Sa(T_1)=sa$, the conditional probability $P(IDR>idr|Sa(T_1)=sa)$ can be obtained by combining the corresponding conditional probabilities for the non-collapse *IDR*s and the collapses, as described below.

Non-collapse IDRs

To calculate the conditional probability $P(IDR>idr|Sa(T_1)=sa)$ for the non-collapse *IDR*s, the probability distribution function of the *IDR*s for the $Sa(T_1)$ levels should be known. Considering available probability distribution functions (e.g., normal, lognormal,

Beta, etc.), the most suitable function can be found by applying the Kolmogorov-Smirnov test (Ang and Tang 1975) to the computed *IDR*s. Such tests for interstorey drifts have been conducted by Baker and Cornell (2005), Shome (1999), and Miranda and Aslani (2003). It has been found that the lognormal probability distribution is suitable for representing the maximum *IDR*s obtained by scaling records to $Sa(T_1)$. Given this, the computed non-collapse *IDR*s at the $Sa(T_1)$ levels discussed earlier are assumed to have lognormal distributions, as illustrated in Fig. 5.4. It is known that if *IDR*s follow lognormal distribution, then the natural logarithms of the *IDR*s (ln*IDR*) follow normal distribution. For each $Sa(T_1)$ level, the mean and the standard deviation of the normal distribution can be calculated using Equations (5.3) and (5.4) respectively (Ang and Tang 1975).

$$\mu_{\ln IDR|Sa(T_1)=sa} = \frac{1}{n}\sum_{i=1}^{n} \ln IDR_i \mid Sa(T_1) = sa \tag{5.3}$$

$$\sigma_{\ln IDR|Sa(T_1)=sa} = \sqrt{\frac{1}{n-1}\sum_{i=1}^{n}\left[\left(\ln IDR_i \mid Sa(T_1) = sa\right) - \mu_{\ln IDR|Sa(T_1)=sa}\right]^2} \tag{5.4}$$

These two quantities fully define the normal distribution. The probability that *IDR* exceeds *idr* given $Sa(T_1)$=*sa* can now be calculated using the normal complementary cumulative distribution function:

$$P(IDR > idr \mid Sa(T_1) = sa, nocollapse) = 1 - \Phi\left(\frac{(\ln idr \mid Sa(T_1) = sa) - \mu_{\ln IDR|Sa(T_1)=sa}}{\sigma_{\ln IDR|Sa(T_1)=sa}}\right) \tag{5.5}$$

where $\Phi(\cdot)$ denotes the standard normal cumulative distribution function.

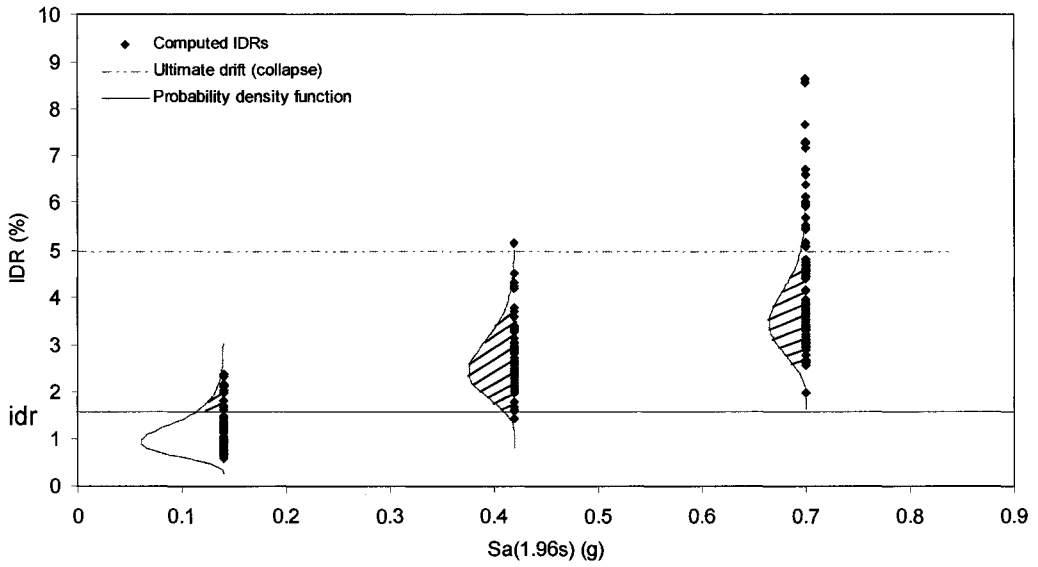

Figure 5.4 Maximum interstorey drifts for the 10S frame for records scaled to three $Sa(T_1)$ levels (0.14 g, 0.42 g, and 0.70 g), and corresponding lognormal probability distributions of the drifts.

Collapses

The calculation of the probability of collapse was done as suggested by Baker and Cornell (2004, 2005). First, the discrete probability that collapse (C) has occurred at a given $Sa(T_1)=sa$ was determined using the equation:

$$P(C|Sa(T_1)=sa) = \frac{\text{number of collapses}}{\text{total number of responses}} \tag{5.6}$$

As indicated by Equation (5.6), the calculation of the collapse probabilities $P(C|Sa(T_1)=sa)$ for each frame was simply done by counting the collapses for each $Sa(T_1)=sa$, and expressing these as a fraction of the total number of responses of 80. The computed discrete probabilities for the 4S, the 10S, and the 16S frames are shown by symbols in Figure 5.5. Since analytical expressions for the collapse prediction are required for PSDA, curves were

fitted (shown in Fig. 5.5) assuming lognormal distribution of the collapses. The curves were represented by the following expression:

$$P(C \mid Sa(T_1) = sa) = \int_{sa} \frac{1}{sa \cdot B \cdot 2\pi} \cdot \exp\left[-\frac{1}{2} \cdot \left(\frac{\ln sa - A}{B} \right)^2 \right] d(sa) \tag{5.7}$$

The coefficients A and B represent the mean and the standard deviation of the natural logarithms of the collapses respectively, and were determined such that the curves fit the computed discrete probabilities (Fig. 5.5).

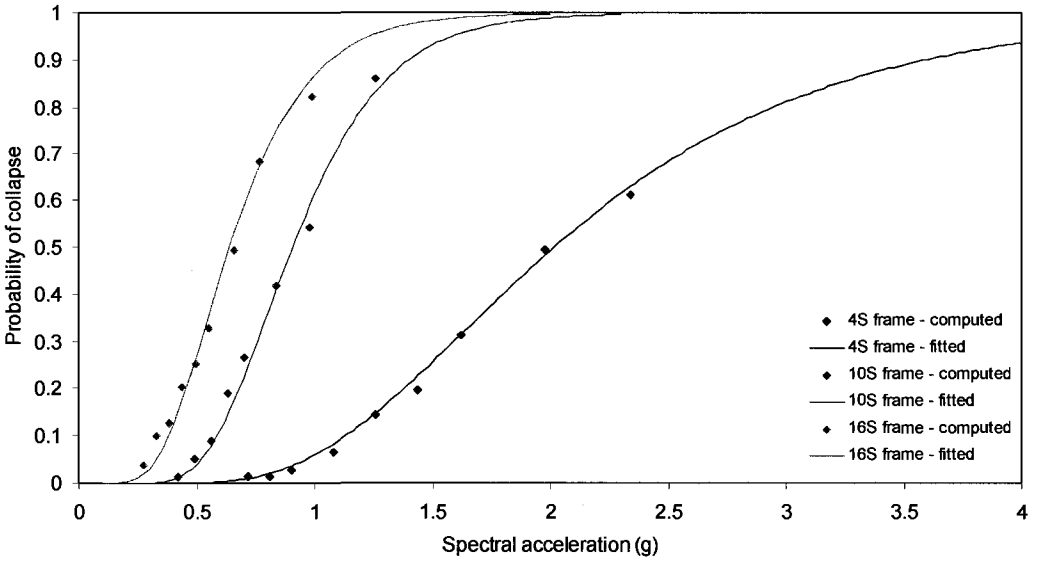

Figure 5.5 Computed probability of collapse (denoted by symbols) and fitted probability of collapse distributions for the 4S, the 10S, and the 16S frames.

Combining non-collapse and collapse results

The probabilities of the non-collapse and the collapse results defined above were combined using the total probability theorem. The probability that *IDR* exceeds a specified value *idr* for a given $Sa(T_1)$=*sa* is expressed as:

$$P(IDR > idr \mid Sa(T_1) = sa) = P(C \mid Sa(T_1) = sa) + \left[1 - P(C \mid Sa(T_1) = sa)\right] \cdot \left[1 - \Phi\left(\frac{\ln idr - \mu_{\ln IDR|Sa(T_1)=sa}}{\sigma_{\ln IDR|Sa(T_1)=sa}}\right)\right] \quad (5.8)$$

This probability was further used in the PSDA of the frames.

For illustration, Fig. 5.6 shows the computed probabilities $P(IDR>idr|Sa(T_1)=sa)$ for the three frames for drift levels of 0.5%, 1.0%, 1.5%, 2.0%, 2.5%, 3.0%, 4.0% and 5.0%. Each curve in the figure represents the probability of exceedance of a given drift level as a function of the spectral acceleration at the fundamental period of the frame. It can be seen from the figure that the curves for the 4S frame (Fig. 5.6(a)) are shifted towards higher $Sa(T_1)$ levels compared to those for the 10S and the 16S frames (Figs. 5.6(b) and 5.6(c)). Namely, for the same probability of exceedance of a given drift, a larger $Sa(T_1)$ level is required for the 4S frame than that for the 10S and the 16S frames. As an example, the probability of 0.5 that the drift of 2.5% will be exceeded corresponds to $Sa(T_1)$ of 1.07 g for the 4S frame, 0.43 g for the 10S frame, and 0.33 g for the 16S frame. As discussed in Section 5.3.1, this is because the 4S frame has a larger lateral stiffness than that of the 10S and the 16S frames, and therefore a higher intensity motion is required in order to obtain the same drift as that of the 10S and the 16S frames. While the probabilities of exceedance represented by the curves in Fig. 5.6 are useful, they are not complete since no time span (or return period) of the exceedance of the drift is given, and that is why further steps are involved in the PSDA.

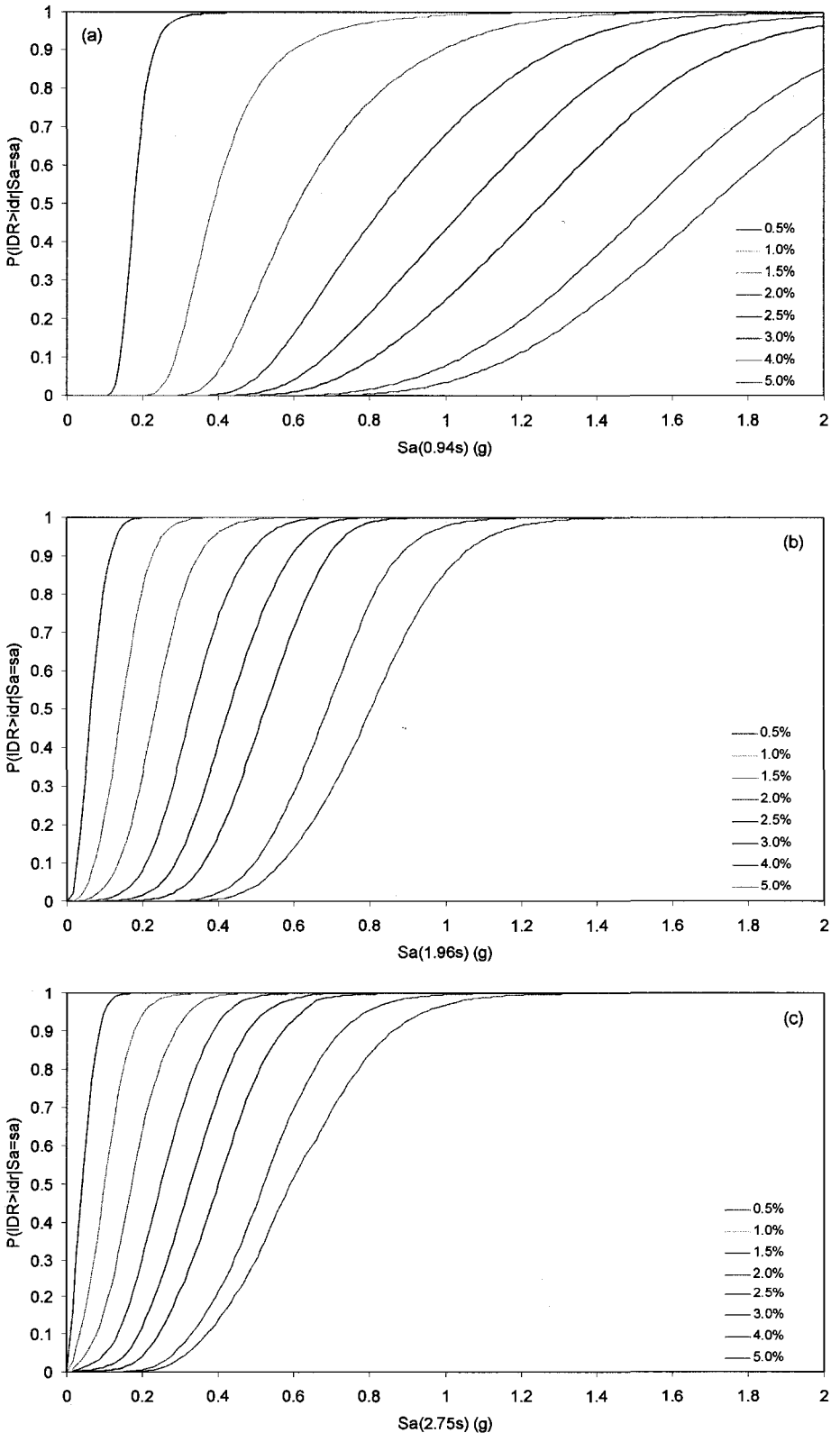

Figure 5.6 Probability $P(IDR>idr|Sa(T_1)=sa)$ for selected *idr* values between 0.5% and 5.0%: (a) for the 4S frame, (b) for the 10S frame, and (c) for the 16S frame.

When curves like those in Fig. 5.6 are linked with the structural damage, they are called *fragility curves*. As an example, FEMA 356 (ASCE 2000) provides descriptions for damage for 1%, 2%, and 4% drifts which can be summarised approximately as moderate, severe, and near collapse damage respectively. So, based on the FEMA 356 specifications, the curves in Fig. 5.6 corresponding to drifts of 1%, 2%, and 4% can be considered as fragility curves for moderate, severe, and near collapse damage respectively. Note that the fragility curves obtained in this way (Fig. 5.6) are in terms of *IM* (i.e., $Sa(T_1)$). Fragility curves in terms of *IM* have been used in some studies, e.g., ATC (1985), and Singhal and Kiremidjian (1996). In PEER research, however, the fragility curves are expressed in terms of response demand, i.e., *EDP* (Moehle and Deierlein 2004), as discussed in the Introduction of this thesis. The development of such fragility curves is beyond the scope of this thesis, and is not discussed here.

5.3.3 Seismic hazard curves, $\lambda_{Sa(T1)}(sa)$

As mentioned above, the seismic hazard in this chapter is represented by the mean annual frequencies of exceeding selected $Sa(T_1)$ values *sa*, and is denoted $\lambda_{Sa(T_1)}(sa)$. Note that T_1 is the fundamental structural period. The *sa* values are chosen within a specified range of interest. $\lambda_{Sa(T_1)}(sa)$ is commonly referred to as the seismic hazard curve and is computed using probabilistic seismic hazard analysis (PSHA). For a given site and a specified $Sa(T_1)$ value *sa*, PSHA combines the hazard contributions of the seismic source zones affecting the site. This is done by considering the seismic activities of the zones and using the attenuation relation for $Sa(T_1)$ (Adams and Halchuk 2003, Atkinson 2004).

For this study, seismic hazard curves for Vancouver were determined for 5% damped *Sa* for periods of 0.94 s, 1.96 s, and 2.75 s, which are the fundamental periods of the 4S, the 10S, and the 16S frame respectively. The curves were computed by Geological Survey of Canada (GSC) (Adams and Halchuk 2007). Note that GSC uses a 'standard' set of attenuation relations for the computation of the seismic hazard for western Canada for periods up to 2.0 s (Adams and Halchuk 2003). To compute the hazard for period of 2.75 s, the attenuation relation for that period was determined by extrapolating the coefficients of the relations for periods below 2.0 s, which was done by fitting regression curves to the coefficients of these relations.

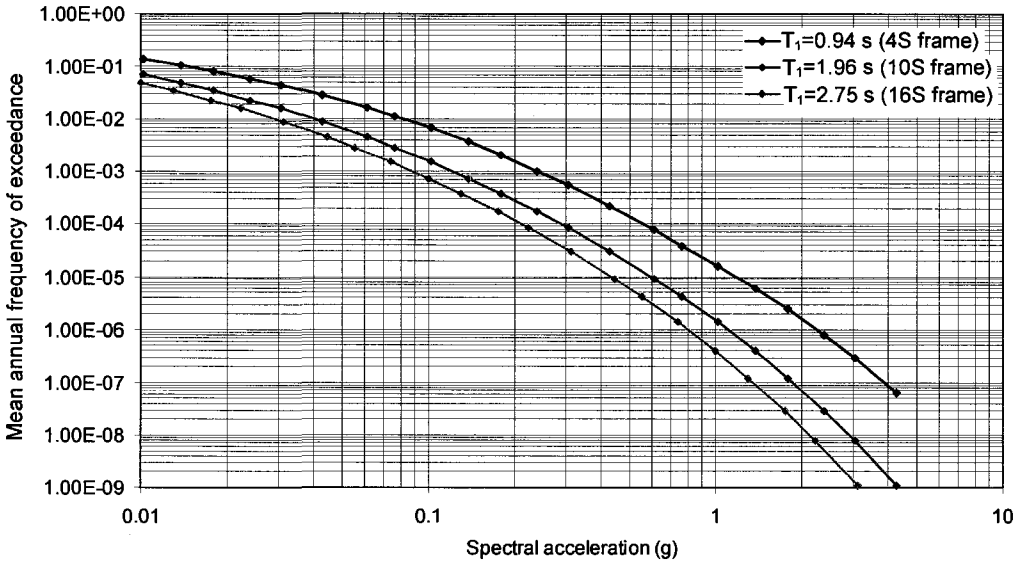

Figure 5.7 Seismic hazard curves for Vancouver expressed in terms of spectral acceleration at the fundamental periods of the 4S, the 10S, and the 16S frames of 0.94 s, 1.96 s, and 2.75 s respectively.

Figure 5.7 shows the seismic hazard curves $\lambda_{Sa(T_1)}(sa)$ for Vancouver, for periods T_1 of 0.94 s, 1.96 s, and 2.75 s. It can be seen in the figure that the mean annual frequencies of exceeding the spectral accelerations for period of 0.94 s are larger than those for periods

of 1.96 s and 2.75 s. This is expected because larger spectral accelerations are normally associated with shorter periods (except for very short periods, e.g., below 0.2 s).

The seismic hazard curves shown in Fig. 5.7 were used in the PSDA to compute the drift hazard curves for the frames considered.

5.3.4 Drift hazard curves for the frames, $\lambda_{IDR}(idr)$

Having determined the probability distributions $P(IDR>idr|Sa(T_1)=sa)$ for the frames, and the seismic hazard curves $\lambda_{Sa(T_1)}(sa)$ for the site, the mean annual frequencies of *IDR* exceeding a set of *idr* values, denoted $\lambda_{IDR}(idr)$, can be computed using Equation (5.2). The function $\lambda_{IDR}(idr)$ is referred to as the drift hazard curve. In this study, numerical integration was used to determine the drift hazard curves, making use of the discrete summation approximation. Values for *sa* ranging between 0.01g and 4.0 g, at a step of 0.01g were used in the numerical integration. Mean annual frequencies (MAF) of exceedance were computed for selected drift values between 0.27% (1.0 cm) and 5.0% (18.25 cm). Note that the drift of 5.0% corresponds to collapse of the frames, as discussed in Section 5.3.1.

The computed drift hazard curves are shown in Fig. 5.8. It is seen that the largest MAF values are for the 16S frame, and the smallest values are for the 4S frame within the entire drift range considered (i.e., between drifts of 0.27% and 5.0%). The MAF values for the 10S frame are in between those for the 16S and the 4S frames. This indicates that among the three frames used in this study, the most vulnerable is the 16S frame and the least vulnerable is the 4S frame.

A quantity that can be obtained directly from the mean annual frequency of exceedance is the mean return period of exceedance. The mean return period of exceedance of a specified drift value is equal to the reciprocal of the mean annual frequency of exceedance of that drift. The return period of exceedance is introduced here since it is commonly used by engineers, and will be used in the discussion that follows.

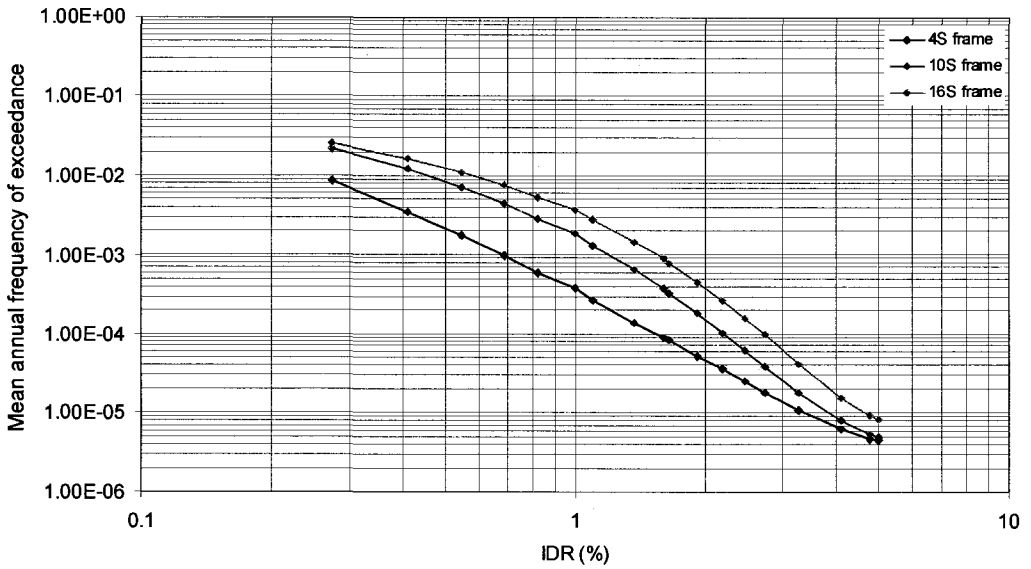

Figure 5.8 Drift hazard curves for the 4S, the 10S, and the 16S frames.

On the use of drift hazard curves

Drift hazard curves provide very useful information on the performance of buildings due to earthquake motions. A general discussion on the use of the drift (i.e., the demand) hazard curves in the performance-based design and in the loss estimations due to earthquakes is given in Chapter 1. However, it is useful at this point to illustrate briefly the use of the drift hazard curves developed for the frames considered in this thesis.

The question that would be normally asked by designers, building owners, or insurance companies for a given building would be "what is the mean annual frequency of

exceeding, for example, *moderate* damage to the building due to earthquake motions?". Since moderate damage corresponds approximately to 1.0% interstorey drift (according to FEMA 356), the question can be answered by determining the annual frequency of exceeding 1.0% drift. It can be found from Fig. 5.8 that the annual frequencies of exceeding 1.0% drift are 0.000375 for the 4S frame, 0.00189 for the 10S frame, and 0.00373 for the 16S frame. The return periods of exceeding this drift are 2670, 530, and 270 years for the 4S, the 10S, and the 16S frames respectively.

Similar question, but for different purposes, that is usually considered by designers and code authorities is: "what is the annual probability of exceedance of the maximum interstorey drift of a building designed for a seismic hazard with a probability of exceedance of 2% in 50 years (i.e., 0.0004 per year) as required by NBCC (NRCC 2005)?" Since the *design* drift for the frames used in this thesis was approximately 1.6% (Chapter 2), the annual frequency of exceeding 1.6% drift is found from Fig. 5.8 to be 0.000081 for the 4S frame, 0.00038 for the 10S frame, and 0.00080 for the 16S frame. It can be seen that the value of the annual frequency of exceeding the design drift for the 10S frame is close to that of the seismic hazard. However the value for the 4S frame is about five times smaller, and that for the 16S frame is twice larger than the annual frequency of exceeding the seismic hazard of 0.0004. This indicates that one should not relate directly the annual frequency of exceeding a specified drift level with that of the seismic hazard. This is because the mean annual frequency of exceedance of drift depends on both the dynamic characteristics of the building and the seismic hazard.

One should keep in mind that the mean annual frequencies discussed above correspond to a specific case, i.e., when $Sa(T_1)$ is used as intensity measure. The mean

annual frequencies obtained from PSDA using improved intensity measures are somewhat different from those corresponding to $Sa(T_1)$, as discussed in Chapter 8. Therefore, the observations for the differences between the mean annual frequencies for drift and that for the seismic hazard should be considered as specific (for $Sa(T_1)$), rather than general observations.

5.4 Disaggregation of seismic drift hazard

The disaggregation method is often used in probabilistic seismic hazard analysis (PSHA) to determine which earthquake scenarios (i.e., magnitude-distance pairs) contribute most to the seismic hazard (Halchuk et al. 2007). In this section, the concept of disaggregation is extended to probabilistic seismic demand analysis (PSDA). The disaggregation of PSDA provides the distribution of the mean annual frequency of exceedance of a specified *IDR* level, expressed as a function of the intensity measure $Sa(T_1)$. This is used for determining the intensities $Sa(T_1)$ that have the largest contributions to the *IDR* level considered.

The disaggregation analysis for a given *IDR* level is normally done by extracting from PSDA the mean annual frequency of exceedance corresponding to each of the $Sa(T_1)$ levels used in the analysis. In this study, disaggregation results were obtained for $Sa(T_1)$ levels between 0.01 g and 4.0 g at a step of 0.01 g, as used in PSDA (Section 5.3.4).

For illustration, Fig. 5.9 shows results from disaggregation analysis for the 10S frame. The distributions of the mean annual frequencies of exceedance of 1.0%, 2.5%, and 5.0% maximum interstorey drifts are presented in the figure. While the mean annual frequencies were computed at discrete time steps, they were connected by line segments in

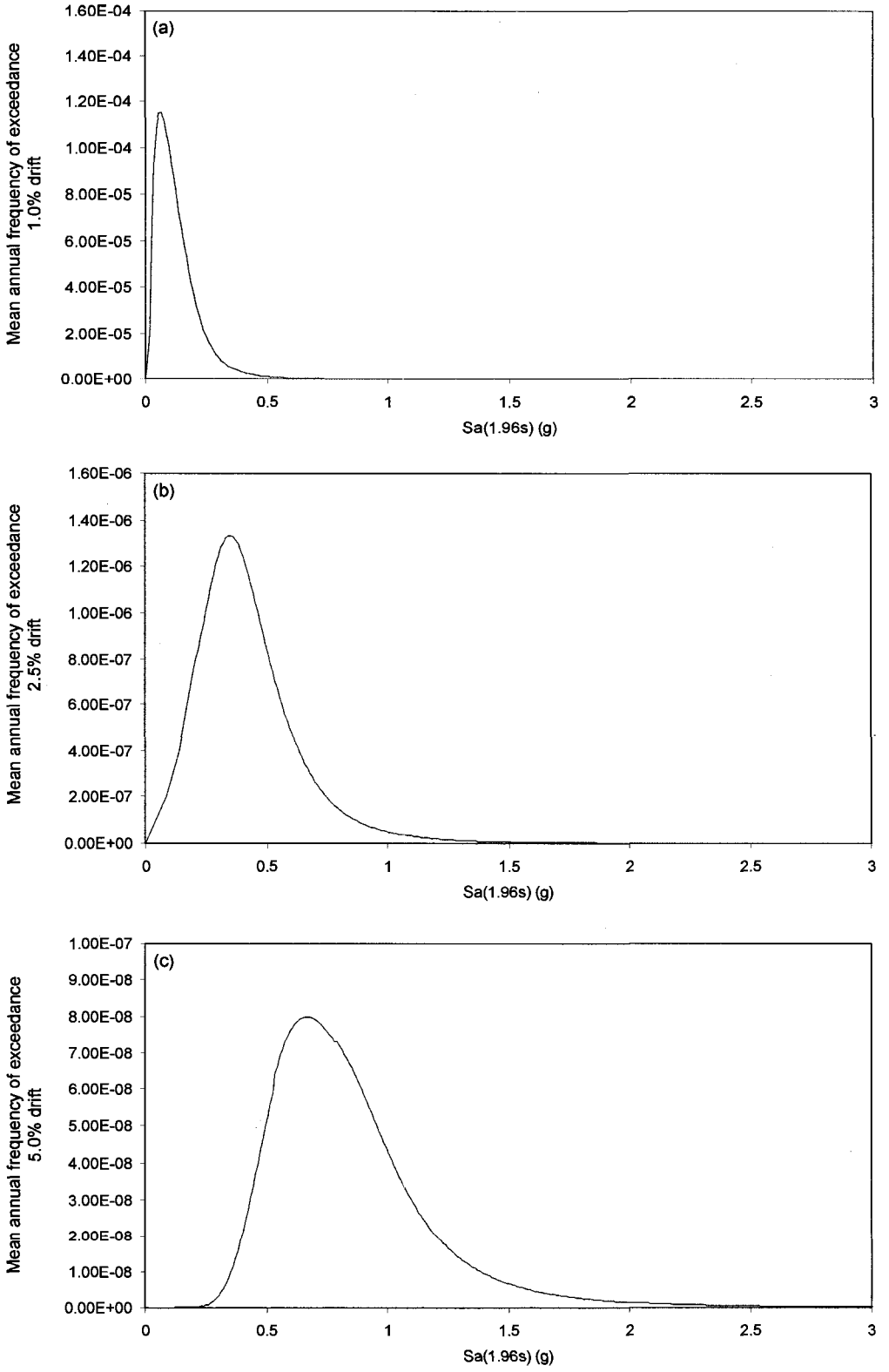

Figure 5.9 Distributions of mean annual frequencies of exceedance of 1.0%, 2.5%, and 5.0% maximum interstorey drifts for the 10S frame: (a) 1.0% drift, (b) 2.5% drift, and (c) 5.0% drift.

the graphs resulting in 'continuous' curves, as shown in the figure. It is seen in the figure that the predominant $Sa(T_1)$ values for the 10S frame are approximately 0.1 g for 1.0% drift, 0.4 g for 2.5% drift, and 0.7 g for 5.0% drift.

The results from disaggregation analysis can also be used to verify whether the range of the intensity levels used in PSDA are appropriate for the computation of the drift hazard curves, i.e., whether the contributions of all possible intensity levels are included in PSDA. As mentioned above, the range of $Sa(T_1)$ values used in PSDA was 0.01 g to 4.0 g. Figure 5.9 shows that $Sa(T_1)$ values up to 2.0 g would be sufficient for the 10S frame, but using $Sa(T_1)$ values up to 1.0 g, for example, would result in an underestimation of the mean annual frequency of exceeding 5% drift for the 10S frame. In general, the results from disaggregation analyses for the three frames showed that the range of $Sa(T_1)$ values between 0.01 g and 4.0 g is appropriate for the computation of the drift hazard curves for the frames.

5.5 Summary

The goal of probabilistic seismic demand analysis (PSDA) is to compute the mean annual frequencies of exceeding given levels of structural response due to future earthquakes. PSDA combines the *structural response* of interest (obtained from nonlinear dynamic analysis) with the *seismic* (i.e., *ground motion*) *hazard* at the location of the structure. In PSDA, the structural response parameter is normally referred to as the engineering demand parameter, and the ground motion intensity is referred to as the intensity measure.

In this chapter, PSDA was applied to the three frames considered in this thesis, i.e., the 4S, the 10S, and the 16S frames. Maximum interstorey drift (*IDR*) was used as engineering demand parameter, and the spectral acceleration of the seismic motion corresponding to the fundamental period of the frame considered ($Sa(T_1)$) was used as intensity measure. *IDR*s were determined from nonlinear time history analyses of the frames using 80 selected ground motion records as excitation motions. For each frame, the records were scaled to a series of $Sa(T_1)$ levels representing different intensities of expected seismic motions. The responses obtained from the analyses for the selected scaling levels ranged from elastic responses to collapses of the frames.

The seismic hazard for each frame was expressed in terms of the intensity measure $Sa(T_1)$. It was represented by the mean annual frequency of exceeding specified $Sa(T_1)$ levels. Note that the seismic hazards for the 4S, the 10S, and the 16S frames are different since their fundamental periods (T_1) are different.

The computed interstorey drifts and the seismic hazards results were combined using PSDA to determine the mean annual frequencies (MAF) of exceeding specified drift levels. Largest MAF values were obtained for the 16S frame, and smallest values were obtained for the 4S frame. The MAF values for the 10S frame were in between those for the 16S and the 4S frames. These results indicate that among the three frames, the most vulnerable to seismic motions is the 16S frame, and the least vulnerable is the 4S frame.

Chapter 6

Development of Improved Intensity Measures

6.1 Introduction

As discussed in Chapter 5, two parameters are involved in probabilistic seismic demand analysis (PSDA), i.e., engineering demand parameter (*EDP*) representing the structural response, and ground motion intensity measure (*IM*) representing the severity of future seismic motions. In the analyses conducted on the frames, the *EDP* was represented by the maximum interstorey drift (*IDR*), and the *IM* was represented by the spectral acceleration of the motions at the fundamental structural period, $Sa(T_1)$.

The *IDR* and the $Sa(T_1)$ (as *EDP* and *IM* respectively) have been widely used in the research work related to performance-based design, undertaken by the Pacific Earthquake Engineering Research (PEER) Center during the last decade. While there is a consensus regarding the suitability of the *IDR* for representing the structural demand, questions have been raised on the efficiency of $Sa(T_1)$ as an intensity measure. This is because $Sa(T_1)$ does not include the effects of the period elongation and the contribution of the higher modes to the structural response. However, $Sa(T_1)$ is still a popular *IM* because it is easy to use and attenuation relations are available for spectral accelerations.

In general, the *IM* is a very important parameter in PSDA, since it represents a link between the response of the structure determined from nonlinear time history analysis, and the ground motion hazard at the location of the structure obtained from probabilistic seismic hazard analysis (PSHA). As discussed in Chapter 1 (Section 1.3), advanced *IM*s have been developed in recent years. However, they are currently not used in practical applications because of different limitations. Given the advantage and the disadvantage of $Sa(T_1)$ relative to other *IM*s (Section 1.3), the focus of this thesis is to improve the *IM* based on $Sa(T_1)$ by including additional parameters to take into account the period elongation and the higher mode effects. For the purpose of this improvement, analyses were conducted to examine the period elongation of the frames used in this thesis. The results from the analyses are described in the following section.

6.2 Investigation of the period elongation

It is well known that reinforced concrete frame structures soften during nonlinear seismic response due to increased cracking and deterioration of the concrete at post-yield levels of deformation. One effect of this softening is the elongation of the structural vibration period. While softening is usually accompanied by a loss of strength, which is an undesirable effect, period elongation can be beneficial in reducing the effect of the seismic excitation because spectral accelerations generally decrease with increasing period. While there has been some evidence of the extent of period elongation from observations of structures damaged during earthquakes, there is limited information on the relationship between the extent of period elongation and intensity of strong seismic ground motions.

The objective of this investigation is to determine the elongation of the first mode periods of the 4S, the 10S, and the 16S frames. This was done using dynamic time history analysis of the frames. This section describes the method used and the results obtained from the analysis.

Analyses for determining the period elongation

When a structure is subjected to a seismic motion, the response of the structure represents a combination of the contributions of different modes. So, the periods of all the modes contributing to the response are contained in the response time history. When an increase in the modal periods occurs, as is the case during nonlinear response, then this increase can be seen in the response time history.

In this investigation, the displacement time histories of the roof responses of the frames were used to determine the period elongation. Each frame was subjected to the 40R set of records (Table B.2 in Appendix B) scaled to five intensity levels in terms of the spectral acceleration at the fundamental period of the frame models, i.e., $Sa(T_1)$. The intensity levels were the same as those used in the investigation of the elastic versus inelastic displacement-based intensity measures in Chapter 4. However, the intensity levels here are expressed in terms of spectral acceleration (rather than in terms of elastic spectral displacement as used in Chapter 4) for consistency with the other results presented in this chapter.

The five intensity levels selected for the analyses were $Sa(T_1)_{ref}$ to $5Sa(T_1)_{ref}$, where $Sa(T_1)_{ref}$ is defined in Chapter 4 (Table 4.1), and is named the *reference* intensity level. As discussed in Chapter 4, records scaled to the reference intensity level are expected to

produce responses corresponding to a 'global' ductility of about 1.0 (i.e., elastic responses). So, the selected intensity levels $Sa(T_1)_{ref}$ to $5Sa(T_1)_{ref}$ are intended to produce 'global' ductilities of approximately 1.0 to 5.0 respectively. Intensity levels higher than $5Sa(T_1)_{ref}$ were not considered since a number of records produce collapses (i.e., interstorey drifts larger than the ultimate drift of 5%). Expressed in terms of spectral acceleration, $Sa(T_1)$, the intensity levels range from 0.18 g to 0.90 g for the 4S frame, from 0.14 g to 0.70 g for the 10S frame, and from 0.11 g to 0.55 g for the 16S frame. The selected intensities are considered to be suitable for the investigation of the period elongation since they produce responses to the frames that are well in the inelastic range (see drift responses corresponding to the foregoing intensity levels in Figs. 4.2(a), 4.3(a), and 4.4(a) in Chapter 4).

For illustration, Fig. 6.1 shows the roof displacement responses of the 10S frame subjected to same motion but scaled to two intensity levels. The response in Fig. 6.1(a) is for the motion scaled to $Sa(T_1)_{ref}$ (i.e., 0.14 g) and that in Fig. 6.1(b) is for the motion scaled to $5Sa(T_1)_{ref}$ (i.e., 0.70 g). Considering the intensity levels of the excitations (discussed above), Fig. 6.1(a) represents elastic response, and Fig. 6.1(b) represents inelastic response of the frame. Note that the duration of the excitation motion is 40 s, and the last 10 seconds of the response time histories are free vibrations of the frame, after the end of the excitation. It can be seen that there are significant differences in the periods of the elastic and the inelastic responses. The elastic response (Fig. 6.1(a)) consists almost entirely of a single-period vibration, i.e., the elastic period of the first mode. The response in Fig. 6.1(b), however, shows much longer period (especially after the 10 s mark), which is the elongated first mode period of the frame as a result of inelastic deformations in the frame members. A

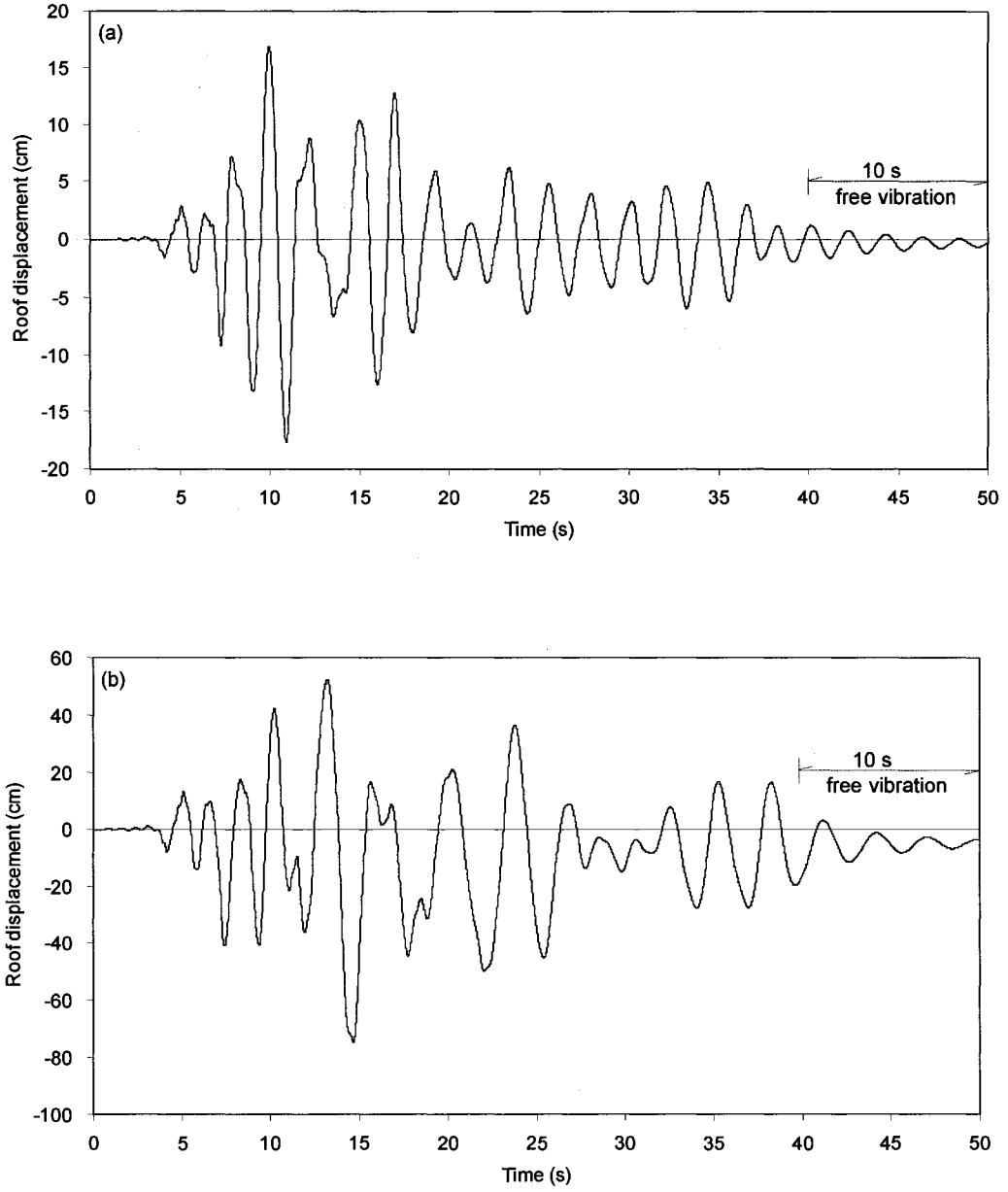

Figure 6.1 Displacement time histories of the roof response of the 10S frame subjected to ground motion scaled to: (a) $Sa(T_1)$=0.14 g, and (b) $Sa(T_1)$=0.70 g.

residual displacement resulting from inelastic deformations is also seen at the end of the free vibration in Fig. 6.1(b).

To quantify the elongation of the first mode period, Fourier amplitude spectra were computed considering the duration of the forced vibration of the responses (e.g., the first 40 seconds in Fig. 6.1). For some of the motions there were difficulties in identifying the elongated first mode period because several vibration periods were present in the Fourier spectra. Given this, the elongation of the first mode period was determined by considering *only* the free vibration, after the end of the excitation motion. For each excitation motion, 10 seconds free vibration was considered. Figure 6.2 shows the Fourier amplitude spectra of the free vibration responses in Fig. 6.1. It is seen that the period of the elastic response (Fig. 6.1(a)) is about 2.0 s which is close to the elastic first mode period of the 10S frame (T_1=1.96 s), and the period of the inelastic response (Fig. 6.1(b)) is 2.9 s, i.e., about 50% larger than T_1=1.96 s. Since these periods are determined from the free vibrations, after the end of the excitation motions, they are referred to as the post-excitation periods.

Discussion of results

The post-excitation first mode periods obtained from the analyses of the 4S, the 10S, and the 16S frames are shown in Figs. 6.3(a), 6.3(b), and 6.3(c) respectively. The five stripes of results correspond to the excitation levels used in the analyses. Lines connecting the mean values of the periods at each excitation level are included in the figures to illustrate the general trends of the computed periods. The *elastic* first mode periods of the frames are also shown in the figures.

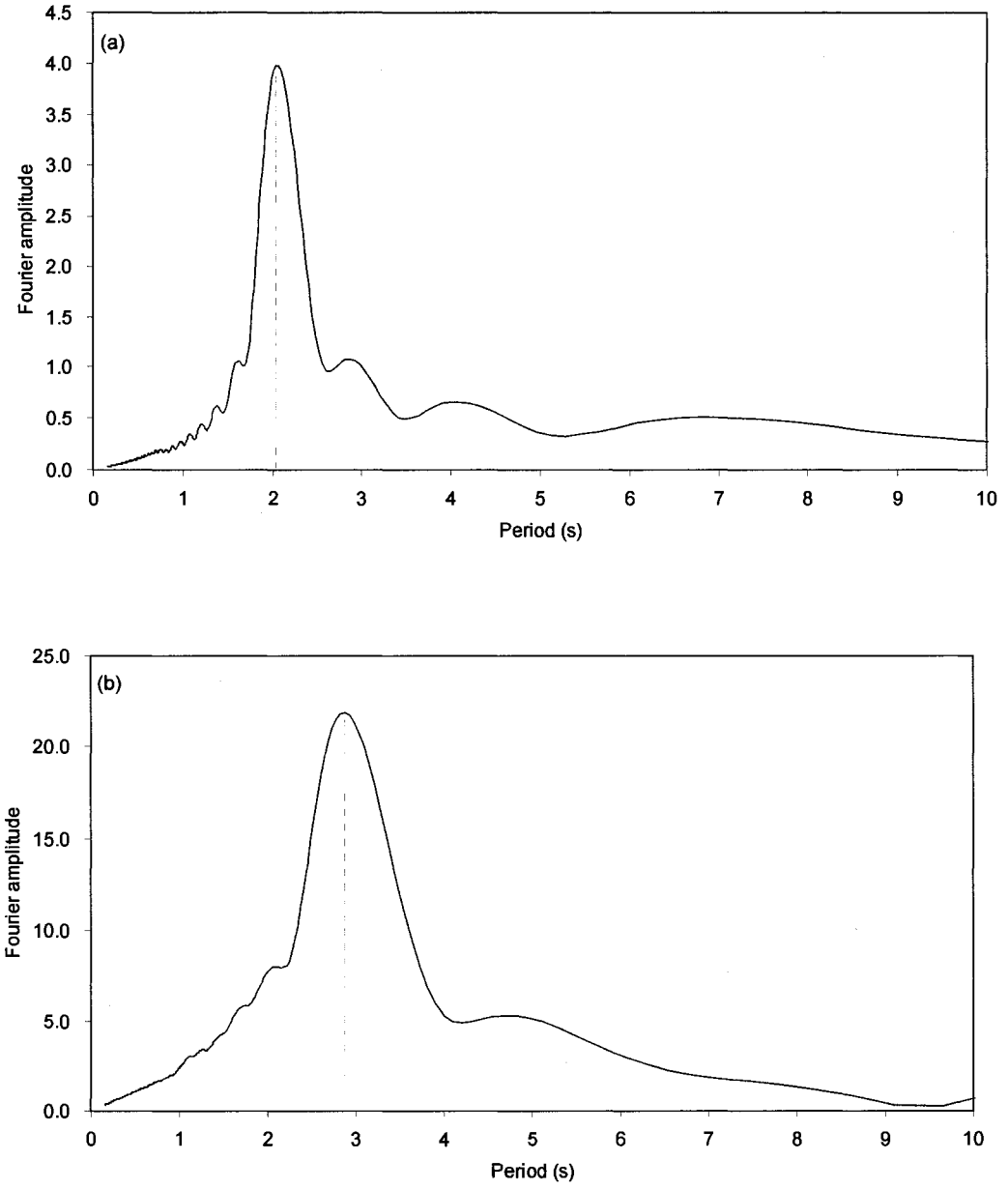

Figure 6.2 Fourier amplitude spectra for the free vibrations of the 10S frame (after the forced vibrations) due to ground motion scaled to: (a) $Sa(T_1)$=0.14 g, and (b) $Sa(T_1)$=0.70 g.

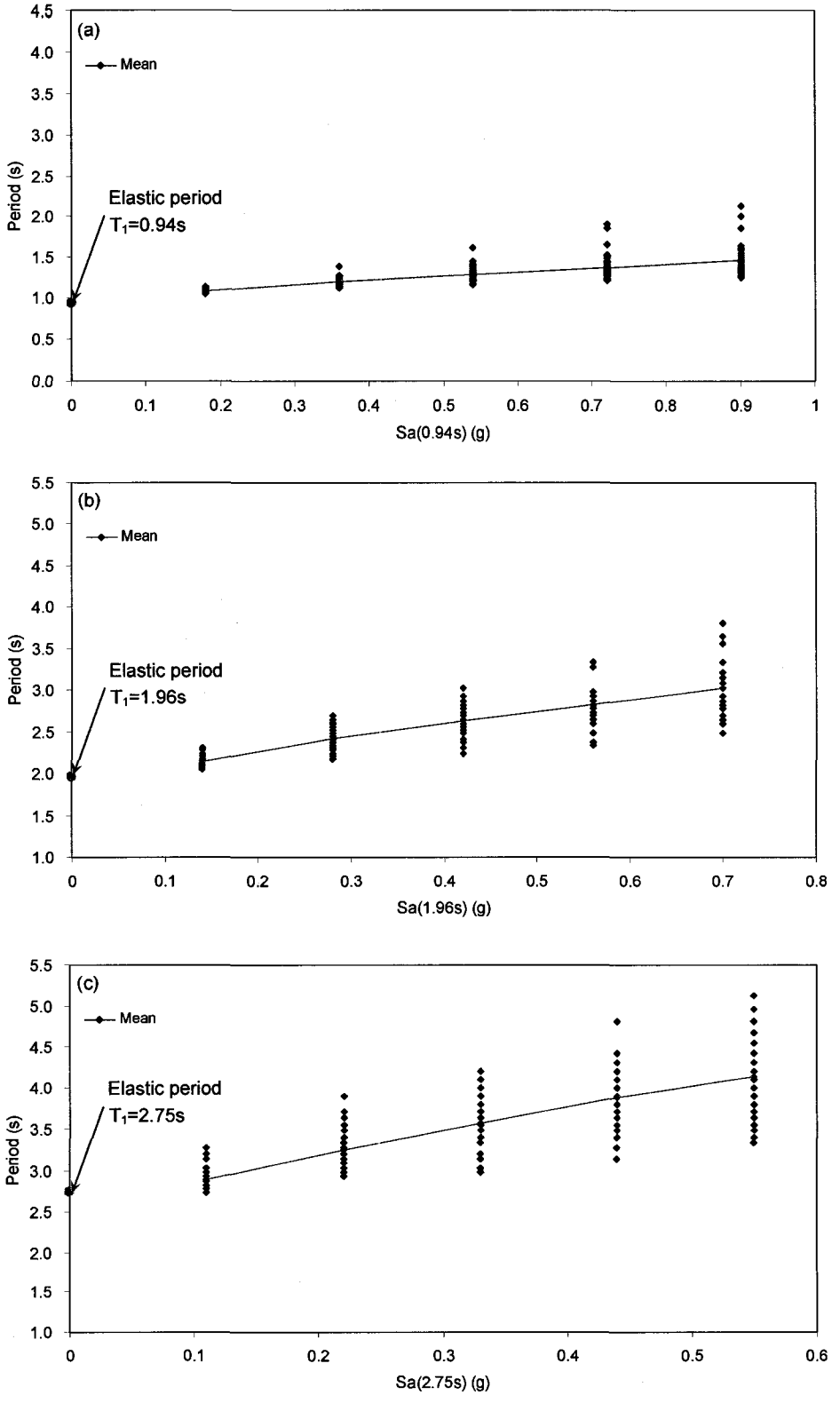

Figure 6.3 Post-excitation periods of the frames for ground motions scaled to five intensity levels of $Sa(T_1)$: (a) for the 4S frame, (b) for the 10S frame, and (c) for the 16S frame.

It can be seen from Fig. 6.3 that the *mean* periods increase almost linearly with the increase of the excitation. It was found from the figure that the mean period increase for the highest excitation level ($5Sa(T_1)_{ref}$) is about 55% for all three frames. This is consistent with the findings reported by Heidebrecht and Naumoski (2000). They investigated the period elongation of a six-storey reinforced concrete frame building designed for Vancouver. The increase of the mean periods for the highest excitation levels shown in Fig. 6.3 is comparable to that observed by Heidebrecht and Naumoski (2000) for similar excitations.

It is also seen in Fig. 6.3 that the dispersion of the periods increases with the increase of the excitation. At the highest excitation level, the dispersion expressed by the coefficient of variation (COV) (which represents the ratio of the standard deviation to the mean period, i.e., σ/μ) is about 0.13 for all three frames.

Figure 6.3 also shows that the computed periods for excitations scaled to the *reference* intensity levels of the frames (i.e., the results for $Sa(T_1)$ of 0.18 g, 0.14 g, and 0.11 g for the 4S, the 10S, and the 16S frame respectively) are somewhat larger than the elastic periods of the frames. This indicates that the responses of the frames at the *reference* intensity levels are not purely elastic, but some inelastic deformations occur during the responses resulting in small lengthening of the elastic periods. This is expected given the assumptions involved in the estimation of the reference levels, as discussed in Chapter 4.

In general, Fig. 6.3 shows that the period elongation can be significant for higher excitation levels as a result of the softening of the frames due to inelastic deformations during the response. Given this, the effects of the period elongation on the structural response need to be taken into account by the intensity measure. An approach for achieving this is described in the following sections.

6.3 Formulation of improved intensity measures

A preferable intensity measure (*IM*) would be one that: (i) takes into account the effects of at least the first and the second modes of vibration, (ii) includes the effects of the first mode period elongation, and (iii) can be easily used in PSDA. It is also important that attenuation relation for the *IM* is available or can be developed using existing attenuation relations. Using spectral acceleration (*Sa*) as a response parameter, an *IM* (designated S_N, where *N* stands for 'new') that satisfies these requirements can be expressed in a general form as:

$$S_N = Sa(T_1)^{\alpha} \cdot Sa(T_2)^{\beta} \cdot Sa(T_f)^{\gamma} \tag{6.1}$$

where T_1 and T_2 are elastic periods of the first and the second modes respectively, and T_f is the lengthened period of the first mode. The exponents α, β, and γ are intended to represent the 'weights' of the contributions of $Sa(T_1)$, $Sa(T_2)$, and $Sa(T_f)$ respectively, to the structural response. The sum of the weights must be 1. Note that the exponents in Equation 6.1 and in similar equations throughout the next chapters, apply to the *Sa* values for the specific periods, and not to the periods in brackets.

While this would be a 'perfect' *IM*, it is difficult to apply such an *IM* because of the complexity associated with the determination of the parameters α, β, γ, and T_f. Even for a single structure, thousands of time-history analyses are required to determine optimum values for these parameters. Other difficulties that would be faced are associated with the accuracy of the attenuation relation for such an *IM*. Based on experience in this study, the uncertainties in the attenuation relation for a given *IM* increase significantly with the increase of the number of structural periods involved in the *IM*.

To simplify the problem, the issues on the period elongation and the second mode effects were considered separately. Two *IM*s were investigated, i.e., one that takes into account the period elongation (denoted S_{N1}) and another one that takes into account the second mode effects (denoted S_{N2}). These are expressed as follows:

$$S_{N1} = Sa(T_1)^{\alpha} \cdot Sa(C \cdot T_1)^{1-\alpha} \tag{6.2}$$

$$S_{N2} = Sa(T_1)^{\beta} \cdot Sa(T_2)^{1-\beta} \tag{6.3}$$

Note that the meanings of the coefficients α and β in these equations are different from the meanings of the same coefficients in Equation (6.1). It can be seen in Equation (6.2) that the elongated period is expressed as a product of the elastic first mode period T_1 and a constant C, i.e., $T_f = C \cdot T_1$. This is a significant approximation since the elongation of the period depends on the excitation level (as discussed in Section 6.2). However, the results showed that even with this approximation, the intensity measure S_{N1} is superior compared to that represented by $Sa(T_1)$ alone (see Section 6.4.1).

Equations (6.2) and (6.3) are based on the assumption that the response of a specific structure is dominated exclusively either by the first mode effects and the period elongation of that mode, or by the first and the second mode effects. While this assumption was based on a preliminary investigation, the results from detailed analyses showed that it is true, as discussed below in this chapter. It should be mentioned that intensity measure similar to that expressed by Equation (6.2) has been considered by Cordova et al. (2000) for composite frames consisting of reinforced concrete columns and steel beams, and steel frames.

The objective of this thesis is to determine the optimal values for the coefficients α, β, and C of the intensity measures S_{N1} and S_{N2} (Equations 6.2 and 6.3) for use in PSDA for moment-resisting reinforced concrete frame buildings. This required a number of time history analyses, as discussed in the following section.

6.4 Analyses for the intensity measures S_{N1} and S_{N2}

For the purpose of determining the coefficients included in S_{N1} and S_{N2}, time history analyses were conducted on the 4S, the 10S, and the 16S frames for excitation motions represented by the records of the 20R set (Table B.3, Appendix B). For each frame, three excitation levels were used in the analyses, i.e., $3Sa(T_1)_{ref}$, $4Sa(T_1)_{ref}$, and $5Sa(T_1)_{ref}$, which are expected to produce responses with average 'global' ductilities of about 3, 4, and 5 respectively (Chapter 4). These levels were selected based on observations in Chapter 5 that intensities between approximately $3Sa(T_1)_{ref}$ and $5Sa(T_1)_{ref}$ have significant contributions to the drift hazard curves for the frames.

The $Sa(T_1)$ intensity levels corresponding to the levels $3Sa(T_1)_{ref}$, $4Sa(T_1)_{ref}$, and $5Sa(T_1)_{ref}$ are given in Table 6.1. The first mode periods of the frames, T_1, are also shown in the table. Note that the $Sa(T_1)$ intensity levels need to be expressed in terms of S_{N1} and S_{N2}

Table 6.1 $Sa(T_1)$ values corresponding to the excitation levels used in the development of the improved intensity measures.

Intensity level	Sa(T_1) values (in g) for:		
	4S frame (T_1=0.94s)	10S frame (T_1=1.96s)	16S frame (T_1=2.75s)
$3Sa(T_1)_{ref}$*	0.54	0.42	0.33
$4Sa(T_1)_{ref}$	0.72	0.56	0.44
$5Sa(T_1)_{ref}$	0.90	0.70	0.55

*The *reference* excitation levels for the frames ($Sa(T_1)_{ref}$) are given in Table 4.1.

levels in order to determine the optimal coefficients of the new intensity measures S_{N1} and S_{N2}, as described in Sections 6.4.1 and 6.4.2.

The standard deviation of the maximum interstorey drifts at each excitation level was used as a criterion for determining the optimal values for the coefficients of the new *IM*s. Optimal coefficients were considered those that provide the smallest standard deviations of the interstorey drifts. The standard deviations corresponding to the optimal coefficients were compared to those obtained from the use of $Sa(T_1)$ as *IM* to see the advantage of the proposed *IM*s relative to $Sa(T_1)$. Two separate sets of analyses were conducted on the frames, i.e., one set for S_{N1} (Equation (6.2)) to determine the coefficients C and α, and another set for S_{N2} (Equation (6.3)) to determine the coefficient β, as described hereafter.

6.4.1 Intensity measure S_{N1} – effects of period elongation

As seen in Equation (6.2), the coefficients C and α need to be determined for the intensity measure S_{N1}. This was done for each of the frames considered in this thesis. To determine the optimal coefficients C and α, 'trial' values for the coefficients were selected for use in the analysis. These include:

- C = 1.5, and 2.0,
- α = 0.25, 0.50, and 0.75.

The values of C=1.5 and C=2.0 were chosen by considering the period elongation of the frames (Fig. 6.3). As seen in Fig. 6.3, C=1.5 corresponds approximately to the *mean* period elongation resulting from excitation motions at intensity level $5Sa(T_1)_{ref}$. It is useful

to mention that C=1.5 is used in the ASCE/SEI 7-05 Standard (ASCE 2006) as a period elongation factor for use in the selection of seismic design motions.

The value of C=2.0, on the other hand, was selected to represent an upper bound of the period elongation for excitation motions at intensity level $5Sa(T_1)_{ref}$. It can be seen from Fig. 6.3 that for C=2.0 almost all the periods in the figure are below the levels $C \cdot T_1$=1.88 s (i.e., 2 x 0.94 s) for the 4S frame, 3.9 s for the 10S frame, and 5.5 s for the 16S frame.

It is important to mention that C is intended to represent an average period elongation factor over the entire range of responses used in PSDA (see Chapter 5). For elastic responses C is approximately 1.0, and for inelastic responses corresponding to the highest excitation levels used in the PSDA, C might be significantly larger than 2.0. The values of C=1.5 and C=2.0, estimated as discussed above, are believed to be close to one third and two thirds of the C range for the excitation levels used in PSDA, and are considered to be appropriate for this study. The objective of the analyses, described hereafter, was to determine which of the 'trial' values for C and α are the most suitable for use in the S_{NI} intensity measure.

Since the conventional *IM* represented by $Sa(T_1)$ is widely used in PSDA, this *IM* was used as a *reference* in the analyses for S_{NI}. This was necessary in order to compare the dispersions (i.e., the standard deviations) of the maximum interstorey drifts (*IDR*s) obtained from the use of S_{NI} and $Sa(T_1)$ as intensity measures. The dispersion was considered because it is an indicator of the efficiency of an intensity measure, as discussed in detail in the next chapter.

Since the dispersion depends on the *mean* value, it was necessary to scale the records such that the *mean* values of the *IDR*s resulting from the use of S_{NI} and $Sa(T_1)$ as

intensity measures are relatively close. This means that for a given intensity level $Sa(T_1)=sa^*$, a corresponding 'target' $S_{N1}=sn1^*$ was required such that the records scaled to $sn1^*$ provide similar mean value of the *IDR*s as that obtained from the records scaled to $Sa(T_1)=sa^*$. This was not straightforward because S_{N1} and $Sa(T_1)$ are different representations of the intensity of ground motions. After considering several approaches, the 'target' intensity level $sn1^*$ was determined using the equation:

$$sn1^* = \left(\frac{\mu_{S_{N1}}}{\mu_{Sa(T_1)}} \right) \cdot sa^* \tag{6.4}$$

where $\mu_{S_{N1}}$ represents the mean of the S_{N1} values of the records for specified C and α, and $\mu_{Sa(T_1)}$ is the mean of the $Sa(T_1)$ values of the records. Having determined the 'target' level $sn1^*$, each record was scaled to this level using the S_{N1} value of the record. It was found that Equation (6.4) is quite suitable for scaling the records, as illustrated by Fig. 6.4.

Figure 6.4 shows the maximum interstorey drifts obtained from time-history analyses of the 4S frame for the records scaled to the three $Sa(T_1)$ levels: 0.54 g, 0.72 g, and 0.90 g (i.e., $3Sa(T_1)_{ref}$, $4Sa(T_1)_{ref}$, and $5Sa(T_1)_{ref}$) and to the corresponding S_{N1} levels of 0.39 g, 0.53 g, and 0.65 g obtained from Equation (6.4). The S_{N1} levels were computed for C=1.5 and α=0.50. Note that the horizontal axis is in terms of the $Sa(T_1)$ levels, and the computed drifts for both types of scaling are shown close to each other for easier comparison. The mean values of the drifts are also shown in the figure. It can be seen that the mean drifts for the S_{N1} scaling are similar to those for the $Sa(T_1)$ scaling, as was intended in the determination of the S_{N1} scaling levels (Equation 6.4). However, the dispersion of the drifts

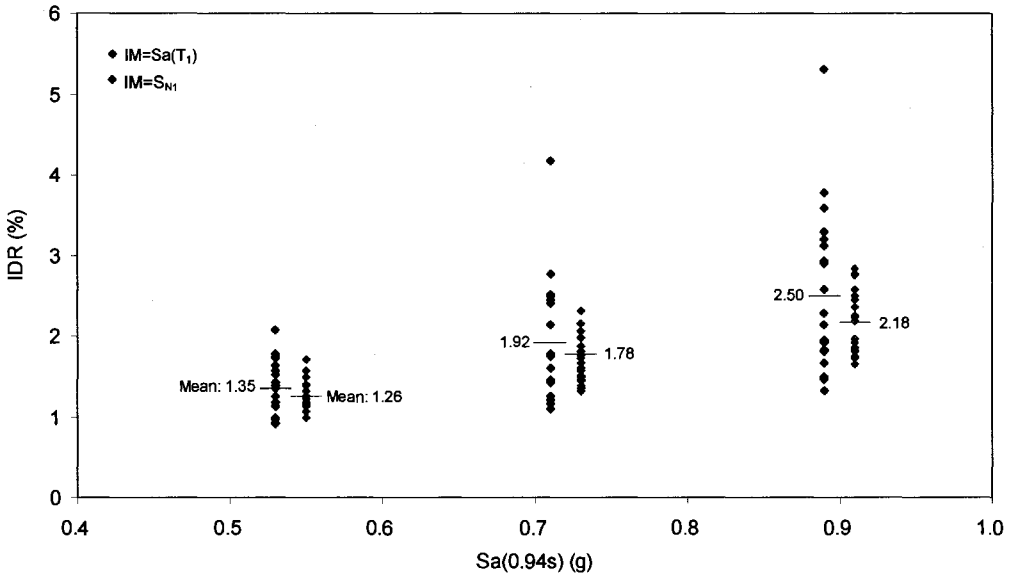

Figure 6.4 Maximum interstorey drifts for the 4S frame for seismic excitations scaled to three intensity levels of $Sa(T_1)$ and S_{N1}.

for the S_{N1} scaling is smaller than that for the $Sa(T_1)$ scaling. A detailed discussion of the dispersion of the drifts is given below in this section.

It is useful to note that the approach for scaling to S_{N1} described above (Equation 6.4) was employed in order to compare the dispersions of the *IDRs* resulting from the use of S_{N1} with those obtained from the use of $Sa(T_1)$. Otherwise, the records can be scaled to any series of selected S_{N1} levels.

The results from the analyses of the 4S, the 10S, and the 16S frames are presented in Figs. 6.5, 6.6, and 6.7 respectively. Figures 6.5(a), 6.6(a), and 6.7(a) show the standard deviations (i.e., the dispersions) of the maximum interstorey drifts, $\sigma_{\ln IDR}$, obtained using the intensity measure S_{N1}. For comparison, the results for $Sa(T_1)$ as *IM* are also shown in these figures. To determine the amounts of decrease (or increase) of the dispersions of the maximum drifts for IM=S_{N1} relative to those for IM=$Sa(T_1)$, Figures 6.5(b), 6.6(b), and

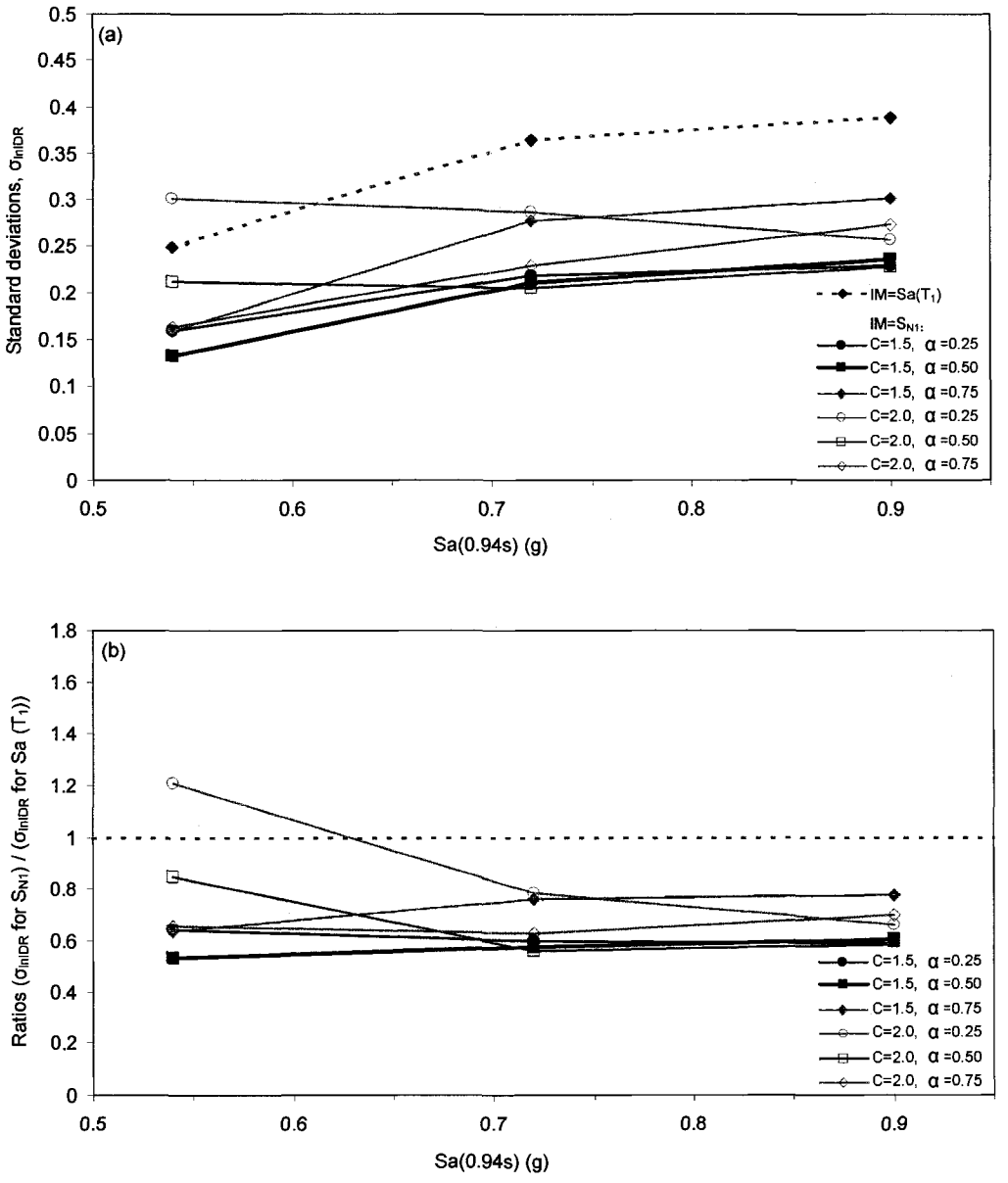

Figure 6.5 Results for dispersion of maximum interstorey drifts for selected C and α for the 4S frame: (a) Standard deviations, $\sigma_{\ln IDR}$, and (b) Ratios ($\sigma_{\ln IDR}$ for S_{N1}) / ($\sigma_{\ln IDR}$ for $Sa(T_1)$).

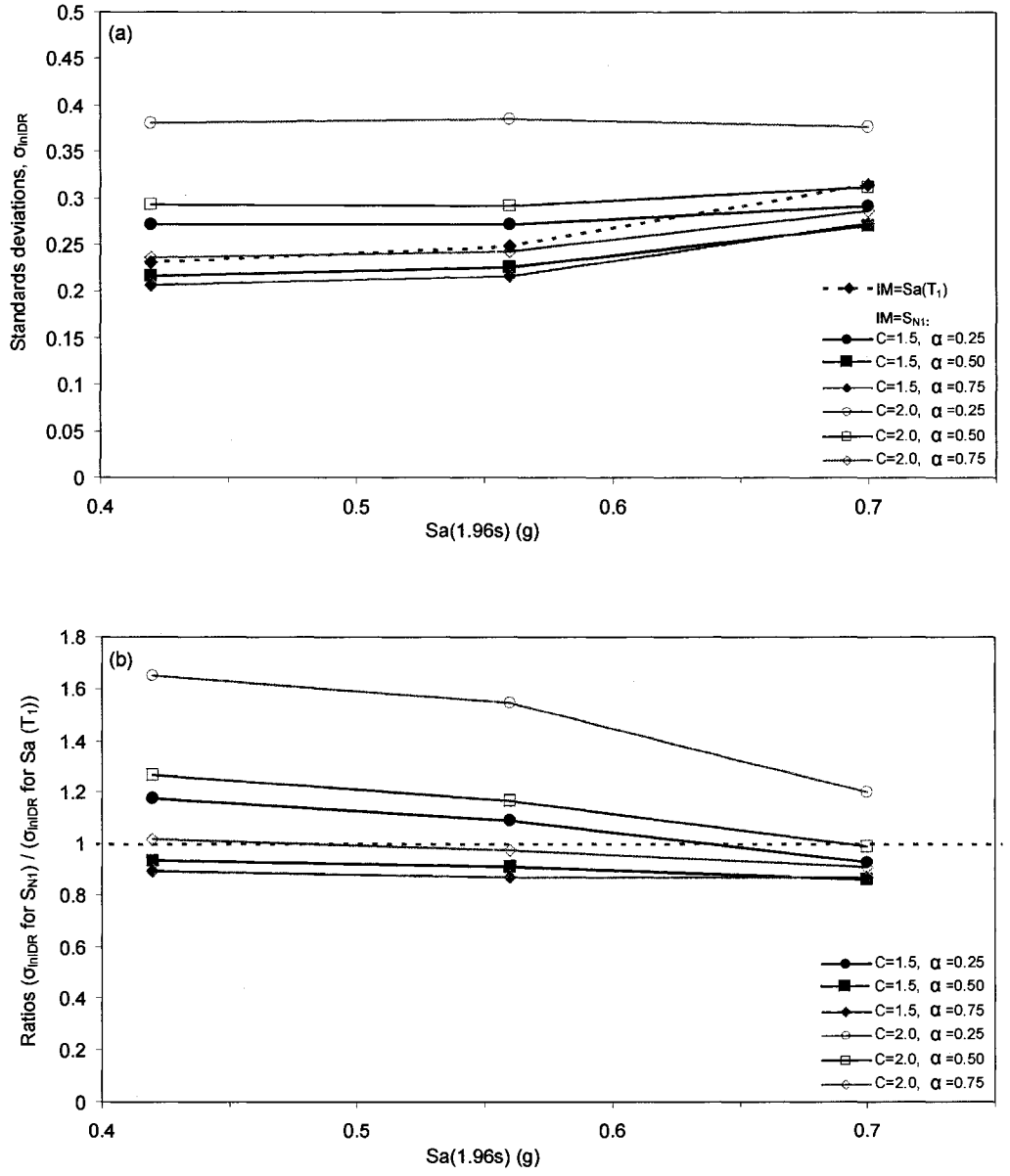

Figure 6.6 Results for dispersion of maximum interstorey drifts for selected C and α for the 10S frame: (a) Standard deviations, $\sigma_{\ln IDR}$, and (b) Ratios ($\sigma_{\ln IDR}$ for S_{N1}) / ($\sigma_{\ln IDR}$ for $Sa(T_1)$).

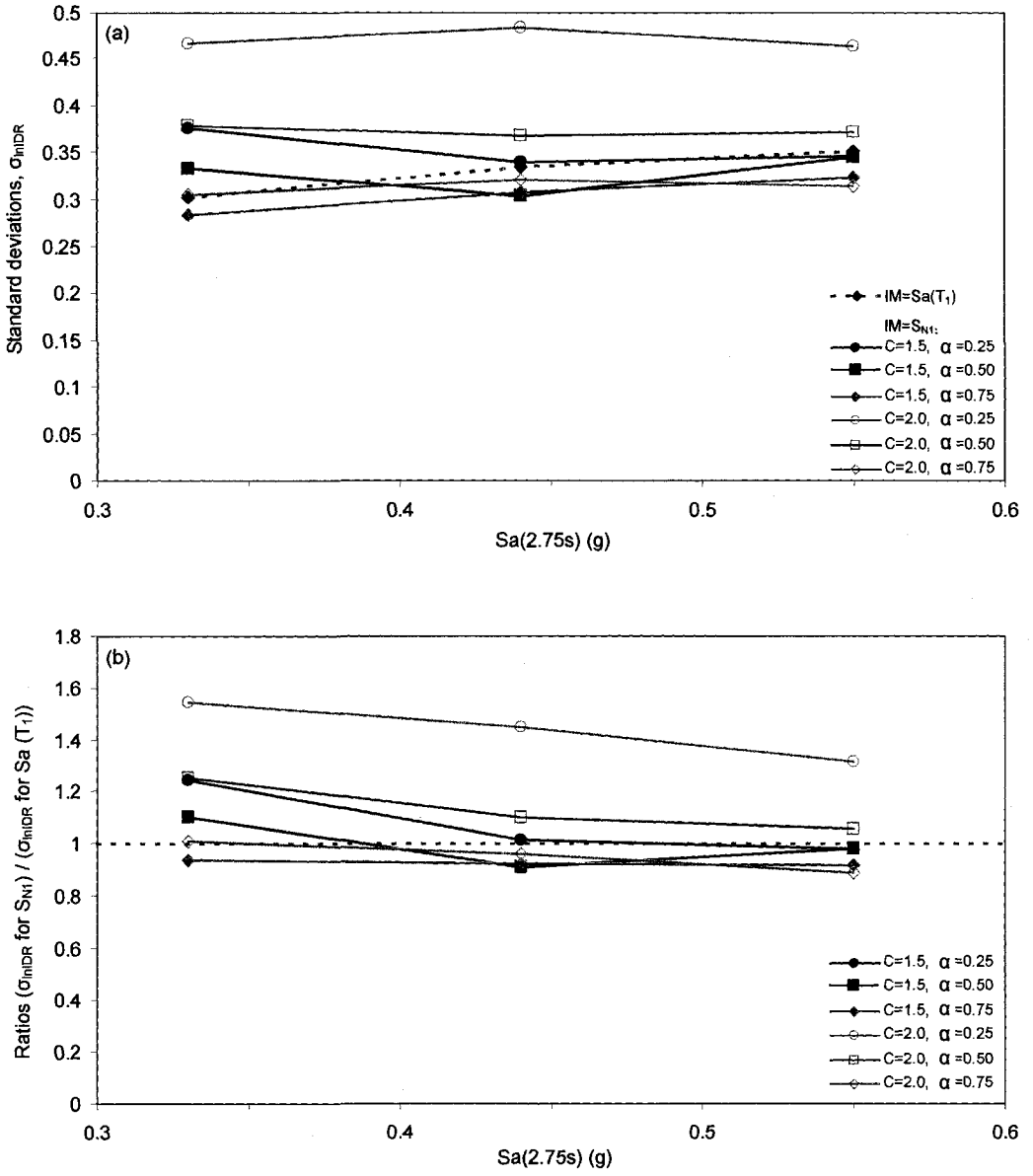

Figure 6.7 Results for dispersion of maximum interstorey drifts for selected C and α for the 16S frame: (a) Standard deviations, $\sigma_{\ln IDR}$, and (b) Ratios ($\sigma_{\ln IDR}$ for S_{N1}) / ($\sigma_{\ln IDR}$ for $Sa(T_1)$).

6.7(b) show the ratios of the standard deviations $\sigma_{\ln IDR}$ for IM=S_{NI} to those for IM=$Sa(T_1)$. These ratios are designated in the figures as ($\sigma_{\ln IDR}$ for S_{NI}) / ($\sigma_{\ln IDR}$ for $Sa(T_1)$). In each figure, the results are presented by three stripes of points (symbols) corresponding to the three excitation levels used in the analyses. For easier identification of the results, the symbols for each C and α combination are connected by lines. The horizontal axes are in terms of the $Sa(T_1)$ levels (Table 6.1).

Figure 6.5(a) shows that for almost all the cases, the $\sigma_{\ln IDR}$ values corresponding to S_{NI} are smaller than those obtained for $Sa(T_1)$. This indicates that S_{NI} is a better intensity measure than $Sa(T_1)$ for the 4S frame. The figure also shows that overall, the smallest $\sigma_{\ln IDR}$ values correspond to C=1.5 and α=0.50 (designated by a bold line in the figure). Given this, the values of C=1.5 and α=0.50 are considered as optimal values for use in S_{NI} for the 4S frame. As shown in Fig. 6.5(b), the dispersion of the interstorey drifts resulting from the use of S_{NI} with C=1.5 and α=0.50 is about 40% to 50% smaller than that resulting from the use of $Sa(T_1)$ as IM.

The observations for the 10S and the 16S frames (Figs. 6.6 and 6.7 respectively) regarding the use of S_{NI} as IM are quite different from those for the 4S frame. Comparing the $\sigma_{\ln IDR}$ results for S_{NI} with the corresponding results for $Sa(T_1)$ in Figs. 6.6(a) and 6.7(a), it is seen that the use of S_{NI} as IM produces a very slight reduction in the $\sigma_{\ln IDR}$ results for some of the α values used with C=1.5, and almost no reduction for the cases with C=2.0. As seen from the ratios of the $\sigma_{\ln IDR}$ values for S_{NI} to those for $Sa(T_1)$ (Figs. 6.6(b) and 6.7(b)), the maximum reduction is less than 15% for the 10S frame and less than 10% for the 16S frame, which is negligible from a practical point of view. This means that the intensity measure S_{NI} does not have an advantage for the 10S and the 16S frames relative to

the intensity measure represented by $Sa(T_1)$. It is believed that the small reduction in the dispersion resulting from the use of S_{N1} as an *IM* is related to the shape of the spectra at long periods. Namely, for periods longer than approximately 2.0 s, the spectra are almost 'flat', i.e., there is no significant change in the spectral shape between T_1 and $C \cdot T_1$, and consequently, the effects of the elongated periods on the structural responses are small.

In summary, the results showed that the new intensity measure S_{N1} (Equation 6.2) with C=1.5 and α=0.50 is effective for the 4S frame, but it is not the case for the 10S and the 16S frames. Using these values for C and α, Equation (6.2) can be written as:

$$S_{N1} = Sa(T_1)^{0.5} \cdot Sa(1.5T_1)^{0.5} \tag{6.5}$$

It is believed that this intensity measure is, in general, effective for short-period (i.e., first mode dominated) frames.

6.4.2 Intensity measure S_{N2} – effects of the second mode

The objective of the analyses described in this section is to determine the optimal value for the coefficient β used in the intensity measure S_{N2} defined by Equation (6.3). As discussed earlier, this *IM* is intended to represent the intensity of seismic motions by taking into account the spectral accelerations at the elastic periods of the first and the second modes of the structure considered, i.e., to take into account the contributions of the first and the second modes to the response.

The procedure for determining the optimal value for the coefficient β used in S_{N2} is the same as that applied in the investigation of the intensity measure S_{N1}, except that now only one coefficient is required to be determined, rather than two as required for S_{N1}. The same records (i.e., the 20R set), and the same excitation levels were used in the analyses.

The scaling of the records is described in the previous section. The equation for determining the 'target' scaling levels $sn2^*$ was the same as Equation (6.4), except that $\mu_{S_{N2}}$ was used instead $\mu_{S_{N1}}$.

The main parameters required for determining the optimal value for the coefficient β are the 'trial' values for β, and the elastic periods of the first and second modes of the frames. The selected 'trial' values for β were 0.50, 0.75, and 0.85. The elastic periods of the first and second modes are T_1=0.94 s and T_2=0.27 s for the 4S frame, T_1=1.96 s and T_2=0.70 s for the 10S frame, and T_1=2.75 s and T_2=1.02 s for the 16S frame (Table 2.2).

The results from the analyses of the 4S, the 10S, and the 16S frame are presented in Figs. 6.8, 6.9, and 6.10 respectively. Figures 6.8(a), 6.9(a), and 6.10(a) show the standard deviations of maximum interstorey drifts, $\sigma_{\ln IDR}$, obtained using the new intensity measure S_{N2} and those obtained using the 'traditional' intensity measure $Sa(T_1)$. Figures 6.8(b), 6.9(b), and 6.10(b) show the ratios of the standard deviations $\sigma_{\ln IDR}$ obtained for S_{N2} to those obtained for $Sa(T_1)$, i.e., ($\sigma_{\ln IDR}$ for S_{N2}) / ($\sigma_{\ln IDR}$ for $Sa(T_1)$).

For the 4S frame, it can be seen in Fig. 6.8(a) that the $\sigma_{\ln IDR}$ values for β=0.75 and β=0.85 are somewhat smaller than those obtained for $Sa(T_1)$. However, the decrease is not significant. Figure 6.8(b) shows that the maximum decrease is about 10%, which is not of importance for practical applications. This shows that S_{N2} as *IM* is not efficient for the 4S frame compared to $Sa(T_1)$. This is because the second mode effects for the 4S frame are quite small, i.e., the response of the frame is dominated by the first mode.

The results for the 10S and the 16S frames in Figs. 6.9(a) and 6.10(a) show that the smallest $\sigma_{\ln IDR}$ values for both frames correspond to β=0.75. Based on this observation, β=0.75 is considered as optimal value for these frames. As shown in Figs. 6.9(b) and

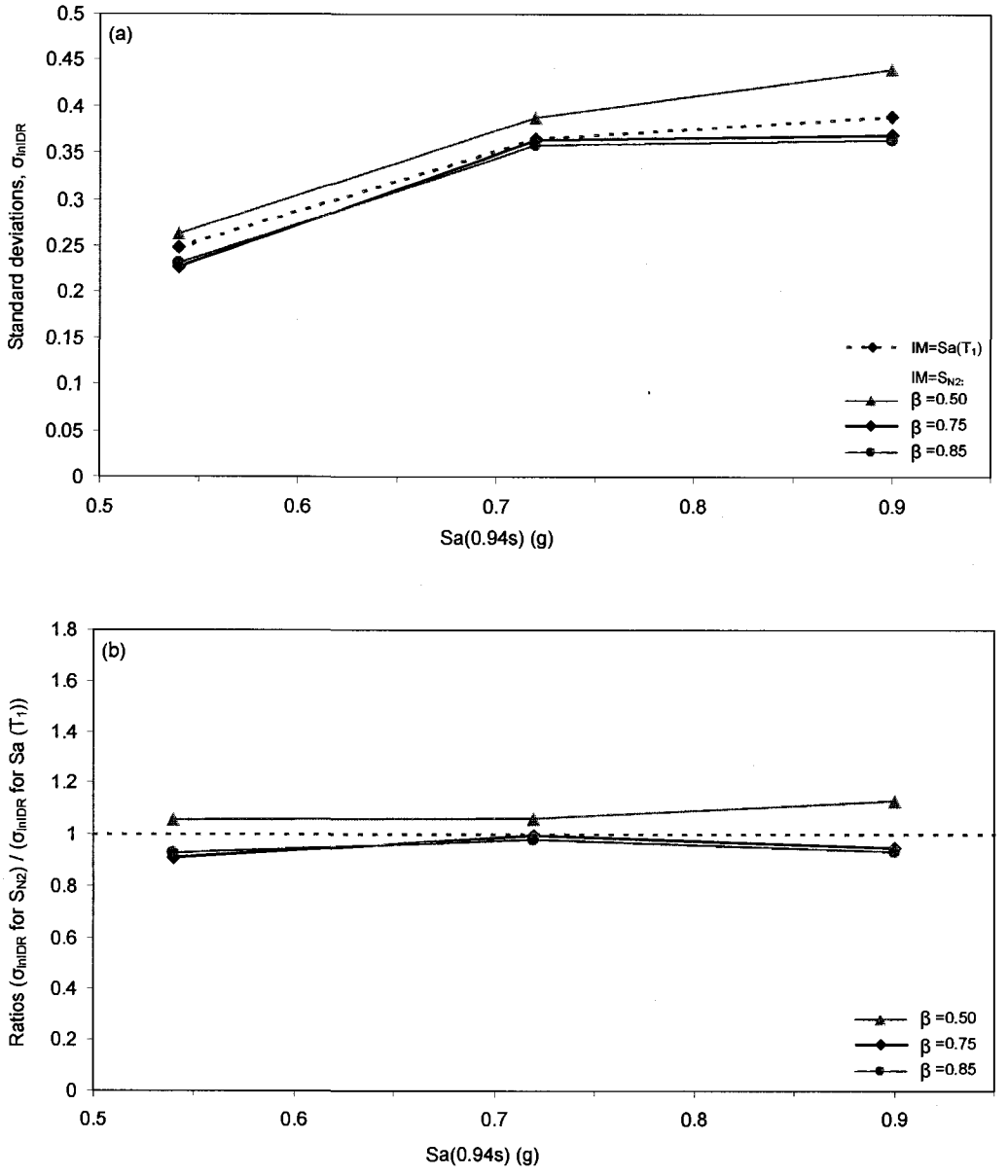

Figure 6.8 Results for dispersion of maximum interstorey drifts for selected β values for the 4S frame: (a) Standard deviations, $\sigma_{\ln IDR}$, and (b) Ratios ($\sigma_{\ln IDR}$ for S_{N2}) / ($\sigma_{\ln IDR}$ for $Sa(T_1)$).

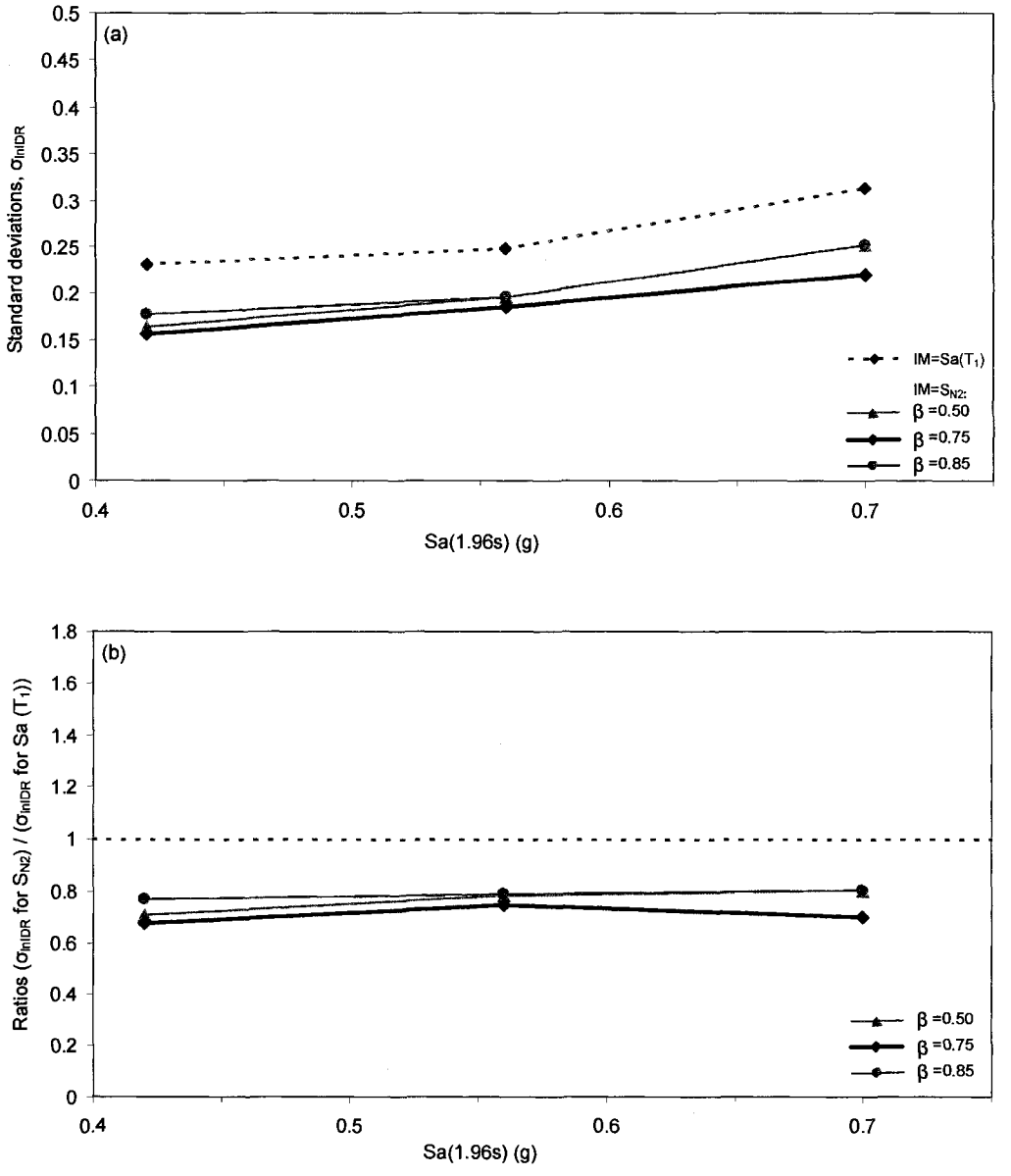

Figure 6.9 Results for dispersion of maximum interstorey drifts for selected β values for the 10S frame: (a) Standard deviations, $\sigma_{\ln IDR}$, and (b) Ratios ($\sigma_{\ln IDR}$ for S_{N2}) / ($\sigma_{\ln IDR}$ for $Sa(T_1)$).

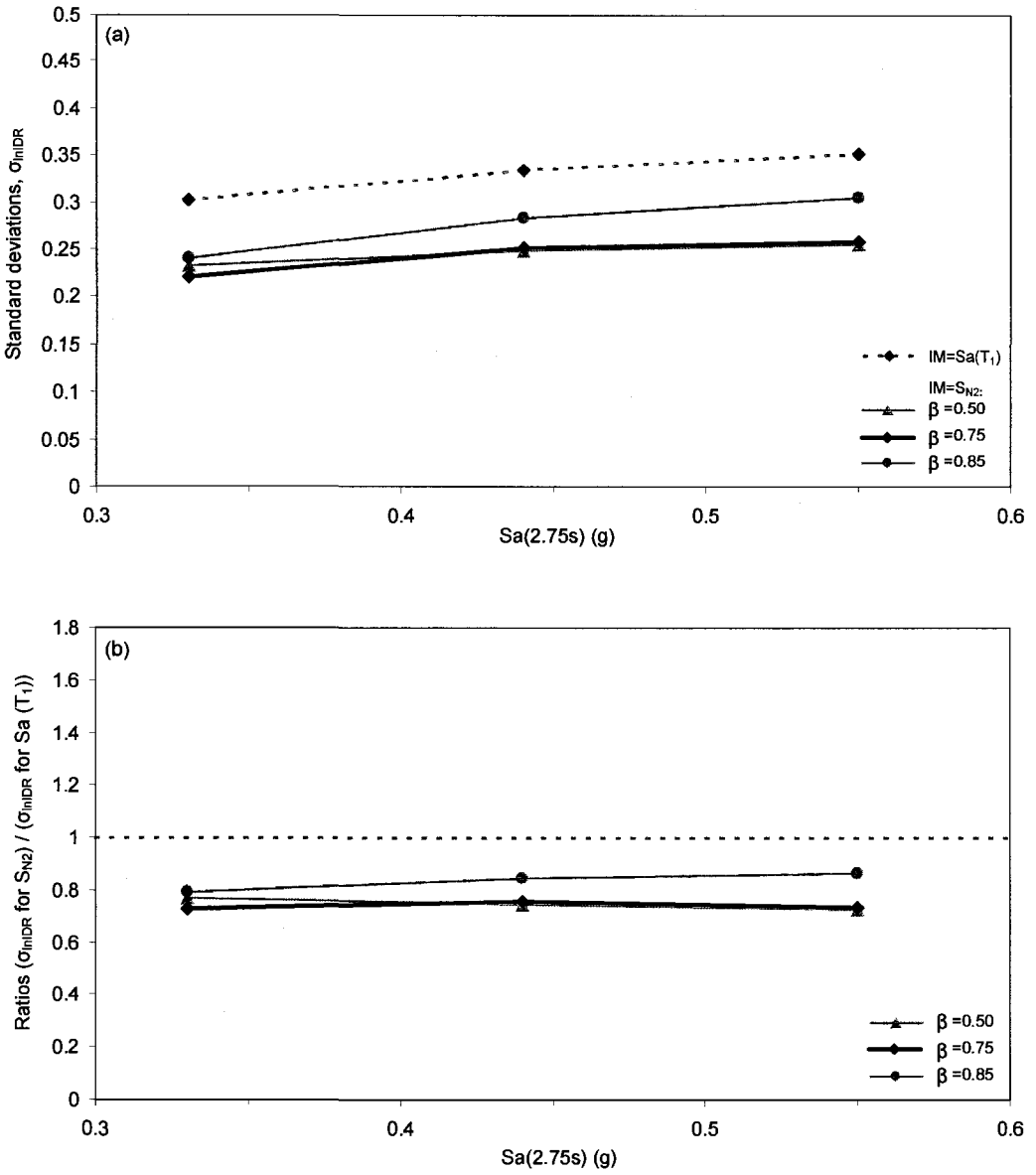

Figure 6.10 Results for dispersion of maximum interstorey drifts for selected β values for the 16S frame: (a) Standard deviations, $\sigma_{\ln IDR}$, and (b) Ratios ($\sigma_{\ln IDR}$ for S_{N2}) / ($\sigma_{\ln IDR}$ for $Sa(T_1)$).

6.10(b), the $\sigma_{\ln IDR}$ values for S_{N2} with β=0.75 are about 25% to 30% smaller than the values for $Sa(T_1)$. This indicates that the second mode has significant contributions to the responses of the 10S and the 16S frames, and the new intensity measure S_{N2} with β=0.75 is efficient for these frames. Using the value for β=0.75, Equation (6.3) is written as:

$$S_{N2} = Sa(T_1)^{0.75} \cdot Sa(T_2)^{0.25} \tag{6.6}$$

While the efficiency of S_{N2} as *IM* was proved for the 10S and the 16S frames, it is believed that this *IM* is, in general, appropriate for long-period structures (e.g., first mode period longer than about 1.5 s, see discussion below) since it is known that the second mode effects are significant for such structures.

6.5 Summary

Two improved intensity measures (*IM*s), designated S_{N1} and S_{N2}, are introduced in this chapter (Equations (6.2) and (6.3)), and their effectiveness is investigated for the frames considered in this thesis (i.e., the 4S, the 10S, and the 16S frames with first mode periods of 0.94 s, 1.96 s, and 2.75 s respectively). The intensity measure S_{N1} takes into account the elongation of the first mode period during nonlinear response of structures, and S_{N2} takes into account the contributions of the first and the second modes to the structural response. The effectiveness of S_{N1} and S_{N2} was assessed relative to the conventional *IM* represented by $Sa(T_1)$.

Both S_{N1} and S_{N2} involve coefficients for which 'optimal' values were required to be determined. This was done by conducting time history analyses on the frames for selected 'trial' values for the coefficients. Two separate sets of analyses were conducted, one set for

S_{N1} and another set for S_{N2}. Twenty earthquake records were used as excitation motions (Table B.3, Appendix B). The records were scaled to three intensity levels, which were selected as representative of ground motion intensities required for probabilistic seismic demand analyses of the frames. For each frame, intensity level, and a 'trial' value for a given coefficient of S_{N1} or S_{N2}, maximum interstorey drifts were computed for the twenty excitation motions. For the purpose of comparison, time history analyses were also performed using $Sa(T_1)$ as intensity measure.

The standard deviation of the maximum interstorey drifts at each excitation level was used as a criterion for determining the optimal values for the coefficients of the proposed *IM*s. Optimal coefficients were considered those that provide the smallest standard deviations of the interstorey drifts. The standard deviations corresponding to the optimal coefficients were compared to those obtained from the use of $Sa(T_1)$ as *IM* to see the advantage of the proposed *IM*s relative to $Sa(T_1)$.

It was found that the intensity measure S_{N1}, which takes into account the period elongation, is more effective than $Sa(T_1)$ for the 4S frame. On the other hand, the intensity measure S_{N2}, which takes into account the first and second mode contributions to the response, is more effective for the 10S and the 16S frames. The general conclusion that can be drawn is that S_{N1} is more suitable than $Sa(T_1)$ for first mode dominated frames (i.e., frames with shorter fundamental periods), and S_{N2} is more suitable for frames for which the second mode contribution to the response is significant (i.e., frames with long fundamental periods). While this study indicates that the period of approximately 1.5 s can be assumed to separate the period ranges of applicability of S_{N1} and S_{N2}, more research is needed to confirm this.

Chapter 7

Validation of the Proposed Intensity Measures

7.1 Introduction

Research work has shown that in order to ensure a satisfactory accuracy in the assessment of the structural performance using probabilistic seismic demand analysis (PSDA) (Equation (5.1)), the intensity measure (*IM*) used in the analysis should satisfy the criteria known as 'the efficiency', 'the sufficiency', and 'the scaling robustness' (Tothong and Cornell 2007, Tothong and Luco 2007, Luco and Cornell 2007). In order to satisfy these criteria, the *IM* should take into account the dominant modes of vibration and the effects of the nonlinear structural behaviour (i.e., the period elongation). This means that the *IM* should include the ground motion characteristics that affect the response of the structure considered, i.e., the spectral accelerations at the periods of the modes that dominate the response, and those at the elongated periods of the structure.

While a given *IM* might satisfy the foregoing criteria, it might not be suitable for PSDA because, for example, of the need of excessive computations for determining the seismic hazard, or because of other difficulties in the use of the *IM* in PSDA, such as the need for the development of attenuation relation for the *IM*. Therefore, in the selection of

an existing *IM* or in the development of a new *IM*, one should keep in mind that the *IM* can be relatively easily applied in PSDA.

This chapter discusses the efficiency, the sufficiency, and the scaling robustness of the intensity measures S_{N1} and S_{N2} proposed in this thesis.

7.2 Efficiency

An *IM* is considered to be efficient if it provides a relatively small dispersion of the structural responses. This is based on one of the main principles in statistics that "a smaller dispersion of a given random variable provides a better estimate of the mean of the variable, i.e., more accurate prediction of the variable" (Ang and Tang 1975). In the context of this thesis, a smaller dispersion of the computed interstorey drifts (*IDR*s) for a given *IM* leads to a higher confidence (i.e., higher accuracy) in the estimation of the mean *IDR* for that *IM*, and consequently to more accurate results from PSDA (Equation (5.1)). Another benefit from a smaller dispersion of the *IDR*s is that a smaller number of time history analyses and ground motion records are necessary to achieve satisfactory accuracy of the PSDA results. This is important because time history analyses are the most time consuming tasks in PSDA.

To illustrate the dispersions of the *IDR*s, Figs. 7.1, 7.2, and 7.3 show the computed maximum *IDR*s for the 4S, the 10S, and the 16S frame respectively, for a series of excitation levels considered in the analysis of the frames. The records of the 80R set were used as excitation motions (Appendix B, Table B.1). For the purpose of comparisons, each figure includes both the *IDR*s computed using the 'traditional' *IM* represented by $Sa(T_1)$ (graph (a) in each figure) and those obtained using the proposed *IM*s, i.e., S_{N1} and S_{N2}

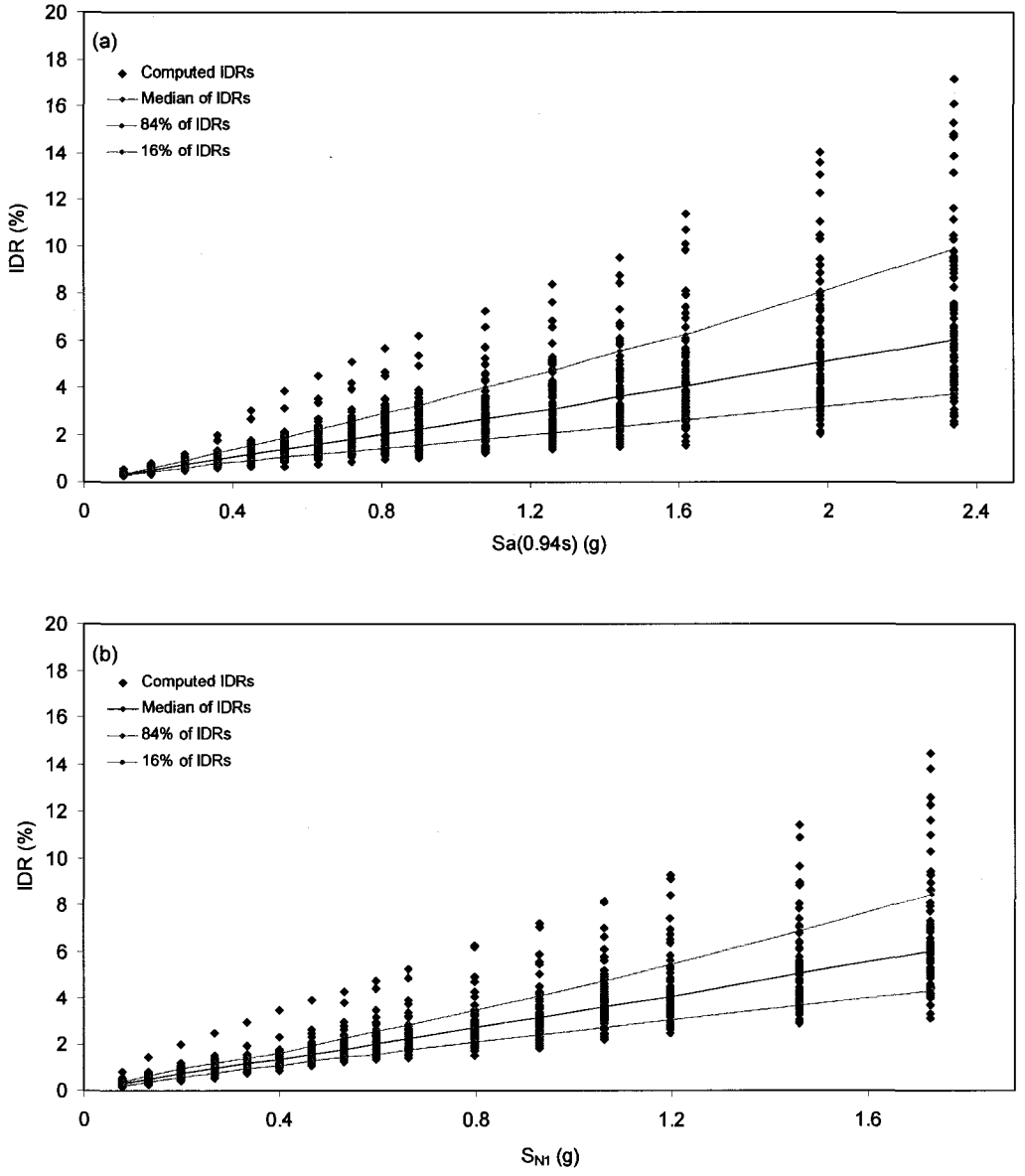

Figure 7.1 Dispersion of maximum interstorey drifts for the 4S frame for intensity measures represented by : (a) $Sa(T_1)$, and (b) S_{N1}.

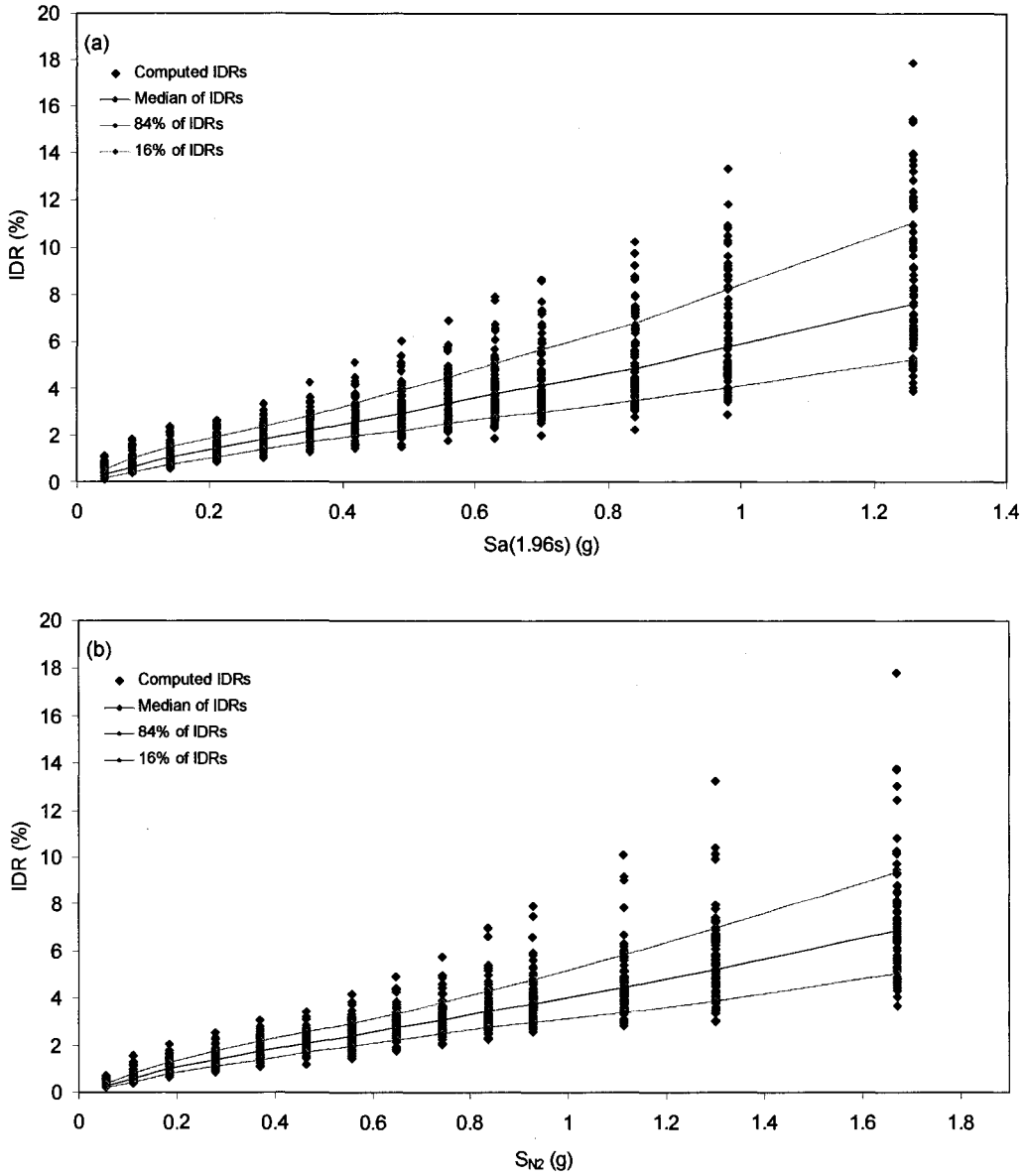

Figure 7.2 Dispersion of maximum interstorey drifts for the 10S frame for intensity measures represented by: (a) $Sa(T_1)$, and (b) S_{N2}.

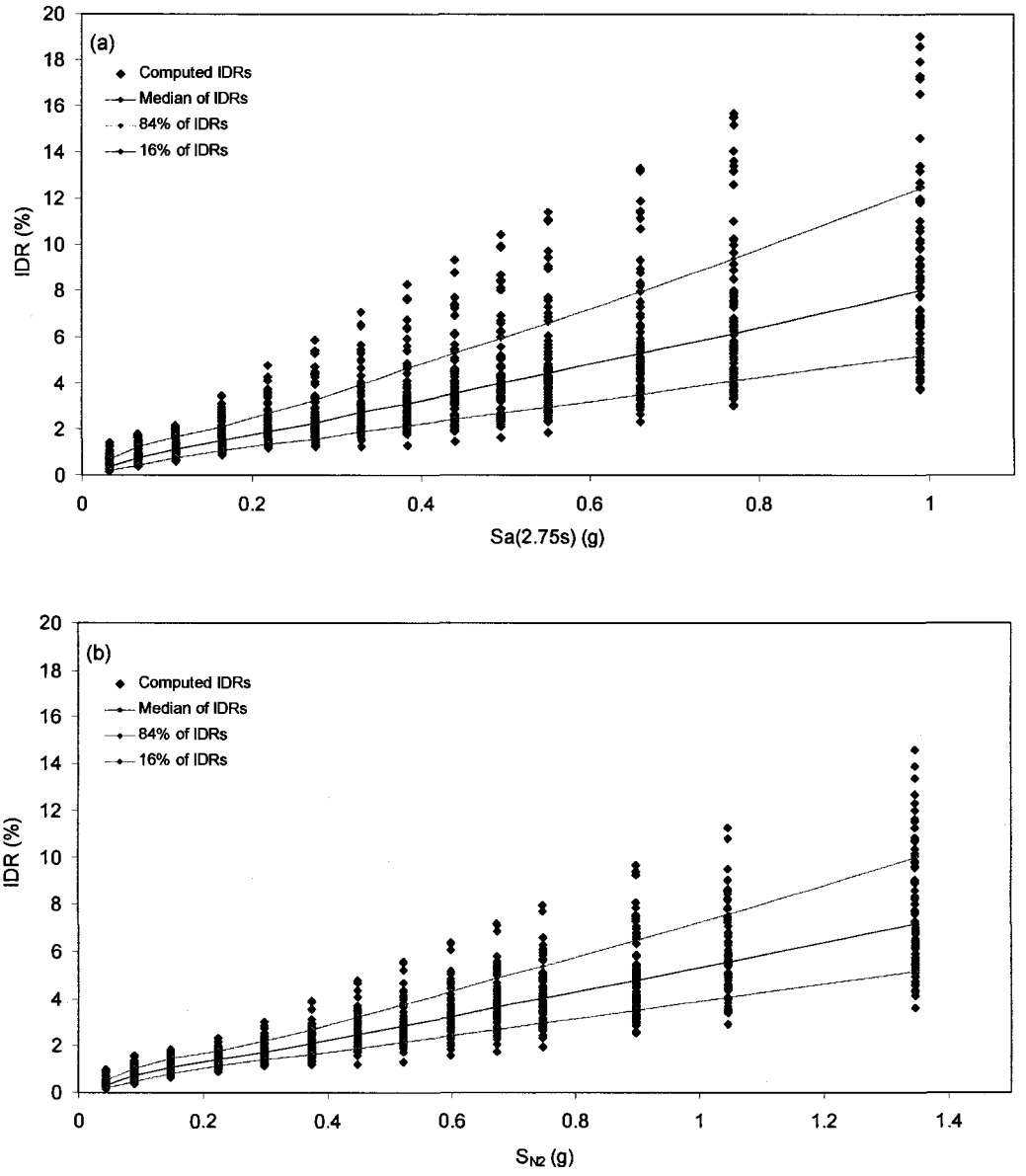

Figure 7.3 Dispersion of maximum interstorey drifts for the 16S frame for intensity measures represented by: (a) $Sa(T_1)$, and (b) S_{N2}.

(graph (b)). Based on the findings in Chapter 6, S_{N1} is used for the 4S frame (Fig. 7.1(b)), and S_{N2} is used for the 10S and the 16S frames (Figs. 7.2(b) and 7.3(b)). It should be mentioned that when S_{N1} or S_{N2} was used as *IM*, the records used in the analyses were scaled such that the mean value of the maximum *IDR*s from the 80 records, for each intensity level considered, is close to that of the *IDR*s obtained using $Sa(T_1)$ as *IM*. So the S_{N1} or S_{N2} values (i.e., intensity levels) corresponding to the *IDR* strips in Figs. 7.1(b), 7.2(b), and 7.3(b) are compatible (in terms of the mean *IDR*s) with the $Sa(T_1)$ values corresponding to the *IDR* strips in Figs. 7.1(a), 7.2(a), and 7.3(a) respectively. A detailed discussion of the scaling of records associated with the use of S_{N1} and S_{N2} as *IM*s is given in Chapter 6. Note that this scaling method was employed in order to compare the dispersions of the *IDR*s resulting from the use of S_{N1} and S_{N2} with those obtained by the use of $Sa(T_1)$ as *IM*. Otherwise, the records can be scaled to any series of preferred S_{N1} or S_{N2} values.

Figures 7.1 to 7.3 also include the 50% (i.e., median), the 84%, and the 16% levels of the computed *IDR*s. These levels were determined assuming lognormal distribution of the *IDR*s. To see the dispersions more clearly, these levels were computed considering all the *IDR*s obtained from the analysis (i.e., non-collapse *IDR*s and collapses together). Comparing the ranges between the 84% and the 16% levels for the proposed *IM*s (S_{N1} and S_{N2} in Figs. 7.1(b) to 7.3(b)) with the corresponding ranges for the *IM* represented by $Sa(T_1)$ (Figs. 7.1(a) to 7.3(a)), it can be seen that the dispersions of the *IDR*s computed using the proposed *IM*s are significantly smaller than those of the *IDR*s obtained using $Sa(T_1)$ as *IM*. Considering these ranges, it was found that the proposed *IM*s lead to a decrease in the dispersion of approximately 35% relative to the dispersion corresponding to the *IM* represented by $Sa(T_1)$. This means that S_{N1} and S_{N2} are more efficient *IM*s than $Sa(T_1)$.

7.3 Sufficiency

A sufficient *IM* is defined as one for which the structural responses (i.e., *EDP*) given *IM* are independent of earthquake magnitude (*M*) and source-to-site distance (*R*). This requirement is related to the term $P(EDP>edp|IM=im)$ in Equation (5.1) which represents the basic equation in PSDA. As seen, this term does not include *M* and *R*, i.e., it is assumed (for simplicity) that *EDP* does not depend on *M* and *R*. This assumption can be true if the *IM* used in the PSDA satisfies the 'sufficiency' criterion. Consequently, if *IM* is sufficient, then the PSDA results represented by the mean annual frequency of exceeding a given *EDP* value *edp* (denoted $\lambda_{EDP}(edp)$, see Equation (5.1)) would not depend on the *M* and *R* (i.e., the *M-R*) values of the selected records.

The sufficiency of a given *IM* can be assessed by investigating the correlation between the computed responses (i.e., *EDP*) and the *M-R* values for the records used in the analysis. If there is a correlation, the *IM* is not sufficient, and if there is no correlation, then the *IM* is considered to be sufficient.

Typical results from the investigation of the sufficiency of the proposed *IM*s (S_{N1} and S_{N2}) are depicted in Fig. 7.4. This figure shows 3-D surfaces of the computed maximum interstorey drifts (*IDR*s) versus magnitudes and distances of the earthquake records used in the analysis of the frames. Note that these are all 80 records of the 80R set. The surfaces were determined by regression analysis of the *IDR*s using the least square fitting method. Figure 7.4(a) illustrates the results for the 4S frame using S_{N1} as *IM*, and Figs. 7.4(b) and 7.4(c) show the results for the 10S and the 16S frames, respectively, using S_{N2} as *IM*. The results for the 4S frame are for S_{N1} level of 0.53 g, and those for the 10S and the 16S frames are for S_{N2} levels of 0.56 g and 0.45 g respectively (see these levels in Figs.

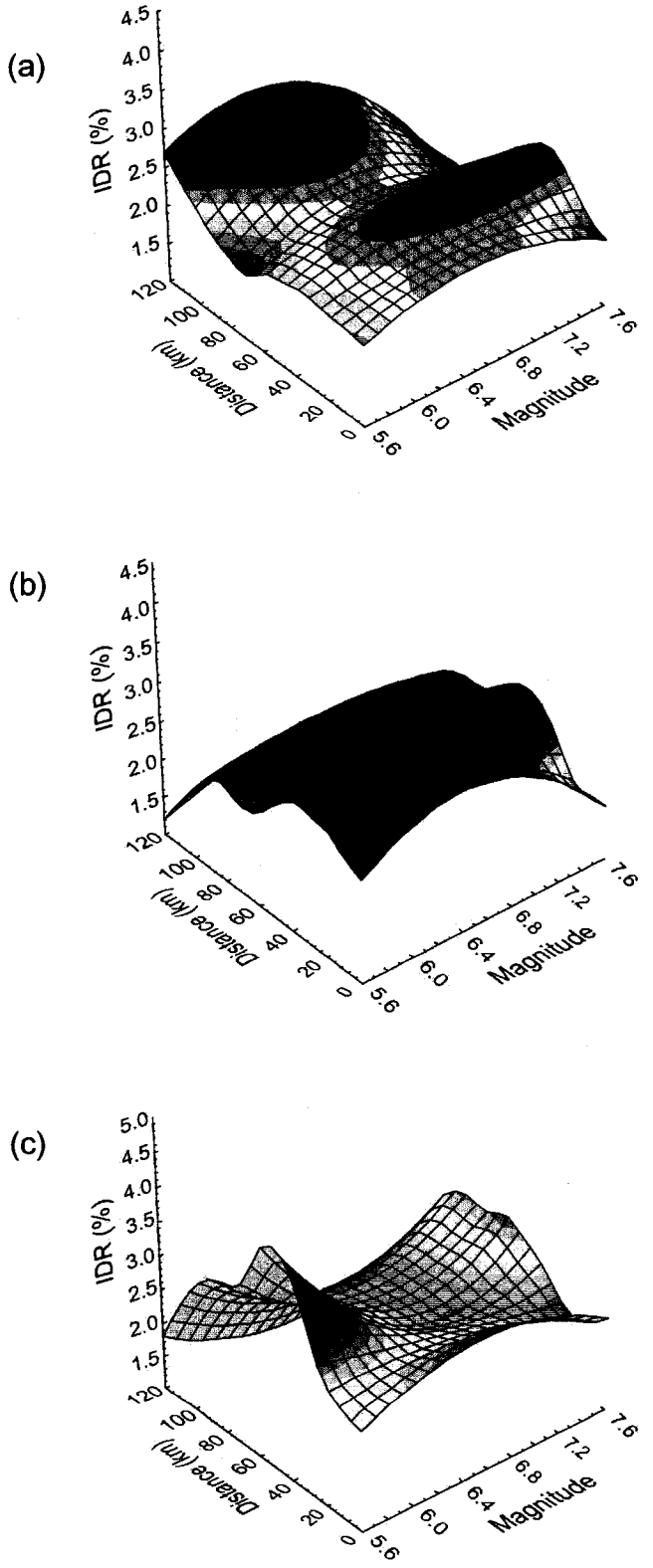

Figure 7.4 Maximum interstorey drifts versus magnitude and distance of earthquake records: (a) 4S frame, S_{N1}=0.53 g, (b) 10S frame, S_{N2}=0.56 g, and (c) 16S frame, S_{N2}=0.45 g. (See the S_{N1} and S_{N2} levels in Figs. 7.1(b), 7.2(b), and 7.3(b)).

7.1(b), 7.2(b) and 7.3(b)). These levels produce significant nonlinear responses of the frames and are considered to be appropriate for illustration of the correlation between the computed *IDR*s and the *M-R* values of the records.

Figure 7.4 shows that there is no correlation between the *IDR*s and the *M-R* values when S_{N1} and S_{N2} are used as *IM*s (S_{N1} for frame 4S – Fig. 7.4(a), and S_{N2} for frames 10S and 16S – Figs. 7.4(b) and 7.4(c)). For each frame, a number of other levels for S_{N1} and S_{N2} were also considered to see the effects of the excitation level on the correlation between *IDR* and *M-R*. The observations from the graphs for all these levels were similar to those from Fig. 7.4. In summary, Fig. 7.4 and the observations from all additional analyses indicate that S_{N1} and S_{N2} are sufficient *IM*s.

Investigations of the correlation between the *IDR*s and the *M-R* were also conducted using $Sa(T_1)$ as *IM*. It was found that there is no such correlation, indicating that $Sa(T_1)$ can also be considered a sufficient *IM*.

7.4 Scaling robustness

In addition to efficiency and sufficiency, an advanced *IM* should be such that the scaling of records to a given level of the *IM* does not cause bias in the structural responses. That is, the responses for records scaled by different factors but to the same *IM* level should not show a trend with respect to the scaling factors, i.e., the structural responses should be independent of the scaling factors of the records. This characteristic, which is called 'the scaling robustness', is important because scaled records are always used in PSDA to compute the conditional structural responses given $IM=im$ (i.e., $P(EDP>edp|IM=im)$, Equation (5.1)).

The scaling robustness for a given *IM* level can be estimated by conducting regression analysis on the response-versus-scaling factor results. Figures 7.5, 7.6, and 7.7 depict computed *IDR*s versus scaling factors for the 4S, the 10S, and the 16S frame respectively. For the purpose of comparison, the figures show both the results for *IM* represented by $Sa(T_1)$ (graphs (a) in the figures) and those for the proposed *IM*s, i.e., S_{N1} and S_{N2} (graphs (b)). As discussed earlier, S_{N1} is used for the 4S frame (Fig. 7.5(b)), and S_{N2} is used for the 10S and the 16S frames (Figs. 7.6(b) and 7.7(b)). The $Sa(T_1)$, S_{N1}, and S_{N2} levels are shown in the figure captions. Note that the S_{N1} and S_{N2} levels are the same as those used in the assessment of the 'sufficiency' (Section 7.3) discussed above. It is important to mention that for each frame, the S_{N1} and S_{N2} levels are consistent with the $Sa(T_1)$ level, i.e., the S_{N1} and S_{N2} levels produce mean responses similar to those corresponding to the $Sa(T_1)$ levels, as discussed in Chapter 6 (Section 6.4.1 and Equation 6.4).

For easier identification of the trends of the *IDR*s, linear regression lines are included in the figures. The scaling robustness can be estimated by considering the slopes of the regression lines. In general, a smaller slope indicates more robust scaling, and a larger slope indicates less robust scaling. As seen in the figures, the slopes of the lines for the proposed *IM*s (Figs. 7.5(b) to 7.7(b)) are significantly smaller than those for the 'traditional' *IM* represented by $Sa(T_1)$ (Figs. 7.5(a) to 7.7(a)). This is especially true for the 4S and the 10S frames for which the regression lines corresponding to the proposed *IM*s are almost horizontal. Based on the coefficients of the regression lines, the slopes for the proposed *IM*s are smaller than those for $Sa(T_1)$ by a factor of 4.4 for the 4S frame, 6.3 for

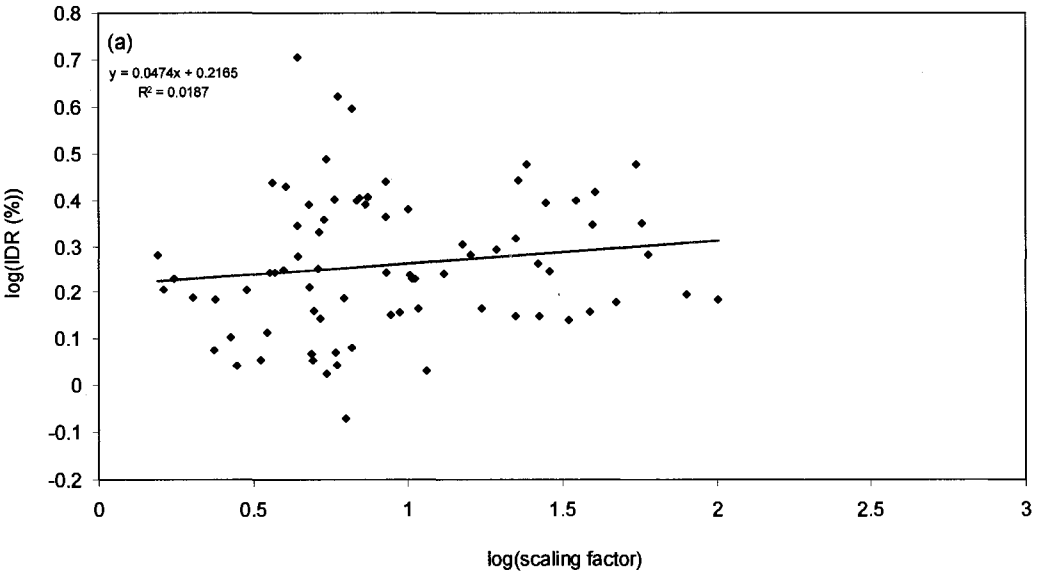

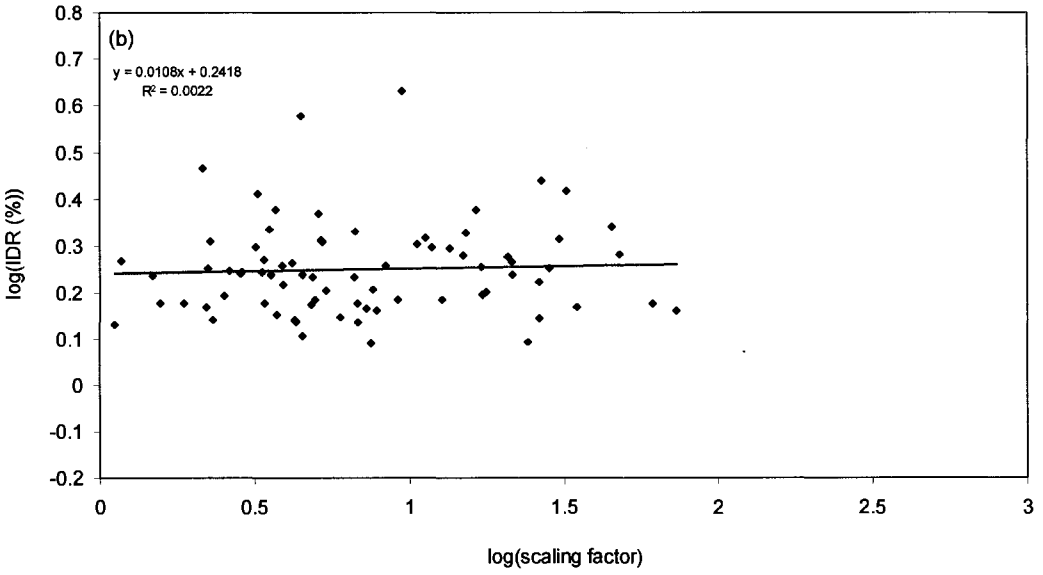

Figure 7.5 Maximum interstorey drifts for the 4S frame versus scaling factors for records scaled to: (a) $Sa(T_1)$=0.72 g, and (b) S_{NI}=0.53 g. (See the $Sa(T_1)$ and S_{NI} levels in Fig. 7.1(a) and 7.1(b)).

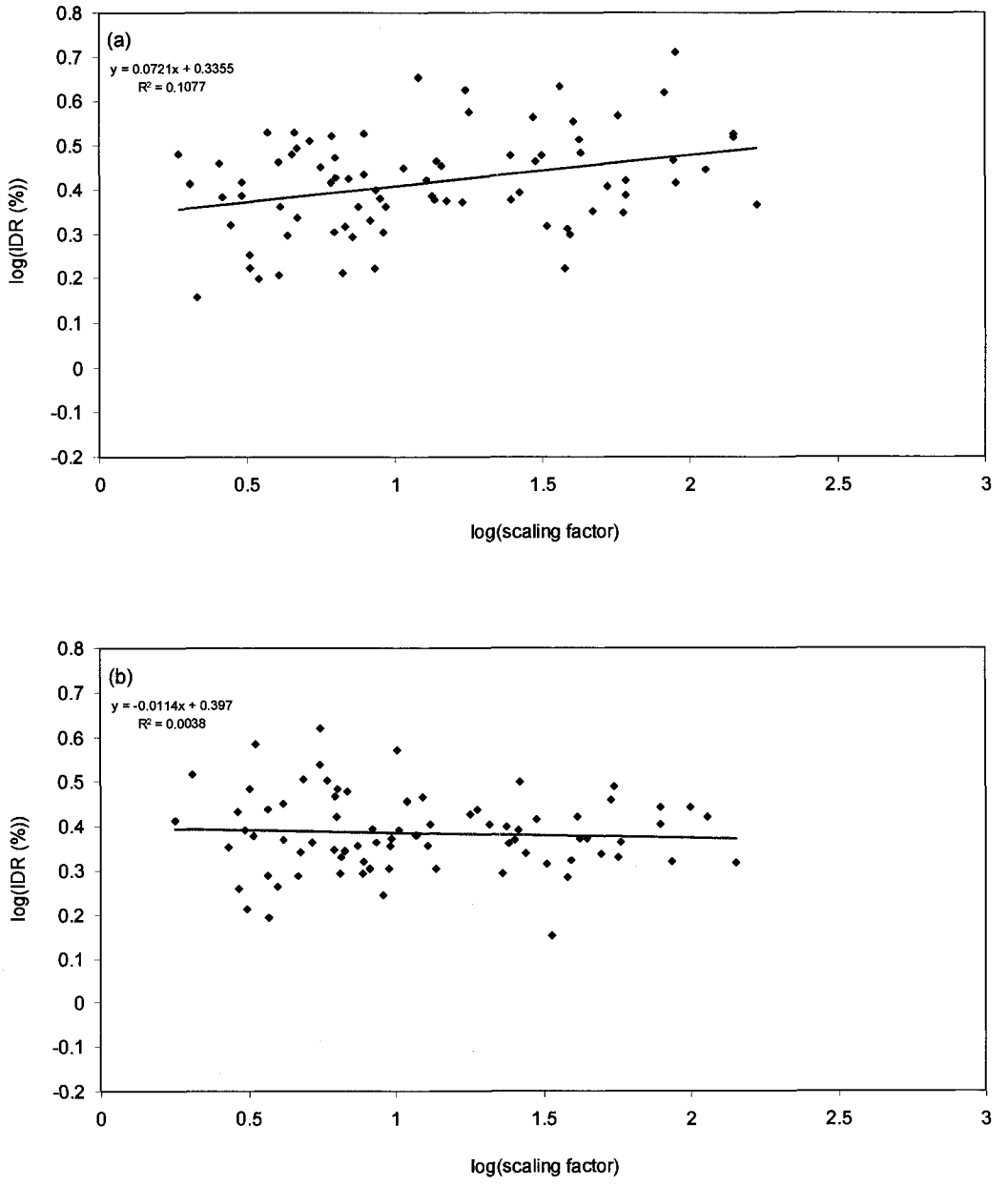

Figure 7.6 Maximum interstorey drifts for the 10S frame versus scaling factors for records scaled to: (a) $Sa(T_1)$=0.42 g, and (b) S_{N2}=0.56 g. (See the $Sa(T_1)$ and S_{N2} levels in Fig. 7.2(a) and 7.2(b)).

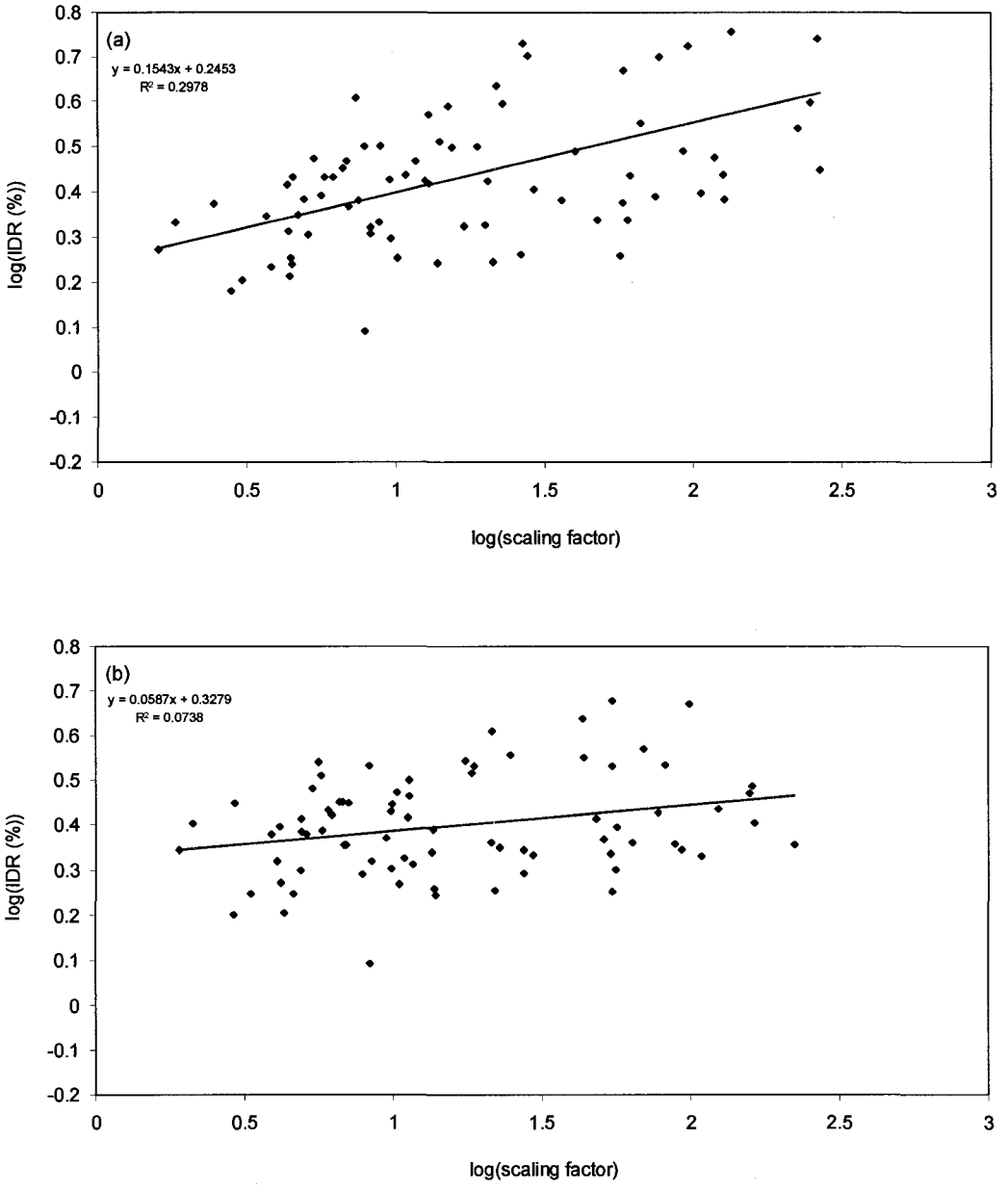

Figure 7.7 Maximum interstorey drifts for the 16S frame versus scaling factors for records scaled to: (a) $Sa(T_1)$=0.33 g, and (b) S_{N2}=0.45 g. (See the $Sa(T_1)$ and S_{N2} levels in Fig. 7.3(a) and 7.3(b)).

the 10S frame, and 2.6 for the 16S frame. This indicates that the scaling of records for the proposed *IM*s is much more robust than that for the *IM* represented by $Sa(T_1)$.

Investigations of the scaling robustness were also conducted for other levels of S_{N1}, S_{N2}, and $Sa(T_1)$. The findings from these investigations were similar to those discussed above.

7.5 Summary

This chapter investigates the suitability of the proposed intensity measures S_{N1} and S_{N2} for use in probabilistic seismic demand analysis. This was done by comparing the major characteristics of the proposed *IM*s with those of the 'traditional' *IM* represented by $Sa(T_1)$. The characteristics that were considered include 'the efficiency', 'the sufficiency', and 'the scaling robustness' of the *IM*s. These characteristics are defined as follows (Tothong and Cornell 2007, Tothong and Luco 2007):

- An *IM* is considered to be *efficient* if it provides a relatively small dispersion of the structural responses.
- A *sufficient IM* is defined as one for which the structural responses are independent of earthquake magnitude (M) and source-to-site distance (R).
- A *scaling robust IM* is considered one for which the responses obtained for records scaled by different factors but to the same *IM* level do not show a trend with respect to the scaling factors, i.e., the responses (as a whole) are independent of the scaling factors of the records.

Based on this investigation it is concluded that the proposed intensity measures S_{N1} and S_{N2} are superior when compared to the intensity measure $Sa(T_1)$, and are appropriate for use in probabilistic seismic demand analysis.

Chapter 8

Probabilistic Seismic Demand Analysis Using the Proposed Intensity Measures

8.1 Introduction

A detailed discussion of the probabilistic seismic demand analysis (PSDA) is given in Chapter 5. For the purpose of the discussion in this chapter, it is helpful to write again here the equation used in PSDA for determining the mean annual frequency of exceeding a specified interstorey drift (*IDR*) level *idr*, designated as $\lambda_{IDR}(idr)$:

$$\lambda_{IDR}(idr) = \int_{im} P(IDR > idr \mid IM = im) \cdot \left| \frac{d\lambda_{IM}(im)}{d(im)} \right| \cdot d(im) \tag{8.1}$$

Note that $\lambda_{IDR}(idr)$ is also called the drift hazard curve. In Equation (8.1), *IDR* represents the *maximum* interstorey drift at any storey of the building, *IM* is a selected intensity measure, and $\lambda_{IM}(im)$ is the mean annual frequency of exceeding a given *IM* value *im* (this is commonly referred to as the seismic hazard curve). Equation (8.1) is the same as Equation (5.1) in Chapter 5, except that maximum *IDR* is used as engineering demand parameter (*EDP*). Detailed explanations for this equation are given in Chapter 5.

This chapter discusses the use of the proposed *IM*s (S_{N1} and S_{N2}) in probabilistic seismic demand analysis. These *IM*s were formulated in Chapter 6 (Equations (6.5) and (6.6)), and their equations are written again here for the purpose of clarity, i.e.,

$$S_{N1} = Sa(T_1)^{0.5} \cdot Sa(1.5T_1)^{0.5} \tag{8.2}$$

$$S_{N2} = Sa(T_1)^{0.75} \cdot Sa(T_2)^{0.25} \tag{8.3}$$

where T_1 and T_2 are the first and the second mode periods of the frames respectively. Note that S_{N1} was used for the 4S frame, and S_{N2} for the 10S and 16S frames (Chapters 6 and 7). Using these *IM*s, Equation (8.1) can be written in terms of S_{N1} as:

$$\lambda_{IDR}(idr)_{S_{N1}} = \int_{sn1} P(IDR > idr \mid S_{N1} = sn1) \cdot \left| \frac{d\lambda_{S_{N1}}(sn1)}{d(sn1)} \right| \cdot d(sn1) \tag{8.4}$$

and in terms of S_{N2} as:

$$\lambda_{IDR}(idr)_{S_{N2}} = \int_{sn2} P(IDR > idr \mid S_{N2} = sn2) \cdot \left| \frac{d\lambda_{S_{N2}}(sn2)}{d(sn2)} \right| \cdot d(sn2) \tag{8.5}$$

where *sn1* and *sn2* represent specific levels of S_{N1} and S_{N2} respectively.

As seen in Equations (8.4) and (8.5) (also in Chapter 5 – Fig. 5.1 and Equation (5.1)), the probabilistic seismic demand analysis using S_{N1} or S_{N2} as intensity measure requires computations of: (i) the maximum *IDR*s for the selected records scaled to a series of intensity levels *sn1* or *sn2* (depending on which *IM* is used, S_{N1} or S_{N2}), (ii) the conditional probability $P(IDR>idr|S_{N1}=sn1)$ or $P(IDR>idr|S_{N2}=sn2)$, and (iii) the seismic hazard curve $\lambda_{S_{N1}}(sn1)$ or $\lambda_{S_{N2}}(sn2)$. The drift hazard curves $\lambda_{IDR}(idr)_{S_{N1}}$ and $\lambda_{IDR}(idr)_{S_{N2}}$ correspond to S_{N1} and S_{N2} respectively and are computed by combining the

conditional probabilities and the seismic hazard curves as defined in Equations (8.4) and (8.5).

Since the main issues in the use of PSDA are covered in Chapter 5, the discussion here is mainly focussed on the differences in the applications of PSDA using the proposed *IM*s relative to the use of $Sa(T_1)$ as *IM*. Specifically, the following issues are discussed here: (i) the computation of the *IDR*s using S_{N1} and S_{N2} as *IM*s, (ii) the development of attenuation relations for S_{N1} and S_{N2} (these are needed in the seismic hazard analysis to determine the seismic hazard curves $\lambda_{S_{N1}}(sn1)$ or $\lambda_{S_{N2}}(sn2)$), and (iii) comparisons of the PSDA results obtained using S_{N1} and S_{N2} with those corresponding to $Sa(T_1)$ as *IM*. The computations of the conditional probabilities $P(IDR>idr|S_{N1}=sn1)$ and $P(IDR>idr|S_{N2}=sn2)$ are the same as those described in Chapter 5 for $Sa(T_1)$ except that S_{N1} and S_{N2} are used rather than $Sa(T_1)$, and therefore, they are not discussed here.

8.2 Calculation of maximum *IDR*s

Maximum *IDR*s were determined from time history analyses of the frame models using the records of the 80R set as excitation motions. The records were scaled to a series of S_{N1} levels for the 4S frame and S_{N2} levels for the 10S and the 16S frames. In total 16 S_{N1} levels were used for the 4S frame ranging from 0.08 g to 1.73 g, and 14 S_{N2} levels for each of the 10S and the 16S frames ranging from 0.06 g to 1.67 g for the 10S frame and from 0.05 g to 1.35 g for the 16S frame.

Figure 8.1 shows the computed *IDR*s versus the selected intensity levels. Each stripe of points in the figure represents the *IDR*s for the 80 records used in the analysis scaled to a given intensity level. The 5% drift level shown in the figure represents the

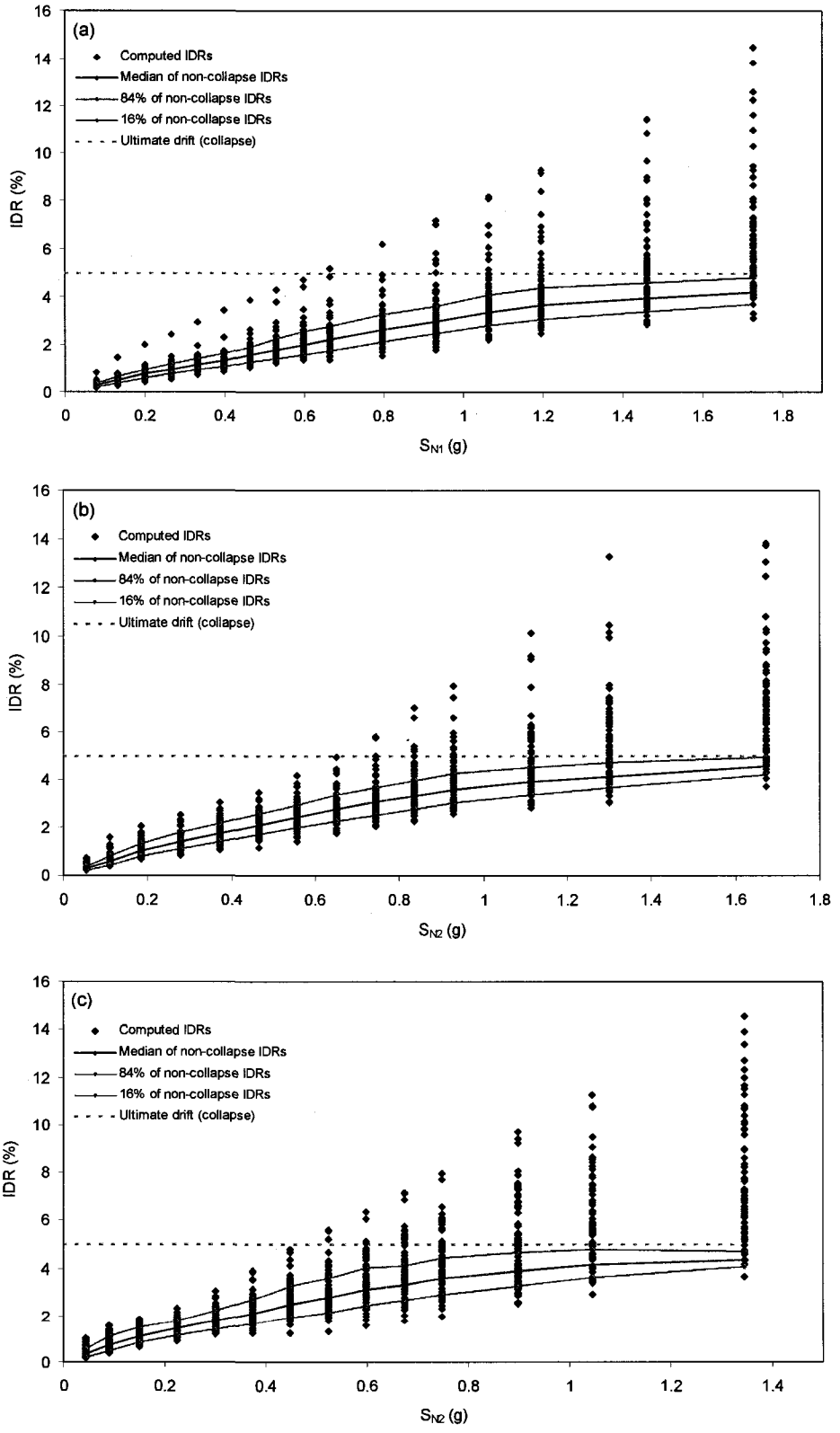

Figure 8.1 Computed maximum interstorey drifts for records scaled to various levels of the proposed intensity measures (S_{N1} for the 4S frame, and S_{N2} for the 10S and the 16S frames): (a) for the 4S frame, (b) for the 10S frame, and (c) for the 16S frame.

ultimate drift limit (i.e., the collapse drift limit). The selection of the 5% drift as ultimate drift limit is discussed in Chapter 5. Drifts smaller than 5% are referred to as the non-collapse drifts, and those above 5% indicate that the frames collapsed and are referred to as the collapses. It can be seen from the figure that the records scaled to the selected intensity levels provide wide ranges of interstorey drifts, from very small drift values (elastic responses) to collapses of the frames. Such response ranges are required for the development of the drift hazard curves for the frames.

8.3 Attenuation relations for use in the analysis

In order to determine the seismic hazard curves for S_{N1} and S_{N2} (i.e., $\lambda_{S_{N1}}(sn1)$ and $\lambda_{S_{N2}}(sn2)$), the *mean* attenuation relations and the corresponding standard deviations for S_{N1} and S_{N2} are required. Since S_{N1} and S_{N2} are related to spectral accelerations (Sa), their attenuation relations and standard deviations were determined from those available for spectral accelerations for western Canada. In this section, first, the available attenuation relations for Sa for western Canada are presented, and then the derivation of those for S_{N1} and S_{N2} is described.

8.3.1 Available attenuation relations for western Canada

The Geological Survey of Canada (GSC), which is responsible for the development of seismic hazard maps of Canada, uses attenuation relations for 5% damped spectral accelerations (Adams and Halchuk 2003, Adams and Atkinson 2003). Depending on the types of the source zones, two sets of attenuation relations are currently used by GSC in performing seismic hazard analysis for western Canada, i.e., one set for crustal source

zones, and another set for subcrustal source zones. Both sets are for class C soil, which is characterised by an average shear wave velocity of 360-750 m/s in the uppermost 30 m (NRCC 2005). The attenuation relations for crustal source zones were originally developed by Boore et al. (1993, 1994). Certain modifications to the relations have been made by GSC regarding the attenuation for distances larger than 100 km. The final attenuation relations for crustal source zones, which represent the *mean* predictions of *Sa* at specified periods, are as follows:

$$\log Sa = b_1 + b_2(M-6) + b_3(M-6)^2 + b_5 \log(R) + b_6 \quad \text{for R<100 km} \tag{8.6}$$

$$\log Sa = b_1 + b_2(M-6) + b_3(M-6)^2 + b_4(R-100) + b_5 \log(100) - \log(R/100) \quad \text{for R>100 km} \tag{8.7}$$

where the spectral acceleration *Sa* is in cm/s^2, *M* is moment magnitude, and *R* is hypocentral distance in km. The earthquake depths are included in the attenuation relations (in *R*) and depend on the period for which *Sa* is estimated. The earthquake depths and the coefficients b_1 to b_6 are given in Boore et al. (1993, 1994) for different periods. Standard deviations of log*Sa* (i.e., $\sigma_{\log Sa}$) for different periods are also provided.

For subcrustal source zones, the attenuation relation developed by Youngs et al. (1997) for 'intraslab' earthquakes has been adjusted by GSC to correspond to class C soil. The modified attenuation relation has the following form:

$$\ln Sa = 0.307 + 1.414M + 1.7818e^{0.554M} + 0.00607h + c_1 + c_2(10-M)^3 + c_3 \ln R + 0.3846c_6 \tag{8.8}$$

where Sa is in g, M is moment magnitude, R is the closest distance to rupture in km, h is earthquake depth in km. A depth of h=50 km is adopted by GSC for the subcrustal source zones in western Canada. The standard deviation of lnSa is given as:

$$\sigma_{\ln Sa} = c_4 + c_5 M \tag{8.9}$$

for magnitudes smaller than 8, and $\sigma_{\ln Sa}=M$ for magnitudes larger than 8. Values for the coefficients c_1 to c_6 for different periods are given in Youngs et al. (1997).

8.3.2 Development of attenuation relations for S_{N1} and S_{N2}

The attenuation relations for S_{N1} and S_{N2} were determined using the existing relations for spectral acceleration (Equations (8.6), (8.7), and (8.8)) discussed above. This involved determining: (i) the *mean* attenuation relations for S_{N1} and S_{N2}, and (ii) the *standard deviations* of the attenuation. The determination of each of these quantities is described in the following subsections. Note that the attenuation relations for S_{N1} and S_{N2} were derived for both the crustal and subcrastal source zones, and were further used in the computation of the seismic hazard. So, it is assumed that S_{N1} and S_{N2}, which were developed considering crustal seismic records, are also effective for subcrustal seismic motions.

Mean attenuation relations

Considering Equations (8.2) and (8.3), the intensity measures S_{N1} and S_{N2} can be expressed in a general form as:

$$S_{N1,N2} = Sa(T_1)^x \cdot Sa(T_z)^y \tag{8.10}$$

where $S_{N1,N2}$ stands for S_{N1} or S_{N2}, T_z stands for $1.5T_1$ or T_2, and x and y represent the exponents in Equations (8.2) and (8.3). Note that T_1 and T_2 are the first and the second mode periods of the frames. Equation (8.10) is introduced to generalise the derivations of the parameters required for the mean attenuation relations for S_{N1} and S_{N2}. In other words, the derivations for $S_{N1,N2}$ are applicable to both S_{N1} and S_{N2}. Now it is necessary to determine the mean attenuation relations for $S_{N1,N2}$ for crustal and subcrustal source zones. Note that for each of the three attenuation relations for *Sa* (Equations (8.6), (8.7), and 8.8), corresponding attenuation relations for $S_{N1,N2}$ are needed.

Since $S_{N1,N2}$ is a function of spectral accelerations at two periods, T_1 and T_z, the attenuation relation for $S_{N1,N2}$ can be derived by combining the GSC attenuation relations for periods T_1 and T_z. As discussed above, the GSC attenuation relations for crustal and subcrustal zones have the same form, but for crustal zones are expressed in log*Sa* and for subcrustal zones in ln*Sa*. Therefore, the method for determining the attenuation relations for $S_{N1,N2}$ is practically the same for crustal and subcrustal zones, except that different logarithms (log or ln) are used. While the use of different logarithms in the derivations of the attenuation relations for $S_{N1,N2}$ (and consequently for S_{N1} and S_{N2}) does not cause any difficulty, it could be avoided if the GSC attenuation relations (Equations (8.6), (8.7) and (8.8)) were rewritten using the same type of logarithm (ln or log). This would require, however, making certain changes in the GSC computer code for seismic hazard analysis.

The method is illustrated in more detail here for the attenuation for crustal zones and for R<100 km. The *Sa* attenuation for this case is defined by Equation (8.6), and this equation will be involved in the derivation of the attenuation relation for $S_{N1,N2}$. First, the Equation (8.10) is expressed in logarithmic form, as shown in Equation (8.11):

$$\log S_{N1,N2} = x \log Sa(T_1) + y \log Sa(T_z) \tag{8.11}$$

Replacing the terms $\log Sa(T_1)$ and $\log Sa(T_z)$ by Equation (8.6) for T_1 and T_z respectively, the coefficients for the mean attenuation relation for $S_{N1,N2}(T_1,T_z)$ are obtained as:

$$b_{iT_1,T_z} = x b_{iT_1} + y b_{iT_z} \tag{8.12}$$

where b_{iT_1} and b_{iT_z} are the coefficients of Equation (8.6) corresponding to periods T_1 and T_z respectively. Note that if the coefficients for specific T_1 and T_z are not available, they can be obtained by interpolation or extrapolation using the available coefficients for the other periods. Having determined the coefficients b_{iT_1,T_z}, the mean attenuation relation for $S_{N1,N2}(T_1,T_z)$ can be written in the same form as Equation (8.6), but with coefficients b_{iT_1,T_z} instead b_i. This results in the following expression:

$$\log S_{N1,N2}(T_1,T_z) = (x b_{1T_1} + y b_{1T_z}) + (x b_{2T_1} + y b_{2T_z})(M-6) + (x b_{3T_1} + y b_{3T_z})(M-6)^2 + (x b_{5T_1} + y b_{5T_z}) \log(R) + (x b_{6T_1} + y b_{6T_z}) \tag{8.13}$$

which represents the mean attenuation relation for $S_{N1,N2}(T_1,T_z)$ for crustal zones and R<100 km. This equation could be simplified but it is not done here because the objective of these derivations is to illustrate the method using general expressions.

The expressions for the attenuation relations for the intensity measures S_{N1} and S_{N2} (i.e., the expressions for $\log S_{N1}$ and $\log S_{N2}$) can now be determined. These expressions have the same form as Equation (8.13) but with values b_{iT_z}, x, and y corresponding to those of the intensity measure (S_{N1} or S_{N2}) considered. For intensity measure S_{N1}, for example,

x=0.5, y=0.5, and the coefficients b_{iT_z} correspond to those of Equation (8.6) for T_z=1.5T_1. Similarly, for intensity measure S_{N2}, the values for x and y are 0.75 and 0.25 respectively, and the coefficients b_{iT_z} are those of Equation (8.6) for T_z=T_2.

The derivation of the attenuation relation for $S_{N1,N2}$ (and consequently for S_{N1} and S_{N2}) for crustal zones and R>100 km was conducted following the approach described above for crustul zones and R<100 km, except that Equation (8.7) was used in the derivation rather than Equation (8.6). Similarly, the derivation of the attenuation relation for $S_{N1,SN2}$ (also for S_{N1} and S_{N2}) for subcrustal zones was done using the same approach except that Equation (8.8) was used in the derivations. Since Equation (8.8) is in terms of lnSa, the derivations for subcrustal zones were conducted using natural logarithms ln rather than 'standard' logarithms log.

Standard deviations

Standard deviations for the attenuation relations for S_{N1} and S_{N2} are also needed for conducting seismic hazard analysis. To determine the standard deviations, the correlation of the spectral accelerations involved in S_{N1} and S_{N2} should be calculated first. For ease of discussion, the general expression for S_{N1} and S_{N2} represented by Equation (8.10), i.e., $S_{N1,N2}$, is used again here, and referring to $S_{N1,N2}$ means referring to both S_{N1} and S_{N2}. Equation (8.10) shows that $S_{N1,N2}$ includes spectral accelerations at periods T_1 and T_z (where T_z is 1.5T_1 for S_{N1}, and T_z =T_2 for S_{N2}), and exponents x and y representing those used in S_{N1} and S_{N2} (i.e., Equations (8.2) and (8.3) respectively). Now the correlation coefficient of $Sa(T_1)$ and $Sa(T_z)$ should be defined.

Investigations of the correlation of spectral accelerations at two periods have been conducted by Inoue and Cornell (1990) and Baker and Cornell (2006) for earthquake

motions recorded in California. The equations for correlation coefficients resulting from these investigations provide very similar results. In this thesis, the equation proposed by Inoue and Cornell (1990) was used. The correlation coefficient for the natural logarithms of the spectral accelerations at periods T_1 and T_z, as formulated in Inoue and Cornell (1990), can be expressed as:

$$\rho_{\ln Sa(T_1),\ln Sa(T_z)} = 1 - 0.33\left|\ln\left(T_z / T_1\right)\right| \tag{8.14}$$

Now the standard deviation of $\ln S_{N1,N2}$ can be written as:

$$\sigma^2_{\ln S_{N1},S_{N2}} = x^2\sigma^2_{\ln Sa(T_1)} + y^2\sigma^2_{\ln Sa(T_z)} + 2\rho_{\ln Sa(T_1),Sa(T_z)}xy\sigma_{\ln Sa(T_1)}\sigma_{\ln Sa(T_z)} \tag{8.15}$$

The correlation coefficients and the standard deviations for S_{N1} and S_{N2} were determined by substituting into Equations (8.14) and (8.15) corresponding values for T_1, T_z, x, y, $\sigma_{\ln Sa(T_1)}$ and $\sigma_{\ln Sa(T_z)}$. Note that for the crustal zones, for which the attenuation relations are expressed using 'standard' logarithms (i.e., $\log S_{N1}$ and $\log S_{N2}$), simple mathematical transformations between log and ln were required to determine $\sigma^2_{\log S_{N1}}$ and $\sigma^2_{\log S_{N2}}$.

8.4 PSDA results using the intensity measures S_{N1} and S_{N2}

The final results from the analysis are the drift hazard curves for the frames, $\lambda_{IDR}(idr)_{S_{N1}}$ and $\lambda_{IDR}(idr)_{S_{N2}}$, corresponding to the intensity measures S_{N1} and S_{N2} respectively (Equations (8.4) and (8.5)). These represent the mean annual frequencies of

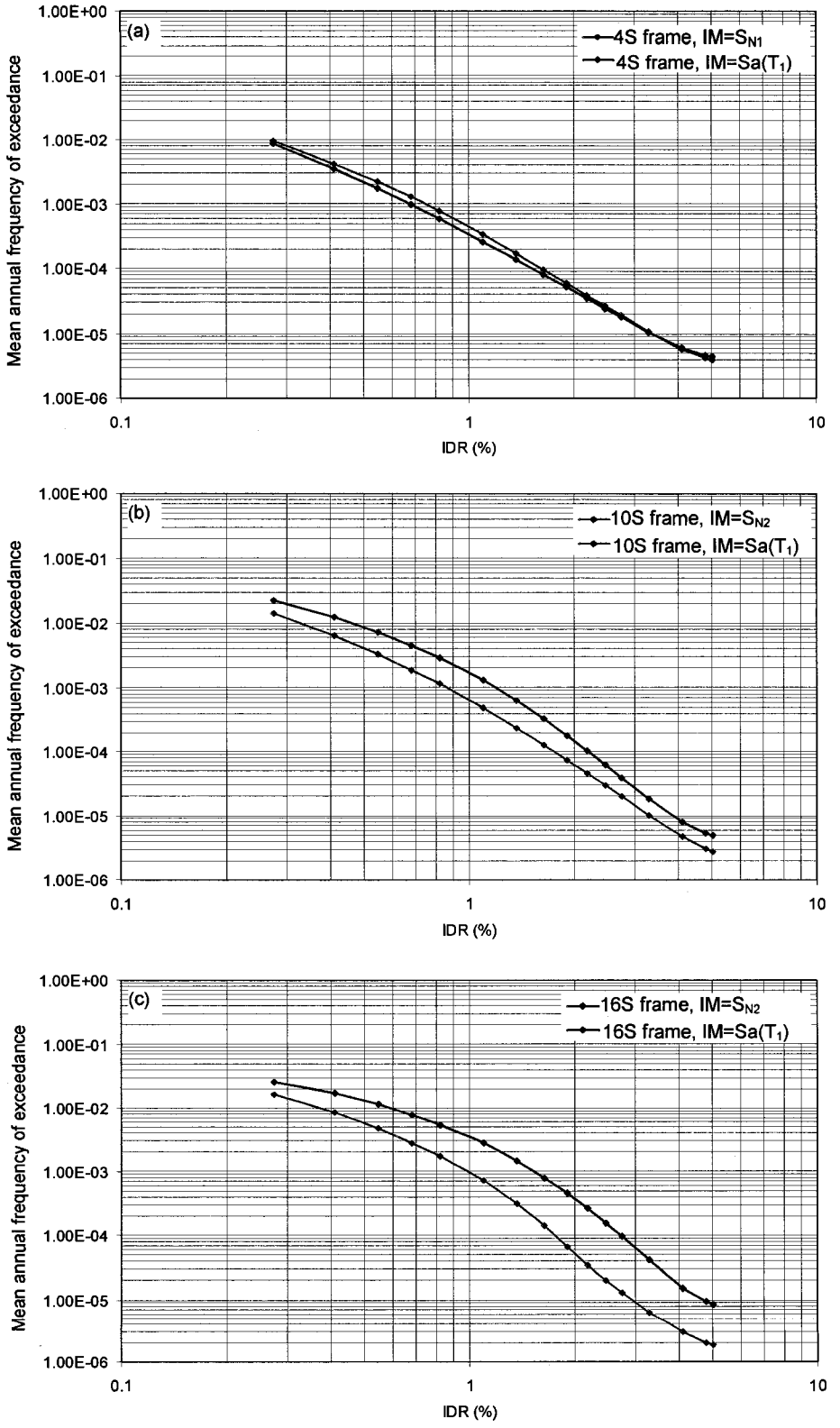

Figure 8.2 Comparison of drift hazard curves obtained using S_{N1} and S_{N2} as *IM*s with those obtained using $Sa(T_1)$ for: (a) the 4S frame, (b) the 10S frame, and (c) the 16S frame. Note that S_{N1} is used for the 4S frame, and S_{N2} is used for the 10S and the 16S frames.

exceeding specified interstorey drift levels *idr*. Figure 8.2 shows the drift hazard curves for the three frames considered in this thesis. The drift hazard curve for the 4S frame corresponds to intensity measure S_{N1}, and those for the 10S and the 16S frames correspond to S_{N2}. For the purpose of comparison, the drift hazard curves obtained using $Sa(T_1)$ as intensity measure are also shown in the figure. It can be seen that the differences in the drift hazard curves corresponding to S_{N1} and $Sa(T_1)$ are relatively small for the 4S frame (Fig. 8.2(a)). The differences are much larger for the 10S and the 16S frames (Figs. 8.2(b) and 8.2(c)). For both frames, the drift hazard curves for S_{N2} are significantly lower than those for $Sa(T_1)$.

Table 8.1 compares the drift hazard curves computed using S_{N1} and S_{N2} as *IM*s with those using $Sa(T_1)$. The comparison is for interstorey drifts of 1.0%, 2.5%, and the ultimate drift (i.e., the collapse drift) of 5.0%. The drift of 1.0% is specified in FEMA 356 as upper drift limit for *immediate occupancy performance level* (ASCE 2000), and the drift of 2.5% is the maximum drift allowed by NBCC 2005 (NRCC 2005) for use in the design.

Table 8.1 Differences between drift hazard results obtained using S_{N1} and S_{N2} as *IM*s and those obtained using $Sa(T_1)$.

Frame analysed and IM used	Difference (in %) at drift of:		
	1.0%	2.5%	5.0%
4S (IM=S_{N1})	+34	+10	-9
10S (IM= S_{N2})	-61	-47	-44
16S (IM= S_{N2})	-68	-85	-78

Note: Percentages are relative to $Sa(T_1)$ as *IM*; + denotes increase, - denotes decrease.

It is seen in the table that the differences in the drift hazard curves, for the three drift levels considered, are approximately 10% to 35% for the 4S frame, 45% to 60% for the 10S frame, and 65% to 85% for the 16S frame. While the differences are quite significant, they were not surprising given the results from other similar studies.

Tothong and Cornell (2007) have investigated the effects of advanced intensity measures on the drift hazard curves for a number of frame models with fundamental periods between 0.3 s and 3.0 s. The intensity measures used in the probabilistic seismic demand analyses include: inelastic spectral displacement (Ruiz-Garcia and Miranda 2005), the so-called $IM_{1I\&2E}$ intensity measure proposed by Luco and Cornell (2007), and the intensity measure consisting of elastic spectral acceleration and 'epsilon' proposed by Baker and Cornell (2005). These intensity measures are described in Chapter 1, Section 1.3. The results from the advanced intensity measures have been compared with those obtained using elastic spectral acceleration at the fundamental period, $Sa(T_1)$, as intensity measure. Two drift levels have been used in the comparisons, i.e., the drifts corresponding to ductility of four, and to collapse. As reported by Tothong and Cornell (2007) and Tothong and Luco (2007), the use of the advanced intensity measures resulted in significantly different drift hazard values compared to those obtained using $Sa(T_1)$ as intensity measure. Differences of up to 90% are observed in these studies. It is useful to note that in almost all the cases, the drift hazard results from the use of the advanced intensity measures have been found to be smaller than those obtained using $Sa(T_1)$, as seen in this thesis for the 10S and the 16S frames (Fig. 8.2(b) and 8.2(c)). In summary, the differences between the drift hazard curves corresponding to the proposed intensity measure S_{N1} and S_{N2}, and those corresponding to $Sa(T_1)$ resulting from the analysis in this thesis are consistent with the findings reported in similar studies on advanced intensity measures.

8.5 Summary

This chapter discusses the use of the proposed intensity measures S_{N1} and S_{N2} in probabilistic seismic demand analysis (PSDA). The PSDA procedure is, in general, the same as that described in Chapter 5 for the use of spectral acceleration at the fundamental structural period ($Sa(T_1)$) as intensity measure. However, attenuation relations for S_{N1} and S_{N2}, as functions of earthquake magnitude and diatance, are required in order to perform PSDA. These were determined using the existing attenuation relations for spectral acceleration for western Canada.

Drift hazard curves corresponding to the proposed intensity measures S_{N1} and S_{N2} were computed for the three frames considered in this thesis. These were compared with the drift hazard curves obtained using the intensity measure represented by $Sa(T_1)$ (Fig. 8.2). The differences between the drift hazard results based on the proposed intensity measures and the results based on $Sa(T_1)$ are consistent with those observed in recent studies on advanced intensity measures.

This chapter shows that the use of the intensity measures S_{N1} and S_{N2} in probabilistic seismic demand analysis is quite straightforward. These intensity measures introduce significant improvements compared to $Sa(T_1)$, and are recommended for probabilistic response analysis of reinforced concrete frame buildings.

Chapter 9

Summary and Conclusions

9.1 General remarks

Probabilistic seismic demand analysis (PSDA) is an important part of the new approach for seismic assessment and design of structures known as performance-based earthquake engineering (PBEE). PSDA for a given structure combines the structural response due to earthquake motions with the ground motion hazard at the location of the structure (Fig. 1.1). The intensity measure is the parameter that connects the structural response with the ground motion hazard. The final results from PSDA for a given structure are the mean annual frequencies of exceeding specified response levels due to future earthquakes, i.e., the *seismic demand hazard curve* for the structure.

While the procedures for the computation of the seismic hazard and the structural response are well established, the intensity measure is still under investigation. The intensity measure is a key parameter in PSDA. This is because the scaling of the ground motion records used in the response analysis is based on the intensity measure (*IM*), and if the *IM* is not adequate, the analysis would result in biased responses.

Substantial research on intensity measures for PSDA has been conducted in recent years (e.g., Baker and Cornell 2005, Tothong and Cornell 2007, Luco and Cornell 2007). This has resulted in the developments of new intensity measures that are summarised in Chapter 1. However, the use of these intensity measures in practice is not straightforward because of different limitations, as discussed in Chapter 1, Section 1.3. Therefore, there is a need for further investigations into the intensity measures.

The main objective of this thesis is to develop improved intensity measures for use in PSDA. Considering the limitations of the existing intensity measures, this thesis is focussed on the development of intensity measures that take into account the contributions of the first and the second vibration modes to the structural response, and the effects of the period elongation during nonlinear response.

For the purpose of this study, three reinforced concrete frames (4-, 10-, and 16-storeys high) of building structures assumed to be located in Vancouver were designed according to the 2005 edition of the National Building Code of Canada (Chapter 2). Earthquake records representative for the Vancouver region were selected for use in the response analyses of the frames (Chapter 3). The main findings from the research work described in Chapters 4 through 8 are summarised hereafter.

9.2 Summary of main findings

9.2.1 Inelastic versus elastic displacement-based intensity measures

An investigation was conducted in Chapter 4 to determine the effects of the use of elastic and inelastic spectral displacements (*Sde* and *Sdi* respectively) as intensity measures. Time history analyses were performed on the three frames using a set of 40 earthquake

records scaled to *Sde* and *Sdi*. The dispersions of the interstorey drifts for scaling to *Sde* and *Sdi* were compared to see which of these two parameters is more appropriate for scaling. The dispersion is an important indicator for the effectiveness of a given intensity measure, i.e., smaller dispersion is always preferred. It was found that the dispersions resulting from scaling to *Sde* and *Sdi* are quite close. Based on this it is concluded that considering the dispersions, the use of *Sdi* as an intensity measure does not have advantage compared to the use of *Sde*, for the frames investigated in this thesis.

9.2.2 Period elongation

An investigation was conducted to determine the elongation (i.e., the increase) of the *first mode periods* of the frames during nonlinear response (Chapter 6). Each frame was subjected to a set of 40 records scaled to five intensity levels. The intensity levels were selected to produce a range of nonlinear responses of the frames. The displacement time histories of the roof responses of the frames were used to determine the period elongation. It was found that the *mean* period elongation is almost linearly proportional to the intensity of the motions (Fig. 6.3). The dispersions of the periods also increase with the increase of the excitation. Based on the results from this investigation, it was estimated that for the highest intensity levels used in probabilistic seismic demand analysis, the actual (or the 'effective') first mode periods of the frames could be longer than the corresponding elastic periods by factors larger than 2 (Chapter 6, Section 6.2).

9.2.3 Development of improved intensity measures

Two improved intensity measures (*IM*s) are introduced in Chapter 6, and are formulated as:

$$S_{N1} = Sa(T_1)^{0.5} \cdot Sa(1.5T_1)^{0.5}$$

$$S_{N2} = Sa(T_1)^{0.75} \cdot Sa(T_2)^{0.25}$$

where T_1 and T_2 represent the first and the second mode periods respectively, and $Sa(T_1)$ and $Sa(T_2)$ are spectral accelerations of ground motions at the first and the second mode periods respectively. The intensity measure S_{N1} takes into account the elongation of the first mode period during nonlinear response, and S_{N2} takes into account the contributions of the first and the second modes to the response. The exponents 0.25, 0.5, and 0.75 included in S_{N1} and S_{N2}, and the constant 1.5 in S_{N1}, represent *optimum* values and were determined from nonlinear time-history analyses of the frames. The excitation motions used in the analyses were represented by a set of 20 earthquake records scaled to selected intensity levels. The standard deviation of the maximum interstorey drifts for each excitation level was used as a criterion for determining the optimal values for the coefficients of the new *IM*s. The effectiveness of the new *IM*s was assessed relative to the 'traditional' *IM* represented by $Sa(T_1)$.

Based on the results from the analyses, S_{N1} is proposed as an intensity measure for use in probabilistic seismic demand analysis for first mode dominated frames (i.e., frames with shorter fundamental periods), and S_{N2} is proposed for frames for which the second mode contribution to the response is significant (i.e., frames with long fundamental periods). While this study indicates that the period of approximately 1.5 s can be assumed

to separate the period ranges of applicability of S_{N1} and S_{N2}, more research is needed to confirm this.

9.2.4 Validation of the proposed intensity measures

An investigation into the effectiveness of the proposed intensity measures S_{N1} and S_{N2} for use in probabilistic seismic demand analysis was conducted in Chapter 7. This was done by comparing the major characteristics of the proposed *IM*s with those of the *IM* represented by $Sa(T_1)$. The characteristics that were considered include 'the efficiency', 'the sufficiency', and 'the scaling robustness' of the *IM*s. These characteristics are defined as follows (Tothong and Cornell 2007, Tothong and Luco 2007):

- An *IM* is considered to be *efficient* if it provides a relatively small dispersion of the structural responses.
- A *sufficient IM* is defined as one for which the structural responses are independent of earthquake magnitude (M) and source-to-site distance (R).
- A *scaling robust IM* is considered one for which the responses obtained for records scaled by different factors but to the same *IM* level do not show a trend with respect to the scaling factors, i.e., the responses (as a whole) are independent of the scaling factors of the records.

Based on this investigation it is concluded that the proposed intensity measures S_{N1} and S_{N2} are superior when compared to the intensity measure $Sa(T_1)$, and are appropriate for use in probabilistic seismic demand analysis.

9.2.5 Attenuation relations for the proposed intensity measures

In the development of new intensity measures it is important that attenuation relations for the intensity measures can be derived. Attenuation relations, as functions of earthquake magnitude and distance, are needed for the computation of the seismic hazard.

The derivation of the attenuation relations for the proposed intensity measures S_{N1} and S_{N2} is described in Chapter 8. Since S_{N1} and S_{N2} are expressed as products of spectral accelerations at two periods, the derivation of their attenuation relations was quite straightforward, and was done using the existing attenuation relations for spectral accelerations. Specifically, the attenuation relations for S_{N1} and S_{N2} derived in Chapter 8 are for western Canada. However, the same approach can be used for any region for which attenuation relations for spectral accelerations are available.

9.2.6 Application of the proposed intensity measures

Probabilistic seismic demand analyses were conducted for the three frames using the proposed intensity measures S_{N1} and S_{N2} (Chapter 8). The maximum interstorey drift was used as a demand parameter. The mean annual frequencies of exceeding specified drift levels (i.e., the *drift hazard curves*) resulting from the analyses were compared with those obtained using the intensity measure $Sa(T_1)$ (Table 8.1 and Fig. 8.2 in Chapter 8). For the 4-storey frame, the drift hazard curve corresponding to S_{N1} is above the curve corresponding to $Sa(T_1)$, and the maximum difference between the curves is approximately 35%. On the other hand, the drift hazard curves for the 10-storey and the 16-storey frames based on S_{N2} are below the curves based on $Sa(T_1)$, and the maximum difference between the curves is about 60% for the 10-storey frame and 85% for the 16-storey frame. Such differences

relative to drift hazard curves based on $Sa(T_1)$ have also been observed in other studies on advanced intensity measures (e.g., Tothong and Cornell 2007, Tothong and Luco 2007).

In summary, the use of the proposed intensity measures in probabilistic seismic demand analysis is straightforward and provides reliable results.

9.3 Conclusions

Based on the foregoing discussion, the main conclusions can be summarised as follows:

- For the frames investigated in this thesis, the use of *inelastic* spectral displacement as an intensity measure does not have advantage compared to the use of *elastic* spectral displacement (or spectral acceleration at the first mode period).

- The elongation (i.e., the increase) of the first mode structural period is almost linearly proportional to the intensity of the motions. The *actual* first mode periods of frame structures corresponding to the highest intensity levels used in probabilistic seismic demand analysis could be longer than the elastic periods by factors larger than 2.

- Two improved intensity measures, designated S_{N1} and S_{N2}, are developed in this thesis. The intensity measure S_{N1} is proposed for first mode dominated frames, and S_{N2} is proposed for frames for which the second mode contribution to the response is significant.

- With respect to the *elastic* first mode periods, the results indicate that S_{N1} can be used for frames with periods shorter than approximately 1.5 s, and S_{N2} can be used for frames with periods longer than about 1.5 s.

- The proposed intensity measures S_{N1} and S_{N2} are superior in comparison with the 'traditional' intensity measure represented by the spectral acceleration at the first mode period ($Sa(T_1)$). The dispersions of the frame responses obtained using S_{N1} and S_{N2} are about 35% smaller than those obtained using $Sa(T_1)$.

- Attenuation relations for the proposed intensity measures are developed using the existing attenuation relations for spectral accelerations for western Canada. The method described in the thesis can be used for any region for which attenuation relations for spectral accelerations are available.

- The drift hazard curves corresponding to the proposed intensity measures S_{N1} and S_{N2} are significantly different from those obtained using $Sa(T_1)$ as intensity measure. The differences are about 35% for the 4-storey frame, 60% for the 10-storey frame, and 85% for the 16-storey frame.

- The drift hazard curves show that among the three frames considered in this thesis, the most vulnerable is the 16-storey (i.e., the high rise) frame and the least vulnerable is the 4-storey (i.e., the low rise) frame.

9.4 Recommendations for future work

The research work presented in this thesis is based on considerations of selected structural models, ground motion records, and the use of maximum interstorey drift as a response parameter. These represent a portion of possible cases for which the proposed intensity measures are intended. Given this, further research is needed as summarised hereafter:

- The research in this thesis is done using structural models of three moment-resisting reinforced concrete frames. Other structural systems (e.g., steel frames, as well as shear-wall and dual systems) need to be analysed following the procedure presented in this thesis to verify the effectiveness of the proposed intensity measures S_{N1} and S_{N2} for different structural systems, and to define more precisely the period ranges of the applicability of S_{N1} and S_{N2}.

- The structural response parameter considered in this thesis is the maximum interstorey drift in frame structures, which is considered to be a good indicator of damage to structural components. It is known, however, that peak acceleration can be more suitable for estimating damage to nonstructural components (e.g., building content, equipment, tanks, etc.). Additional studies are needed to verify the effectiveness of the proposed intensity measures for predicting peak floor accelerations in building structures.

- The records used in this thesis were selected from earthquakes in California, and are considered to be representative of expected ground motions due to *crustal* earthquakes in the Vancouver region. The effectiveness of the proposed intensity measures needs to

be verified for other types of earthquake motions, e.g., pulse-like near-fault ground motions, as well as motions from subduction earthquakes, and deep subcrustal earthquakes.

Appendix A

Design of Frames

A.1 Gravity loads

The gravity loads used in the design of the frames are shown in Table A.1. The weights of the beams and the columns represent average values for all three frames. The weights of the frames, W, used in the base shear formula were calculated by considering the dead loads on the roof and the floors over strips of 9.0 m x 27.0 m [i.e., (distance between transverse frames) x (width of building)]. The calculated weights for the 4S, the 10S, and the 16S frames are 7 460 kN, 19 124 kN, and 30 788 kN respectively. Snow loads were not considered.

Table A.1 Design gravity loads (kN/m^2).

	Dead load		Live load
Roof	Weight of slab	3.6	
	Weight of beams	1.8	
	Weight of columns	0.3	
	Roof insulation	0.5	
	Mechanical services	0.5	
	Total	6.7	1.0
Floor	Weight of slab	3.6	
	Weight of beams	2.1	
	Weight of columns	0.8	
	Partitions	1.0	
	Mechanical services	0.5	
	Total	8.0	2.4

A.2 Seismic loads

The computed seismic base shears forces, V, for the 4S, the 10S and the 16S frames are 664 kN, 880 kN, and 1078 kN respectively. These forces were distributed over the height of the frames in accordance with the NBCC specifications. The distributed seismic forces are shown in Table A.2. These were used in the elastic analysis of the frames, in combinations with the gravity loads as prescribed in NBCC and CSA A23.3-04.

Table A.2 Distribution of seismic design forces (kN).

Floor No.	Frame		
	4S	10S	16S
16			215.5
15			107.8
14			100.6
13			93.4
12			86.2
11			79.1
10		195.7	71.9
9		136.9	64.7
8		121.6	57.5
7		106.4	50.3
6		91.2	43.1
5		76.0	35.9
4	237.9	60.8	28.7
3	213.1	45.6	21.6
2	142.0	30.4	14.4
1	71.0	15.2	7.2
Total	664.0	880.0	1078.0

A.3 Longitudinal reinforcement in columns and beams of the frames

Table A.3.1 Percentages of longitudinal reinforcement in columns and beams of the 4S frame.

Storey No.	Exterior columns		Interior columns		Beams			
	Size (cm)	Reinforc. (%)	Size (cm)	Reinforc. (%)	Floor No.	Size (cm)	Reinforcement (%) Top	Bottom
4	55x55	1.45	65x65	1.23	4	40x75	0.67	0.40
3	55x55	1.45	65x65	1.23	3	40x75	1.00	0.50
2	55x55	1.45	65x65	1.23	2	40x75	1.17	0.50
1	55x55	1.45	65x65	1.23	1	40x75	1.40	0.60

Table A.3.2 Percentages of longitudinal reinforcement in columns and beams of the 10S frame.

Storey No.	Exterior columns		Interior columns		Beams			
	Size (cm)	Reinforc. (%)	Size (cm)	Reinforc. (%)	Floor No.	Size (cm)	Reinforcement (%) Top	Bottom
10	55x55	1.19	65x65	1.04	10	40x75	0.67	0.40
9	55x55	1.19	65x65	1.04	9	40x75	0.83	0.40
8	55x55	1.19	65x65	1.04	8	40x75	1.00	0.50
7	60x60	1.22	70x70	1.06	7	45x80	0.97	0.56
6	60x60	1.22	70x70	1.06	6	45x80	1.17	0.56
5	60x60	1.22	70x70	1.06	5	45x80	1.17	0.56
4	65x65	1.04	75x75	1.21	4	45x85	1.10	0.53
3	65x65	1.42	75x75	1.99	3	45x85	1.28	0.65
2	65x65	1.61	75x75	2.84	2	45x85	1.28	0.65
1	65x65	1.61	75x75	2.84	1	45x85	1.28	0.65

Table A.3.3 Percentages of longitudinal reinforcement in columns and beams of the 16S frame.

Storey No.	Exterior columns		Interior columns		Beams			
	Size (cm)	Reinforc. (%)	Size (cm)	Reinforc. (%)	Floor No.	Size (cm)	Reinforcement (%) Top	Bottom
16	55x55	1.19	65x65	1.04	16	40x75	0.67	0.40
15	55x55	1.19	65x65	1.04	15	40x75	0.83	0.40
14	55x55	1.19	65x65	1.04	14	40x75	1.00	0.50
13	60x60	1.22	70x70	1.06	13	45x80	0.97	0.56
12	60x60	1.22	70x70	1.06	12	45x80	1.17	0.56
11	60x60	1.22	70x70	1.06	11	45x80	1.17	0.56
10	65x65	1.04	75x75	1.21	10	45x85	1.10	0.53
9	65x65	1.42	75x75	1.21	9	45x85	1.28	0.65
8	65x65	1.61	75x75	1.71	8	45x85	1.28	0.65
7	70x70	1.39	80x80	1.69	7	50x90	1.09	0.56
6	70x70	1.71	80x80	2.31	6	50x90	1.09	0.56
5	70x70	1.96	80x80	2.94	5	50x90	1.09	0.56
4	75x75	1.71	85x85	2.60	4	50x95	1.03	0.53
3	75x75	2.13	85x85	3.32	3	50x95	1.03	0.53
2	75x75	2.42	85x85	3.88	2	50x95	1.03	0.53
1	75x75	2.84	85x85	4.43	1	50x95	1.03	0.53

Appendix B

Characteristics of Selected Records

Table B.1 Characteristics of the 80R set.

Record No.	Record ID	Earthquake Name	Station	Mag. (M)	Dis. (km)	Comp.1 (Degree)	PGA (g)	Comp.2 (Degree)	PGA (g)
1	P0807	1992 Cape Mendocino	Eureka-Myrtle&West	7.1	35.8	0	0.15	90	0.18
2	P0811	1992 Cape Mendocino	Shelter Cove Airport	7.1	32.6	0	0.23	90	0.19
3	P0860	1992 Landers	Barstow	7.3	36.1	0	0.13	90	0.14
4	P0755	1989 Loma Prieta	APPEL 7- Pulgas	6.9	46.5	0	0.16	90	0.09
5	P0756	1989 Loma Prieta	APEEL 9-Crystal Springs	6.9	46.4	137	0.11	227	0.10
6	P0767	1989 Loma Prieta	Hayward-BART sta	6.9	57.7	220	0.16	310	0.16
7	P0453	1984 Morgan Hill	Gilroy Array #6	6.2	11.8	0	0.22	90	0.29
8	P0901	1994 Northridge	Inglewood-Union Oil	6.7	40.0	0	0.09	90	0.10
9	P0903	1994 Northridge	LA-Baldwin Hills	6.7	26.2	90	0.24	360	0.17
10	P0905	1994 Northridge	LA-Century City	6.7	18.3	90	0.26	360	0.22
11	P0034	1996 Parkfield	Temblor Pre-1969	6.1	9.9	205	0.36	295	0.27
12	P0282	1980 Trinidad California	Rio Overpass	7.2	71.9	0	0.06	270	0.15
13	P0629	1987 Whittier Narrows	Inglewood-Union Oil	6.0	25.2	0	0.30	90	0.25
14	P0631	1987 Whittier Narrows	LA-Baldwin Hills	6.0	27.0	0	0.14	90	0.16
15	P0688	1987 Whittier Narrows	Rancho-Cucamonga Law&J	6.0	44.3	90	0.06	360	0.05
16	P0515	1986 N. Palm Springs	Anza Tule Canyon	6.0	55.4	270	0.11	360	0.10
17	P0165	1979 Imperial Valley	Cerro Prieto	6.5	23.5	147	0.17	237	0.16
18	P0191	1979 Imperial Valley	Supersition Mtn Camera	6.5	26.0	45	0.11	135	0.20
19	P0816	1992 Landers	Joshua Tree	7.3	11.3	0	0.27	90	0.28
20	P0820	1992 Landers	Puerta La Cruz	7.3	93.1	0	0.05	90	0.04
21	P0859	1992 Landers	Baker Fire Station	7.3	88.3	50	0.11	140	0.11
22	P0861	1992 Landers	Boron Fire Station	7.3	90.6	0	0.12	90	0.09
23	P0764	1989 Loma Prieta	Gilroy Gavilan Coll.	6.9	10.9	67	0.36	337	0.33
24	P0522	1986 N. Palm Springs	Hurkey Creek Park	6.0	34.9	45	0.24	135	0.19
25	P0532	1986 N. Palm Springs	Puerta La Cruz	6.0	71.9	258	0.08	348	0.06
26	P0534	1986 N. Palm Springs	Riverside Airport	6.0	71.1	180	0.05	270	0.04
27	P0957	1994 Northridge	Featherly Park	6.7	82.5	0	0.10	90	0.10
28	P1006	1994 Northridge	Riverside Airport	6.7	100.4	180	0.06	270	0.06
29	P0085	1971 San Fernando	Pearblossom Pump	6.6	37.4	0	0.10	270	0.14
30	P0093	1971 San Fernando	Upland-San Antonio Dam	6.6	58.1	15	0.06	285	0.08
31	P0281	1980 Trinidad California	Rio dell Overpass	7.2	71.9	0	0.16	270	0.13
32	P0283	1980 Trinidad California	Rio dell Overpass	7.2	71.9	0	0.15	270	0.16
33	P0591	1987 Whittier Narrows	Csatatic-Old Ridge Route	6.0	78.3	0	0.07	90	0.07
34	P0661	1987 Whittier Narrows	Malibu point Dume	6.0	65.3	180	0.05	270	0.04
35	P0014	1952 Kern Country	Pasaadena CIT Athenaeum	7.4	109.0	180	0.05	270	0.05
36	P0015	1952 Kern Country	Santa Barbara Courthouse	7.4	85.0	42	0.09	132	0.13
37	P0016	1952 Kern Country	Taft Lincoln School	7.4	41.0	21	0.16	111	0.18
38	P0188	1979 Imperial Valley	Parachute Test Site	6.5	14.0	225	0.11	315	0.20
39	P0817	1992 Landers	Morongo Valley	7.3	17.7	0	0.19	90	0.14
40	P0317	1981 Westmorland	Parachute Test Site	5.8	24.1	225	0.24	315	0.16

Note: ID=identification No. in PEER database; M=moment magnitude; PGA=peak ground acceleration.

Table B.2 Characteristics of the 40R set.

Record No.	Record ID	Earthquake Name	Station	Mag. (M)	Dis. (km)	Comp. (Degree)	PGA (g)
1	P0807	1992 Cape Mendocino	Eureka-Myrtle&West	7.1	35.8	90	0.18
2	P0811	1992 Cape Mendocino	Shelter Cove Airport	7.1	32.6	0	0.23
3	P0860	1992 Landers	Barstow	7.3	36.1	90	0.14
4	P0755	1989 Loma Prieta	APPEL 7- Pulgas	6.9	46.5	0	0.16
5	P0756	1989 Loma Prieta	APEEL 9-Crystal Springs	6.9	46.4	137	0.11
6	P0767	1989 Loma Prieta	Hayward-BART sta	6.9	57.7	220	0.16
7	P0453	1984 Morgan Hill	Gilroy Array #6	6.2	11.8	90	0.29
8	P0901	1994 Northridge	Inglewood-Union Oil	6.7	40.0	90	0.10
9	P0903	1994 Northridge	LA-Baldwin Hills	6.7	26.2	90	0.24
10	P0905	1994 Northridge	LA-Century City	6.7	18.3	90	0.26
11	P0034	1996 Parkfield	Temblor Pre-1969	6.1	9.9	205	0.36
12	P0282	1980 Trinidad California	Rio Overpass	7.2	71.9	270	0.15
13	P0629	1987 Whittier Narrows	Inglewood-Union Oil	6.0	25.2	0	0.30
14	P0631	1987 Whittier Narrows	LA-Baldwin Hills	6.0	27.0	90	0.16
15	P0688	1987 Whittier Narrows	Rancho-Cucamonga Law&J	6.0	44.3	90	0.06
16	P0515	1986 N. Palm Springs	Anza Tule Canyon	6.0	55.4	270	0.11
17	P0165	1979 Imperial Valley	Cerro Prieto	6.5	23.5	147	0.17
18	P0191	1979 Imperial Valley	Supersition Mtn Camera	6.5	26.0	135	0.20
19	P0816	1992 Landers	Joshua Tree	7.3	11.3	90	0.28
20	P0820	1992 Landers	Puerta La Cruz	7.3	93.1	0	0.05
21	P0859	1992 Landers	Baker Fire Station	7.3	88.3	50	0.11
22	P0861	1992 Landers	Boron Fire Station	7.3	90.6	0	0.12
23	P0764	1989 Loma Prieta	Gilroy Gavilan Coll.	6.9	10.9	67	0.36
24	P0522	1986 N. Palm Springs	Hurkey Creek Park	6.0	34.9	45	0.24
25	P0532	1986 N. Palm Springs	Puerta La Cruz	6.0	71.9	258	0.08
26	P0534	1986 N. Palm Springs	Riverside Airport	6.0	71.1	180	0.05
27	P0957	1994 Northridge	Featherly Park	6.7	82.5	0	0.10
28	P1006	1994 Northridge	Riverside Airport	6.7	100.4	270	0.06
29	P0085	1971 San Fernando	Pearblossom Pump	6.6	37.4	270	0.14
30	P0093	1971 San Fernando	Upland-San Antonio Dam	6.6	58.1	285	0.08
31	P0281	1980 Trinidad California	Rio dell Overpass	7.2	71.9	0	0.16
32	P0283	1980 Trinidad California	Rio dell Overpass	7.2	71.9	270	0.16
33	P0591	1987 Whittier Narrows	Csatatic-Old Ridge Route	6.0	78.3	0	0.07
34	P0661	1987 Whittier Narrows	Malibu point Dume	6.0	65.3	180	0.05
35	P0014	1952 Kern Country	Pasaadena CIT Athenaeum	7.4	109.0	270	0.05
36	P0015	1952 Kern Country	Santa Barbara Courthouse	7.4	85.0	132	0.13
37	P0016	1952 Kern Country	Taft Lincoln School	7.4	41.0	111	0.18
38	P0188	1979 Imperial Valley	Parachute Test Site	6.5	14.0	315	0.20
39	P0817	1992 Landers	Morongo Valley	7.3	17.7	0	0.19
40	P0317	1981 Westmorland	Parachute Test Site	5.8	24.1	225	0.24

Note: ID=identification No. in PEER database; M=moment magnitude; PGA=peak ground acceleration.

Table B.3 Characteristics of the 20R set.

Record No.	Record ID	Earthquake Name	Station	Mag. (M)	Dis. (km)	Comp. (Degree)	PGA (g)
1	P0860	1992 Landers	Barstow	7.3	36.1	90	0.14
2	P0860	1992 Landers	Barstow	7.3	36.1	0	0.13
3	P0755	1989 Loma Prieta	APPEL 7- Pulgas	6.9	46.5	0	0.16
4	P0756	1989 Loma Prieta	APEEL 9-Crystal Springs	6.9	46.4	137	0.11
5	P0901	1994 Northridge	Inglewood-Union Oil	6.7	40.0	90	0.10
6	P0903	1994 Northridge	LA-Baldwin Hills	6.7	26.2	90	0.24
7	P0905	1994 Northridge	LA-Century City	6.7	18.3	90	0.26
8	P0282	1980 Trinidad California	Rio Overpass	7.2	71.9	270	0.15
9	P0631	1987 Whittier Narrows	LA-Baldwin Hills	6.0	27.0	90	0.16
10	P0515	1986 N. Palm Springs	Anza Tule Canyon	6.0	55.4	270	0.11
11	P0191	1979 Imperial Valley	Supersition Mtn Camera	6.5	26.0	135	0.20
12	P0816	1992 Landers	Joshua Tree	7.3	11.3	90	0.28
13	P0859	1992 Landers	Baker Fire Station	7.3	88.3	50	0.11
14	P0861	1992 Landers	Boron Fire Station	7.3	90.6	0	0.12
15	P0957	1994 Northridge	Featherly Park	6.7	82.5	0	0.10
16	P0281	1980 Trinidad California	Rio dell Overpass	7.2	71.9	0	0.16
17	P0281	1980 Trinidad California	Rio dell Overpass	7.2	71.9	0	0.13
18	P0015	1952 Kern Country	Santa Barbara Courthouse	7.4	85.0	132	0.13
19	P0016	1952 Kern Country	Taft Lincoln School	7.4	41.0	111	0.18
20	P0188	1979 Imperial Valley	Parachute Test Site	6.5	14.0	315	0.20

Note: ID=identification No. in PEER database; M=moment magnitude; PGA=peak ground acceleration.

References

Adams, J., and Halchuk, S. 2003. Fourth generation seismic hazard maps of Canada: Values for over 650 Canadian localities intended for the 2005 National Building Code of Canada. Open File Report 4459, Geological Survey of Canada, Ottawa, Ont., 155 p.

Adams, J., and Atkinson, G. 2003. Development of seismic hazard maps for the proposed 2005 edition of the National Building Code of Canada. Canadian Journal of Civil Engineering, **30**: 255-271.

Adams, J., and Halchuk, S. 2007. Personal communication.

Ang, A.H-S., and Wilson, H.T. 1975. Probability concepts in engineering planning and design, Volume I – Basic principles. John Wiley & Sons, 409 p.

Anglin, F.M., Wetmiller, R.J., Horner, G.C., Rogers, G.C., and Drysdale, J.A. 1990. Canadian Geophysical Atlas, Seismicity Map of Canada, Map 15, scale 1:10 000 000. Geological Survey of Canada, Ottawa, Ont.

ASCE. 2000. Prestandard and commentary for the seismic rehabilitation of buildings. Report FEMA 356, American Society of Civil Engineers, Reston, Virginia.

ASCE. 2006. Minimum design loads for building and other structures. ASCE standard ASCE/SEI 7-05, American Society of Civil Engineers, Danvers, MA.

ATC. 1985. Earthquake damage evaluation data for California. Report ATC-13, Applied Technology Council, Redwood City, CA, 492 p.

Atkinson, G.M. 2006. Personal communication.

Atkinson, G.M. 2004. An overview of developments in seismic hazard analysis. 13th World Conference on Earthquake Engineering, on CD-ROM, Paper No. 5001, Vancouver, Canada, 22 p.

Baker, J.W., and Cornell, C.A. 2004. Choice of a vector of ground motion intensity measures for seismic demand hazard analysis. Proceedings of the 13th World Conference on Earthquake Engineering, on CD-ROM, Paper No. 3384, Vancouver, Canada, 15 p.

Baker, J.W., and Cornell, C.A. 2005. A vectored-valued ground motion intensity measure consisting of spectral acceleration and epsilon. Earthquake Engineering and Structural Dynamics, **34**: 1193-1217.

Baker, J.W., Cornell, C.A., and Tothong, P. 2005. Disaggregation of seismic drift hazard. 9th International Conference on Structural Safety and Reliability, Rome, Italy, 7 p.

Baker, J.W., and Cornell, C.A. 2006. Correlation of response spectral values for multicomponent ground motions. Bulletin of the Seismological Society of America, **96**(1): 215-227.

Baker, J.W. 2007. Probabilistic structural response assessment using vector-valued intensity measures. Earthquake Engineering and Structural Dynamics, **36**: 1861-1883.

Boore, D.M., Joyner, W.B., and Fumal, T.E. 1993. Estimation of response spectra and peak accelerations from western North American earthquakes: An interim report, U.S. Geological Survey, Open-file Report 93-509.

Boore, D.M., Joyner, W.B., and Fumal, T.E. 1994. Estimation of response spectra and peak accelerations from North American earthquakes: An interim report, Part 2, U.S. Geological Survey, Open-file Report 94-127.

Boore, D.M., Joyner, W.B., and Fumal, T.E. 1997. Equations for estimating horizontal response spectra and peak acceleration from western North American earthquakes: A summary of recent work. Seismological Research Letters, **68**: 128-153.

Carr, A.J. 2004. RUAUMOKO – Inelastic dynamic analysis program. Department of Civil Engineering, University of Canterbury, Christchurch, New Zealand.

Computers and Structures, Inc. 2000. SAP2000 – Computer program for three dimensional static and dynamic finite element analysis and design of structures. Berkeley, CA.

Cordova, P.P., Deierlein, G.G., Mehanny, S.S.F., and Cornell, C.A. 2001. Development of two-parameter seismic intensity measure and probabilistic assessment procedure. The Second U.S. – Japan Workshop on Performance-based Earthquake Engineering Methodology for Reinforced Concrete Building Structures, Sapporo, Japan, 187-206.

Cornell, C.A., and Krawinkler, H. 2000. Progress and challenges in seismic performance assessment. PEER Center News, **3**(2), 4 p. http://peer.berkeley.edu/news/2000spring/performance.html.

CSA. 2004. Design of concrete structures. CSA Standard A23.3-04, Canadian Standards Association, Rexdale, Ont.

DeVall, R. 2007. Personal communication.

Fajfar, P. 2000. A nonlinear analysis method for performance-based seismic design. Earthquake Spectra, **16**(3): 573-592.

Halchuk, S., Adams, J., and Anglin, F. 2007. Revised deaggregation of seismic hazard for selected Canadian cities. Proceedings of the Ninth Canadian Conference on Earthquake Engineering, Ottawa, Ont., on CD-ROM, Paper No. 1188, 420-432.

Hamburger, R.O. 2007. Development of next-generation procedures for performance-based earthquake engineering. 9th Canadian Conference on Earthquake Engineering, Ottawa, Ont., Canada, on CD-ROM, p. 45-54.

Heidebrecht, A.C. 1997. Seismic level of protection for building structures. Canadian Journal of Civil Engineering, **24**: 20-33.

Heidebrecht, A.C., and Naumoski, N. 2000. Periods of reinforced concrete frames during nonlinear earthquake response. Twelfth World Conference on Earthquake Engineering, Wellington, New Zealand, on CD-ROM, Paper No. 208, 7 p.

Inoue, T., and Cornell, C.A. 1990. Seismic hazard analysis of multi-degree-of-freedom structures. Reliability of Marine Structures, Report RMS-8, Stanford University, Stanford, CA, 70 p.

Luco, N., and Cornell, C.A. 2007. Structure-specific scalar intensity measures for near-source and ordinary earthquake motions. Earthquake Spectra, **23**(2): 357-391.

Mander, J.B., Priestley, M.J.N., and Park, R. 1988. Theoretical stress-strain model for confined concrete. ASCE Journal of Structural Engineering, 114: 1804-1849.

Moehle, J., and Deierlein, G.G. 2004. A framework methodology for performance-based earthquake engineering. 13th World Conference on earthquake Engineering, Vancouver, B.C., Canada, on CD-ROM, 13 p.

Miranda, E., and Aslani, H. 2003. Probabilistic response assessment for building-specific loss estimation. PEER 2003/03, Pacific Earthquake Engineering Research Center, University of California at Berkeley, Berkeley, CA, 49 p.

NRCC. 2005. National Building Code of Canada 2005. Institute for Research in Construction, National Research Council of Canada, Ottawa, Ont.

Paulay, T., and Priestley, M.J.N. 1992. Seismic design of reinforced concrete and masonry buildings. John Wiley & Sons, Inc., New York.

Perus, I., Poljansek, K., and Fajfar, P. 2006. Flexural deformation capacity of rectangular RC columns determined by the CAE method. Earthquake Engineering and Structural Dynamics, **35**: 1453-1470.

Pujol, S., Sozen, M., and Ramirez, J. 2000. Transverse reinforcement for columns of RC frames to resist earthquakes. Journal of Structural Engineering, **126**(4): 461-466.

Ruiz-Garcia, J., and Miranda, E. 2005. Performance-based assessment of existing structures accounting for residual displacements. Report No. 153, The John. A. Blume Earthquake Engineering Center, Department of Civil and Environmental Engineering, Stanford University, Stanford, CA, 407 p.

Saatcioglu, M., and Razvi, S.R. 2002. Displacement-based design of reinforced concrete columns for confinements. ACI Structural Journal, **99**(1): 3-11.

Shome, N., Cornell, C.A., Bazzurro, P., and Carballo, J.E. 1998. Earthquakes, records, and nonlinear responses. Earthquake Spectra, **14**(3): 469-500.

Shome, N. 1999. Probabilistic seismic demand analysis of nonlinear structures. Report RMS-35, RMS Program, Department of Civil and Environmental Engineering, Stanford University, Stanford, CA, 320 p.

Singhal, A., and Kiremidjian, A.S. 1996. A method for earthquake motion-damage relationships with application to reinforced concrete frames. Report No. 119, John. A. Blume Earthquake Engineering Center, Department of Civil and Environmental Engineering, Stanford University, Stanford, CA, 186 p.

Taghavi, S., and Miranda, E. 2003. Probabilistic study of peak floor acceleration demands in linear structures. Proceedings of the Ninth International Conference on Applications of Statistics and Probability in Civil Engineering, San Francisco, California.

Tothong, P., and Cornell, C.A. 2007. Probabilistic seismic demand analysis using advanced ground motion intensity measures, attenuation relationships, and near-fault

effects. PEER Report 2006/11, Pacific Earthquake Engineering Center, University of California, Berkeley, 205 p.

Tothong, P., and Luco, N. 2007. Probabilistic seismic demand analysis using advanced intensity measures. Earthquake Engineering and Structural Dynamics, **36**: 1837-1860.

Tremblay, R. 1998. Development of design spectra for long-duration ground motions from Cascadia subduction earthquakes. Canadian Journal of Civil Engineering, **25**: 1078-1090.

Tremblay, R., and Atkinson, G.M. 2001. Comparative study of the inelastic seismic demand of eastern and western Canadian sites. Earthquake Spectra, **17**(2): 333-358.

Vamvatsikos, D., and Cornell, C.A. 2004. Applied incremental dynamic analysis. Earthquake Spectra, **20**(2): 523-553.

Vision 2000 Committee. 1995. Performance based seismic engineering of buildings. Structural Engineers Association of California (SEAOC), San Francisco, CA.

Youngs, R.R., Chiou, S.-J., Silva, W.J., and Humphrey, J.R. 1997. Strong ground motion relationships for subduction zone earthquakes. Seismological Research Letters, **68**: 58-73.